On the Motion of Objects Immersed in Fermi Liquids

Juri Kuorelahti

University of Oulu Graduate School
University of Oulu
Faculty of Science
Nano and Molecular Systems Research Unit

Abstract

Interacting many-body problems are central to most fields of physics. In condensed matter physics, the systems of interest consists of a number of bodies on the order of Avogadro's constant, $\sim 10^{23}$. The precise modeling of such systems is usually impossible. Under certain circumstances however, even these problems can become tractable. One such circumstance is that of a Fermi liquid. At sufficiently low temperatures, in describing the dynamics of a system of interacting fermions, it is possible to forgo description of the fermions themselves, and instead concentrate on the collective excitations of the entire fermion system. These collective excitations are called quasiparticles.

In this thesis we study two phenomena related to the motion of objects in a Fermi liquid. First, we study the transmission of transverse oscillations through a thin film of normal Fermi liquid. The dynamics of normal Fermi liquid are described by Landau's Fermi liquid theory. Landau's theory predicts the existence of new modes of sound under conditions where sound ordinarily would not propagate. Using the equations of motion for the Fermi liquid quasiparticles, we calculate the linear response of a Fermi liquid film to the transverse oscillations of a planar substrate under a wide range of conditions. We present the linear response in terms of the film's acoustic impedance and study the effects of quasiparticle collisions and of the Fermi liquid interactions.

The second phenomenon we study is the supercritical motion of a wire in a superfluid Fermi liquid. The prevailing assumption is that if the velocity of an object moving in a superfluid Fermi liquid surpasses a characteristic critical velocity, the object experiences a sudden onset of viscous forces. This viscosity is caused by the escape of quasiparticles, produced by pair breaking on the surface of the object, into the surrounding superfluid. We study Andreev reflection of the quasiparticles by the surrounding superfluid flow field, and modifications to the flow caused by pair breaking, as possible mechanisms for low-dissipation motion above the critical velocity.

Keywords: ^{3}He, Normal Fermi liquid, Fermi liquid theory, Transverse zero sound, Acoustic impedance, Fermi superfluid, Supercritical motion, Pair breaking, Andreev reflection

Acknowledgements

<div align="center">Oulu, June 2019 Juri Kuorelahti</div>

List of original publications

The present thesis consists of an introductory part and the following papers which will be referred to in the text by their assigned Roman numerals.

  I J. A. Kuorelahti, J. A. Tuorila and E. V. Thuneberg, *Fermi liquid theory applied to a film on an oscillating substrate*, Phys. Rev. B **94**, 184103 (2016).

  II J. A. Kuorelahti and E. V. Thuneberg, *Two-parameter boundary condition applied to transverse acoustic impedance of a Fermi liquid*, Journal of Physics: Conference Series **969**, 012010 (2018).

  III J. A. Kuorelahti, S. M. Laine, E. V. Thuneberg, *Models for supercritical motion in a superfluid Fermi liquid*, Phys. Rev. B **98**, 144512 (2018).

The author of this thesis has had a central role in all publications. He has done all of the numerical work in Pubs. I and II, and most of that in Pub. III. He has written an initial draft of Pub. I and contributed to the writing of all publications.

Contents

1

Introduction

Everything flows.

– Heraclitus

Particles in the Universe can be divided into two groups; *fermions* and *bosons*. This division is delineated by a particle's *spin*, a form of internal angular momentum. The spin of a particle can "point" in different directions, but its magnitude is intrinsic to the type of particle. Bosons have an integer spin, while fermions have a half-integer spin. The important distinction between fermions and bosons is that fermions are subject to the *Pauli exclusion principle*. The wave function of a system of fermions has to be antisymmetric with respect to the exchange of particles. Alternatively, no two fermions can simultaneously occupy the same quantum state. This has a profound effect on the statistical behavior of particles. In a low energy system of bosons, particles can all crowd into the lowest available energy state. In a system of fermions, particles must fill the available energy states starting from the bottom up, with only a single particle fitting into each individual state.

Generally speaking, matter is made of fermions, while particles that intermediate forces are bosons. In the presence of a binding force, particles may group together to form a composite particle, such as an atomic nucleus. This composite particle can then be either a boson or a fermion, depending on the sum of the spins of the constituent particles. The element helium has two stable isotopes, one bosonic and one fermionic. A helium atom has two electrons. In the ground state, the spins of the electrons point in opposite directions. As a result, the spin of a helium atom is completely due to the spin of its nucleus. The nucleus of the more common helium isotope, ^{4}He, consists of two protons and two neutrons. The spins of these particles cancel each other, leaving a total spin of zero. The ^{4}He atom is thus a boson. The other isotope, ^{3}He on the

other hand, has two protons but only one neutron, producing a total spin of 1/2, making it a fermion.

Helium is the only substance known to exists in a liquid state at absolute zero. In the context of classical physics, we would expect all liquids to solidify at this temperature, as the thermal motion of atoms has stopped. One of the consequences of quantum mechanics is that the position and momentum of a specific particle cannot simultaneously have absolute certain values. This phenomenon, called the Heisenberg uncertainty principle, is a result of the fact that position and momentum are conjugate variables. An eigenstate of position, i.e., a state where the position of a particle is known without ambiguity, is a state where the momentum of the particle is completely uncertain, and vice versa. A curious ramification of this is that atoms continue to move at absolute zero in what is called *zero-point motion*. In the case of helium, this zero-point motion is enough to preserve a liquid state at absolute zero. Helium exhibits this behavior because helium atoms are very light, which amplifies the zero-point motion. Helium is also an inert gas, so the interatomic forces that would bind the atoms into a solid are very weak. No other element fulfills these conditions; the other inert gases are much heavier than helium, and the other light elements, such as hydrogen and lithium, are highly reactive.

Near absolute zero, instead of solidifying, helium becomes the most freely moving substance in nature, a *superfluid*. This has to do with the concept of Bose–Einstein condensation. In a low temperature system, bosons occupy the single-particle state with the lowest energy. Because the particles are in the same quantum state, their behavior is coherent and the system as a whole exhibits macroscopic quantum mechanical properties. ^{4}He atoms are bosons and readily form a condensate. For ^{4}He the transition to a superfluid state takes place at the temperature of a few kelvin [1]. ^{3}He atoms on the other hand are fermions and so cannot occupy the same state en masse. At these temperatures, ^{3}He behaves like a degenerate Fermi gas, where the single-particle states are filled by individual particles, starting from the state with the lowest energy. ^{3}He in this state is called *normal liquid*, to distinguish it from the superfluid state.

In comparison to ^{4}He, the superfluid transition of ^{3}He takes place at the much lower temperature of a few millikelvin [1, 2]. This is because in order to form a condensate, ^{3}He must first form *Cooper pairs*. The concept of Cooper pairing was originally introduced to explain the related phenomenon of superconductivity, where certain metals, once cooled to a sufficiently low temperature, exhibit zero electrical resistance. In a Cooper pair, two fermions pair together to form a composite boson as

a means of reaching a lower energy state. It can be shown that Cooper pairs are formed as long as there exists an arbitrarily small attractive potential between the particles. In a superconductor, Cooper pairs are formed by conduction electrons and the attraction is provided by the ionic lattice through which the electrons move. In helium, there is a direct van der Waals-type attraction between the atoms [1]. Both superconductivity and ^{3}He superfluidity may here be understood as the condensation of Cooper pairs into the same quantum state. In ^{3}He, the Cooper pairs are not formed directly by the helium atoms themselves, but rather by ^{3}He quasiparticles, particle-like elementary excitations of the fluid. Collectively, the superfluid phases of helium, normal state ^{3}He, and the conduction electrons in metals are referred to as *quantum liquids*.

The history of quantum liquids arguably begins with the liquefaction of helium by Heike Kamerlingh Onnes in 1908, an achievement which soon led Kamerlingh Onnes to also discover the phenomenon of superconductivity [3]. Given that these discoveries took place well before the full formulation of quantum mechanics, theoretical explanations were not offered until decades later. The first steps in the theoretical study of quantum liquids were made by Satyendra Nath Bose and Albert Einstein, who in 1924 proposed that a system of bosons at low temperature would condense into the lowest available energy state and thus exhibit macroscopic quantum mechanical properties [4]. This theoretical concept became reality thirteen years later, when ^{4}He superfluidity was discovered in 1937, independently by Pyotr Kapitza [5], and by John Allen and Don Misener [6]. Fritz London suggested that the underlying cause of this, then called "λ-phenomenon", was related to Bose–Einstein condensation [7].

The first theoretical explanation for ^{4}He superfluidity was provided by Lev Landau in 1941 [8]. Landau argued that the underlying cause of superfluidity was the impossibility of the creation of low energy excitations of the fluid. Later, starting in 1956, Landau introduced his theory of Fermi liquids, a description of the properties of a low temperature Fermi system [9, 10]. This theory predicted that a low energy system of interacting fermions, a Fermi liquid, would behave in a manner similar to a degenerate Fermi gas. The theory also introduced the concept of a Fermi liquid quasiparticle, a low energy excitation of the Fermi liquid with particle-like properties.

The concept of Cooper pairing was proposed as an explanation for the phenomenon of superconductivity by Leon Cooper in 1956 [11]. Soon after this discovery, Cooper together with his colleagues John Bardeen and Robert Schrieffer would formulate the microscopic theory of superconductivity, the BCS theory [12]. Following the work of Bardeen, Cooper,

and Schrieffer, efforts were made to study the possibility of different kinds of Cooper pairing. The Cooper pairs of BCS theory form in a zero angular momentum, i.e. $l = 0$ state. The possibility of pairings with higher angular momentum were studied theoretically well before the discovery of superfluid ^{3}He, particularly by Philip Anderson and Pierre Morel [13], and Roger Balian and Nathan Werthamer [14] who introduced the ABM and WB pairing states with $l = 1$. Superfluidity of ^{3}He was finally discovered by Douglas Osheroff, Robert Richardson, and David Lee in 1971 [2]. It was found that ^{3}He has two superfluid phases, now called A and B. It soon became clear that these phases could be understood as the Cooper pairing of the quasiparticles of Landau's Fermi liquid theory in the ABM and BW states. The names of the two phases were solidified as the result of a historical coincidence, as the experimentally observed phase transitions corresponding to the ABM and BW states were fittingly named A and B as they were first recorded. Initially, these phase transitions were thought to be taking place in solid ^{3}He, but this misconception was soon corrected [15].

In this thesis we study two separate phenomena related to the motion of a Fermi liquid. The first phenomenon under study is the transmission of transverse sound waves through a thin film of normal Fermi liquid. Landau's Fermi liquid theory predicts the propagation of new modes of sound, called zero sound. Unlike ordinary sound, which propagates by means of interparticle collisions, for zero sound the mechanism of propagation is a nonlocal interaction between Fermi liquid quasiparticles. In Pub. I, we study the linear response of a thin film of normal state Fermi liquid to the transverse oscillations of a substrate. The linear response is stated in terms of the film's acoustic impedance. The acoustic impedance depends on both the presence of transverse zero sound, as well as the frequency of quasiparticle collisions. The relative strength of these contributions depend on the mean free path of the quasiparticles, and the strength of the Fermi liquid interactions. This study is partially motivated by experiments that show a film of normal state ^{3}He decoupling from a mechanical oscillator as the temperature is lowered [16, 17]. We study Fermi liquid interactions as a possible source of this decoupling. In Pub. II, we investigate a more accurate modeling of quasiparticle scattering from a surface, and what effect this has on the acoustic impedance.

The second phenomenon we study is the supercritical motion of a wire moving in a Fermi superfluid. The most famous property of superfluids is that they flow without viscosity. In a Fermi superfluid, the fundamental reason for this is the formation of Cooper pairs and the associated binding energy, which, below the Landau critical velocity, prevents the creation of excitations in the fluid. It is expected that if the motion of

the fluid surpasses the critical velocity, there is a sudden onset of viscous forces. However, recent experiments have shown that a wire moving with uniform velocity in superfluid ^{3}He does not experience this anticipated onset of viscosity and instead is able to move at velocities well above the critical velocity while experiencing only minor dissipation [18]. We refer to this as supercritical motion. In Pub. III, we attempt to shed light on this unexpected phenomenon by calculating the drag force on a macroscopic cylindrical object moving in a Fermi superfluid. This calculation is formulated in terms of the elementary excitations of the Fermi superfluid. We consider the effects of Andreev reflection, as well as the alterations to the superfluid flow caused by the production of elementary excitations on the surface of the wire as mechanisms for the low-dissipation motion.

The body of this thesis consists of two chapters, each focusing on one of the aforementioned topics of research. In Chap. 2 we discuss the motion of a normal Fermi liquid film on an oscillating substrate. In Chap. 3 we study the supercritical motion of a wire in superfluid Fermi liquid. Finally, Chap. 4 offers a conclusion and summary of the results.

2

Fermi liquid film on an oscillating substrate

We investigate the transmission of transverse sound waves through a thin film of normal state Fermi liquid. We begin in Sec. 2.1 with an introduction to Fermi liquid theory and introduce kinetic equations that describe the dynamics of Fermi liquid quasiparticles. In Sec 2.2 we apply these equations to the problem of a thin film of normal Fermi liquid on top of an oscillating substrate. Finally, in Sec. 2.3 we discuss the details of the numerical approach, along with some analytically solvable limiting cases and present results of the numerical simulation.

2.1   Fermi liquid

A group of non-interacting fermions is called a *Fermi gas*. Or rather, there is no direct interaction between the fermions, but they still adhere to the Pauli exclusion principle. The energy of a non-interacting particle is its kinetic energy,

$$\epsilon = \frac{p^2}{2m},\tag{2.1}$$

where p is the momentum of the particle and m the mass of the particle. The probability that in a system of fermions at temperature T a state with energy ϵ is occupied is given by the Fermi–Dirac distribution

$$n(\epsilon) = \frac{1}{\exp\left[(\epsilon - \mu)/k_B T\right] + 1},\tag{2.2}$$

where k_B is the Boltzmann constant and μ the chemical potential.

The ground state of a Fermi gas is one where the particles fill the states from the bottom up, with each particle occupying the state with

the lowest available energy. The energy and momentum magnitude associated with the highest occupied energy state are called *Fermi energy* ϵ_F and *Fermi momentum* p_F, respectively. By studying the Fermi–Dirac distribution, we see that the ground state is achieved when $T = 0$ and $\mu = \epsilon_F$. Since the energy of a particle with momentum $\boldsymbol{p}$ is proportional to p^2, in momentum space the ground state forms a sphere. This is called the *Fermi sphere*. Excited states of this system can be created by adding particles outside the Fermi sphere and thus producing particle-like excitations, or by removing them from within, producing hole-like excitations. These are called the *elementary excitations* of the Fermi gas. The energy of such an excitation is

$$|\epsilon_{\boldsymbol{p}} - \epsilon_F| = |\frac{p^2}{2m} - \epsilon_F| \approx |\frac{p_F}{m}(p - p_F)|. \qquad (2.3)$$

where $\epsilon_F = p_F^2/2m$. The linearized approximation can be made when the excitation is close to the Fermi surface. The absolute value ensures that hole-like excitations, which have momentum below p_F, also have positive energy.

In contrast to a Fermi gas, a *Fermi liquid* is characterized by strong interactions between the constituent particles. In ^{3}He for instance, in addition to experiencing a nonlocal interatomic attraction, a ^{3}He atom must push other atoms aside as it moves. These conditions obviously hold true for all liquids. Fermi liquid theory, originally formulated by Lev Landau [9, 10], is based on the idea that an interacting Fermi system can have elementary excitations that are similar in nature to those of the non-interacting system. The excitations can no longer be identified with individual particles, but instead correspond to collective excitations of the entire interacting system. These are referred to as *quasiparticles*.

How could a system with strong interactions behave like a non-interacting system? As the excitations have energies very close to the Fermi energy ϵ_F, and since all the states inside the Fermi sphere are filled, the Pauli exclusion principle severely restricts the scattering of quasiparticles. For a particle with momentum $\boldsymbol{p}$ to scatter from a particle inside the Fermi sphere, the final state of the interaction has to be one with two particles outside the Fermi sphere and an empty state or hole inside. Otherwise the initial and final states are indistinguishable. This means that the initial particle can only scatter from particles within a thin shell of thickness $|p - p_F|$ on the surface of the Fermi sphere, since this is how 'deep' it can reach without yielding all of its own energy. The closer the particle is to the Fermi surface, the more severe this restriction becomes. This means that at low temperature the quasiparticles have

long lifetimes and it is reasonable to use them to describe the state of the system.

In comparison to the particles of a Fermi gas, the energies of the Fermi liquid quasiparticles are changed by the inclusion of interactions. The kinetic energy of the quasiparticle is changed, as it has to move against the background of the particles that fill the Fermi sphere. The quasiparticle has an *effective mass* greater than the mass of a bare particle, as some of this background is dragged along with it. In addition to its kinetic energy, a quasiparticle also has an interaction energy with other excited quasiparticles. These changes to the energy in turn change the quasiparticle distribution, it being a function of energy.

The occupation of a specific quasiparticle state with momentum $\boldsymbol{p}$ and spin σ is given by the distribution function $n_{\boldsymbol{p}\sigma}$. For the ground state the distribution is the same as for a Fermi gas:

$$n_{\boldsymbol{p}\sigma}^0 = \begin{cases} 1, & \text{if } p \leq p_F \\ 0, & \text{if } p > p_F. \end{cases} \tag{2.4}$$

The energy of a quasiparticle becomes a functional of the distribution, $\epsilon_{\boldsymbol{p}\sigma} = \epsilon_{\boldsymbol{p}\sigma}\{n_{\boldsymbol{p}'\sigma'}\}$. If we assume that the distribution of quasiparticles $n_{\boldsymbol{p}\sigma}$ differs only a little from the ground state distribution $n_{\boldsymbol{p}\sigma}^0$, we can express the quasiparticle energy in terms of a series expansion [19, 20]:

$$\epsilon_{\boldsymbol{p}\sigma} - \epsilon_F = \frac{p_F}{m^*}(p - p_F) + \frac{1}{V}\sum_{\boldsymbol{p}'\sigma'} f(\boldsymbol{p}, \sigma, \boldsymbol{p}', \sigma')\delta n_{\boldsymbol{p}'\sigma'} + \dots, \tag{2.5}$$

where m^* is the effective mass, $\delta n_{\boldsymbol{p}\sigma} = (n_{\boldsymbol{p}\sigma} - n_{\boldsymbol{p}\sigma}^0)$ and V is the volume of the system. The interaction energy between two quasiparticles is given by $f(\boldsymbol{p}, \sigma, \boldsymbol{p}', \sigma')/V$, and this energy is summed over the momentum and spin states where the distribution differs from the ground state distribution. The interaction is symmetric with regard to the exchange of particles, $f(\boldsymbol{p}, \sigma, \boldsymbol{p}', \sigma') = f(\boldsymbol{p}', \sigma', \boldsymbol{p}, \sigma)$. The inclusion of the leading correction is necessary for the energy equation to satisfy Galilean invariance. If this term was not included, Galilean invariance would require that $m^* = m$. Effective mass is defined using the Fermi velocity v_F as

$$v_F = \left(\frac{\partial \epsilon_{\boldsymbol{p}\sigma}^0}{\partial p}\right)_{p=p_F} = \frac{p_F}{m^*}, \tag{2.6}$$

where $\epsilon_{\boldsymbol{p}\sigma}^0 = \epsilon_{\boldsymbol{p}\sigma}\{n_{\boldsymbol{p}'\sigma'}^0\}$, the energy of a particle added to a system that is otherwise in its ground state.

The interaction between quasiparticles is generally dependent on spin. In the context of normal ^{3}He, the spin depence may be written in terms

of a *spin symmetric* and a *spin anti-symmetric* component [9, 19, 20]. Using matrix notation the interaction becomes

$$f(\boldsymbol{p}, \boldsymbol{p}') = f^s(\boldsymbol{p}, \boldsymbol{p}') + \boldsymbol{\sigma} \cdot \boldsymbol{\sigma}' f^a(\boldsymbol{p}, \boldsymbol{p}'). \tag{2.7}$$

where $\boldsymbol{\sigma}$ are Pauli spin matrices. The anti-symmetric term describes the exchange interaction between particles. In the absence of an external magnetic field there is no preferred spin state and the anti-symmetric component of the interaction energy will disappear in a summation over spin states. Hereafter, the phenomena we discuss are such that we can ignore the anti-symmetric component of the quasiparticle interaction.

2.1.1   Sounds in Fermi liquid

Sound in an everyday context is a moving density fluctuation, consisting of sequential regions of increased and decreased density. This fluctuation is transmitted by particle collisions. If a region of fluid has an increased density and pressure, the particles within this region push nearby particles through collisions. If ω is the frequency of sound and τ a typical mean free time of the fluid particles, a requirement for the transmission of ordinary sound is that $\omega\tau \ll 1$. This means that the collisions have to occur quickly enough, that the pushing is coherent and that by the time the next sound wave maximum arrives, the particles in the volume element have returned to a thermodynamic equilibrium. In the context of liquid ^{3}He, a sound wave that is transmitted through particle collisions is called *first sound*.

If $\omega\tau \approx 1$, only part of the originally displaced particles have collided with others and returned to their equilibrium state. As a result, there is no clearly defined front to the density fluctuation and sound is dissipated into the random motion of particles.

Sound also has a transverse mode, in which the oscillations occur perpendicular to the direction of propagation. This is more commonly associated with solids, where the parallel layers of the medium are strongly tied by atomic bonds, so that transverse movement in one layer is easily transmitted to nearby layers. In an ordinary fluid, this type of shear wave is very quickly dissipated, as there is an obvious difficulty associated with the transmission of momentum in a perpendicular direction through particle collisions.

In a free Fermi gas there are no particle collisions and therefore no sound waves. One might assume that the same holds true for a Fermi liquid in the collisionless regime $\omega\tau \gg 1$. In reality however, the interaction between quasiparticles that characterises Fermi liquid gives rise to a new unique form of sound, *zero sound*. The idea of zero sound

was first presented by Landau in his second publication on Fermi liquids [10]. A region with increased density can push coherently on neighboring elements through modification of the quasiparticle interaction term in Eq. (2.5). Zero sound has transverse and longitudinal modes. Since the propagation occurs via a nonlocal interaction instead of particle collisions, transverse zero sound does not suffer from the same difficulties with propagation that transverse first sound does.

2.1.2 Quasiparticle dynamics

Dynamics of a Fermi liquid can be studied by concentrating on the Fermi liquid quasiparticles, the elementary excitations of the fluid. To this end, we formulate an equation of motion for the quasiparticles. We examine the time evolution of the distribution function $n_{\boldsymbol{p}}(\boldsymbol{r}, t)$ that decribes the mean number of quasiparticles in an element of phase space with volume $d\boldsymbol{r}d\boldsymbol{p}/(2\pi\hbar)^3$. A theory that employs a distribution function that depends on both position and momentum is inherently classical. Quantum mechanics will enter in the way we define the energy distribution of the quasiparticles and how we describe interparticle collisions. The resulting model is then called semi-classical. We can get away with this by ensuring that the systems we study are in a scale where we are not at risk of violating the Heisenberg uncertainty principle $\Delta r \Delta p \geq \hbar/2$. For a system at temperature T, the Fermi distribution function changes significantly with the characteristic momentum variance $\Delta p = k_B T/v_F$. Therefore [19],

$$\Delta r \gg \frac{\hbar v_F}{k_B T}. \tag{2.8}$$

By taking the total time derivative of the distribution function $n_{\boldsymbol{p}}(\boldsymbol{r}, t)$, we arrive at the *Landau kinetic equation* [10]

$$\frac{dn_{\boldsymbol{p}}}{dt} = \frac{\partial n_{\boldsymbol{p}}}{\partial t} + \frac{\partial n_{\boldsymbol{p}}}{\partial \boldsymbol{r}} \cdot \dot{\boldsymbol{r}} + \frac{\partial n_{\boldsymbol{p}}}{\partial \boldsymbol{p}} \cdot \dot{\boldsymbol{p}} = I(n_{\boldsymbol{p}}) \tag{2.9}$$

The kinetic equation is a continuity equation that describes the rate of change in the occupation of a given volume of phase space. The term added to the right side of the kinetic equation is called the *collision integral*. Interparticle collisions are considered instantaneous and can lead to a net change in the occupation of a given volume element. If there are no collisions, the distribution is constant, $dn_{\boldsymbol{p}}/dt = 0$.

With the aid of Hamilton's equations, $\dot{\boldsymbol{r}} = \partial H/\partial \boldsymbol{p}$ and $\dot{\boldsymbol{p}} = -\partial H/\partial \boldsymbol{r}$, the kinetic equation can be recast into the form

$$\frac{dn_{\boldsymbol{p}}}{dt} = \frac{\partial n_{\boldsymbol{p}}}{\partial t} + \boldsymbol{\nabla} n_{\boldsymbol{p}} \cdot \frac{\partial \epsilon_{\boldsymbol{p}}}{\partial \boldsymbol{p}} - \frac{\partial n_{\boldsymbol{p}}}{\partial \boldsymbol{p}} \cdot \boldsymbol{\nabla} \epsilon_{\boldsymbol{p}} = I(n_{\boldsymbol{p}}), \tag{2.10}$$

where we have replaced the Hamiltonian with the quasiparticle energy $\epsilon_{\boldsymbol{p}}$ and written the partial derivatives with respect to $\boldsymbol{r}$ using the $\boldsymbol{\nabla}$-operator.

In order to solve the kinetic equation, we assume that the excitations of the system are low-lying, meaning that they all have momentum with magnitude p_F and exist on the Fermi surface. We can freely make this assumption, since it is a part of the definition of a Fermi liquid. We write both the quasiparticle distribution function and energy in terms of an equilibrium value and a small deviation from equilibrium as [10]

$$n_{\boldsymbol{p}}(\boldsymbol{r}, t) = n_p^0 + \delta n_{\boldsymbol{p}}(\boldsymbol{r}, t), \qquad (2.11)$$

$$\epsilon_{\boldsymbol{p}}(\boldsymbol{r}, t) = \epsilon_p^0 + \delta\epsilon_{\boldsymbol{p}}(\boldsymbol{r}, t). \qquad (2.12)$$

By comparing the equation for the quasiparticle energy $\epsilon_{\boldsymbol{p}}(\boldsymbol{r}, t)$ with that introduce previously in Eq. (2.5), we can identify the deviation $\delta\epsilon_{\boldsymbol{p}}(\boldsymbol{r}, t)$ with the quasiparticle interaction energy. By introducing Eqs. (2.11) and (2.12) into the kinetic equation and neglecting all nonlinear terms, we arrive at the linearized kinetic equation

$$\frac{\partial \delta n_{\boldsymbol{p}}}{\partial t} + v_F \hat{\boldsymbol{p}} \cdot \boldsymbol{\nabla} \left(\delta n_{\boldsymbol{p}} - \frac{\partial n_p^0}{\partial \epsilon_p} \delta\epsilon_{\boldsymbol{p}} \right) = I_{\hat{\boldsymbol{p}}}. \qquad (2.13)$$

This is the kinetic equation describing the motion of the excited quasiparticles. The term inside the parentheses is often written as $\delta\bar{n}_{\boldsymbol{p}}$. It can also be stated as $\delta\bar{n}_{\boldsymbol{p}} = n_{\boldsymbol{p}} - n^0(\epsilon_p^0 + \delta\epsilon_{\boldsymbol{p}})$ and is called the *deviation from local equilibrium*. Function $n^0(\epsilon_p^0 + \delta\epsilon_{\boldsymbol{p}})$ has the form of the Fermi–Dirac distribution where the energies have been shifted by the quasiparticle interaction energy. Next, we introduce the energy-integrated distribution functions

$$\phi_{\hat{\boldsymbol{p}}}(\boldsymbol{r}, t) = \int \delta n(\hat{\boldsymbol{p}}, \epsilon, \boldsymbol{r}, t) d\epsilon \approx \int \delta n(\hat{\boldsymbol{p}}, \epsilon, \boldsymbol{r}, t) v_F dp, \qquad (2.14)$$

$$\psi_{\hat{\boldsymbol{p}}}(\boldsymbol{r}, t) = \int \delta\bar{n}(\hat{\boldsymbol{p}}, \epsilon, \boldsymbol{r}, t) d\epsilon \approx \int \delta\bar{n}(\hat{\boldsymbol{p}}, \epsilon, \boldsymbol{r}, t) v_F dp, \qquad (2.15)$$

where the approximations have been made assuming that $\delta n_{\boldsymbol{p}}$ and $\delta\bar{n}_{\boldsymbol{p}}$ differ from zero only near the Fermi surface. In terms of $\psi_{\hat{\boldsymbol{p}}}(\boldsymbol{r}, t)$, the kinetic equation becomes

$$\frac{\partial}{\partial t}(\psi_{\hat{\boldsymbol{p}}} - \delta\epsilon_{\hat{\boldsymbol{p}}}) + v_F \hat{\boldsymbol{p}} \cdot \nabla\psi_{\hat{\boldsymbol{p}}} = I_{\hat{\boldsymbol{p}}}. \qquad (2.16)$$

Since we assume that all excited quasiparticles are close to the Fermi surface, the interaction energy between two quasiparticles should depend

(a) Legendre polynomials $P_l(\hat{\boldsymbol{p}} \cdot \hat{\boldsymbol{p}}')$

(b) Deformations of the Fermi surface
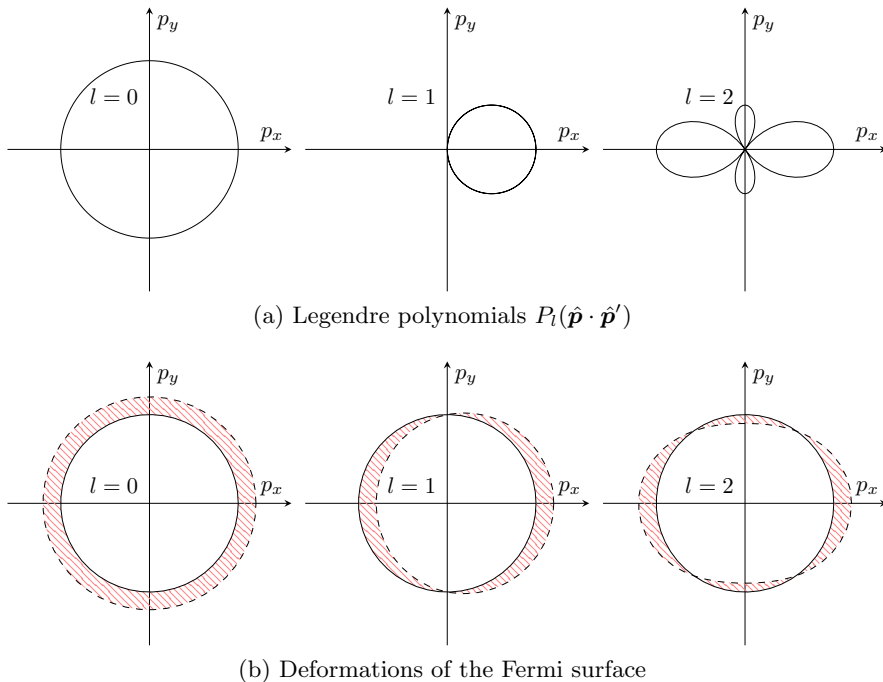
Figure 2.1: In (a) are shown the first three Legendre polynomials $P_l(\hat{\boldsymbol{p}} \cdot \hat{\boldsymbol{p}}')$, assuming that $\hat{\boldsymbol{p}}'$ is aligned with $\hat{\boldsymbol{x}}$. In (b), types of deformations of the Fermi surface corresponding to the different terms in the Legendre polynomial expansion in Eq. (2.17). The solid black line depicts the equilibrium Fermi surface, and the dashed line the deformed surface. The red hatching depicts the region where $\delta n_{\boldsymbol{p}} \neq 0$, which is exaggerated for clarity.

only on the relative directions of their momenta. This allows the expansion of the interaction energy as a series of Legendre polynomials, in terms of the two distributions $\phi_{\hat{\boldsymbol{p}}}$ and $\psi_{\hat{\boldsymbol{p}}}$, as

$$\delta\epsilon_{\hat{\boldsymbol{p}}} = \sum_{l=0}^{\infty} F_l^s \langle P_l(\hat{\boldsymbol{p}} \cdot \hat{\boldsymbol{p}}')\phi_{\hat{\boldsymbol{p}}'} \rangle_{\hat{\boldsymbol{p}}'} = \sum_{l=0}^{\infty} A_l^s \langle P_l(\hat{\boldsymbol{p}} \cdot \hat{\boldsymbol{p}}')\psi_{\hat{\boldsymbol{p}}'} \rangle_{\hat{\boldsymbol{p}}'}, \qquad (2.17)$$

where the two expansion coefficients are related by

$$A_l^s = \frac{F_l^s}{1 + F_l^s/(2l+1)}. \qquad (2.18)$$

The brackets $\langle \ldots \rangle_{\hat{\boldsymbol{p}}}$ denote averaging over momentum directions

$$\langle P_l(\hat{\boldsymbol{p}} \cdot \hat{\boldsymbol{p}}')\phi_{\hat{\boldsymbol{p}}'} \rangle_{\hat{\boldsymbol{p}}'} = \frac{1}{4\pi} \int P_l(\hat{\boldsymbol{p}} \cdot \hat{\boldsymbol{p}}')\phi_{\hat{\boldsymbol{p}}'} \, d\Omega_{\hat{\boldsymbol{p}}'}, \qquad (2.19)$$

where

$$\int d\Omega_{\hat{\boldsymbol{p}}} = \int_0^{2\pi} \int_0^{\pi} \sin\theta_p \, d\theta_p \, d\phi_p. \tag{2.20}$$

The *Landau parameters* F_l^s describe the strength of the quasiparticle interaction. Legendre polynomials are an orthogonal system of polynomials, which means that $\langle P_m(\hat{\boldsymbol{p}}\cdot\hat{\boldsymbol{p}}')P_n(\hat{\boldsymbol{p}}\cdot\hat{\boldsymbol{p}}')\rangle_{\hat{\boldsymbol{p}}} = 0$ if $m \neq n$. A function which is orthogonal to a given Legendre polynomial will not "survive" averaging over momentum direction $\langle\ldots\rangle_{\hat{\boldsymbol{p}}}$. The series expansion in Eq. (2.17) thus split $\phi_{\hat{\boldsymbol{p}}}$ and $\psi_{\hat{\boldsymbol{p}}}$ into components that are parallel with a given $P_l(\hat{\boldsymbol{p}}\cdot\hat{\boldsymbol{p}}')$. This is illustrated in Fig. 2.1.

The first symmetric Landau parameter F_1^s is related to the effective mass of quasiparticles as

$$\frac{m^*}{m} = 1 + \frac{F_1^s}{3}. \tag{2.21}$$

The origin of this relation is discussed in App. A. If $F_1^s > -3$, the effective mass is positive. This is a reasonable requirement. The value of effective mass can be extracted from specific heat measurements which show it to be pressure dependent. In this way, the Landau parameter F_1^s can and has been measured [21]. For example, at zero pressure $F_1^s = 5.4$. A similar relation can also be derived for the zeroth symmetric Landau parameter F_0^s which relates its value to the speed of first sound [22]. The antisymmetric Landau parameters F_0^a and F_1^a are dependent on magnetic susceptibility [22, 23] and spin diffusion [24], respectively. One motivation behind the study of zero sound is that it may allow the measurement of the higher Landau parameters, such as F_2^s.

2.1.3   Quasiparticle collisions

The term on the right side of the kinetic equation in Eq. (2.16) is called the collision integral. We approximate the collision integral by assuming that the gas of excited quasiparticles is rarefied enough that collisions only take place between two individual quasiparticles. In the same vein, we assume that the distributions of individual quasiparticles are uncorrelated, so that a multiparticle distribution can be represented by their product. Generally, for a sparse gas, the collision integral can be written as [25]

$$\begin{aligned} I_{\boldsymbol{p}_1} = -\int d\rho_1' d\rho_2 d\rho_2' \Big\{ &w(\boldsymbol{p}_1', \boldsymbol{p}_2'; \boldsymbol{p}_1, \boldsymbol{p}_2) f(\boldsymbol{p}_1) f(\boldsymbol{p}_2) \\ &- w(\boldsymbol{p}_1, \boldsymbol{p}_2; \boldsymbol{p}_1', \boldsymbol{p}_2') f(\boldsymbol{p}_1') f(\boldsymbol{p}_2') \Big\}. \end{aligned} \tag{2.22}$$

Function $f(\boldsymbol{p})$ is the distribution function and $d\rho_i = d^3p_i/(2\pi\hbar)^3$, a momentum space volume element. $w(\boldsymbol{p}_1', \boldsymbol{p}_2'; \boldsymbol{p}_1, \boldsymbol{p}_2)$ is the probability of a collision where particles with momenta $\boldsymbol{p}_1$ and $\boldsymbol{p}_2$ collide and end up with momenta $\boldsymbol{p}_1'$ and $\boldsymbol{p}_2'$. In our case we can assume that the principle of detailed balance holds, i.e.

$$w(\boldsymbol{p}_1', \boldsymbol{p}_2'; \boldsymbol{p}_1, \boldsymbol{p}_2) = w(\boldsymbol{p}_1, \boldsymbol{p}_2; \boldsymbol{p}_1', \boldsymbol{p}_2'). \tag{2.23}$$

Additionally, for fermions we have to require that the state a particle scatters into is empty. The collision integral can be written as

$$\begin{aligned} I_{\boldsymbol{p}_1} = &- \int d\rho_1' d\rho_2 d\rho_2' w(\boldsymbol{p}_1, \boldsymbol{p}_2; \boldsymbol{p}_1', \boldsymbol{p}_2') \\ &\times \left\{ f_1' f_2' (1 - f_1)(1 - f_2) - f_1 f_2 (1 - f_1')(1 - f_2') \right\}, \end{aligned} \tag{2.24}$$

where we have used shorthand notations $f_i = f(\boldsymbol{p}_i)$ and $f' = f(\boldsymbol{p}')$.

For practical purposes, the collision integral outlined above is too complicated. It does however inform on the form that other, approximate approaches can take. One such approach is the relaxation time approximation [19]

$$I_{\boldsymbol{p}} = -\frac{\delta n_{\boldsymbol{p}}^{\text{l.e.}}}{\tau}, \tag{2.25}$$

where $\delta n_{\boldsymbol{p}}^{\text{l.e.}}$ is the deviation from the local equilibrium distribution, and τ the relaxation time. This reflects the fact that a system of particles left to its own devices should spontaneously evolve towards an equilibrium state. Once this state is reached, the collision integral disappears.

What is the distribution $n_{\boldsymbol{p}}^{\text{l.e.}}$ where the system has reached equilibrium? An elastic collision between two particles should conserve particle number, momentum and kinetic energy [25]. Other conserved quantities can be written as a linear combination of these independent collision invariants. If φ is an additive conserved quantity carried by a particle, then in a collision of two particles

$$\varphi_1 + \varphi_2 = \varphi_1' + \varphi_2'. \tag{2.26}$$

In an equilibrium state, the entropy of the system, and the distribution function, should be constant, i.e. $dn_{\boldsymbol{p}}/dt = I_{\boldsymbol{p}} = 0$. This can be achieved by requiring that the term inside the curly brackets in Eq. (2.24) is zero. This in turn means that at equilibrium the quantity $\ln(f/(1-f))$ satisfies the conservation condition Eq. (2.26) and is thus a collision invariant. We may write it in terms of the other collision invariants [25]

$$\ln\left(\frac{f}{1-f}\right) = C \cdot 1 + \boldsymbol{B} \cdot \boldsymbol{p} + AE. \tag{2.27}$$

where f is the distribution where the collision integral disappears, i.e. the local equilibrium distribution, and C, $\boldsymbol{B}$, and A are constant to be determined later. By writing $A = 1/k_B T$, $\boldsymbol{b} = -\boldsymbol{B}/A$, and $c = -C/A$, the deviation from local equilibrium distribution can now be written

$$\delta n_{\boldsymbol{p}}^{\text{l.e.}} = n_{\boldsymbol{p}} - n^0(\epsilon_p^0 + \delta\epsilon_{\boldsymbol{p}} - c - \boldsymbol{b} \cdot \boldsymbol{p}), \tag{2.28}$$

where n^0 is the Fermi–Dirac distribution. Distribution $\delta n_{\boldsymbol{p}}^{\text{l.e.}}$ is the deviation from local equilibrium, $\delta\bar{n}_{\boldsymbol{p}}$, defined in conjuction with Eq. (2.13), but with chemical potential c and drift velocity $\boldsymbol{b}$. The energy integrated form of Eq. (2.28) is simply

$$\delta\psi_{\hat{\boldsymbol{p}}}^{\text{l.e.}} = \psi_{\hat{\boldsymbol{p}}} - c - \boldsymbol{b} \cdot \hat{\boldsymbol{p}}. \tag{2.29}$$

where we have defined $\delta\psi_{\hat{\boldsymbol{p}}}^{\text{l.e.}} = \int \delta n_{\boldsymbol{p}}^{\text{l.e.}} d\epsilon$. What is left is to determine the constants c and $\boldsymbol{b}$. This is done by ensuring that the collision integral

$$I_{\hat{\boldsymbol{p}}} = -\frac{\delta\psi_{\hat{\boldsymbol{p}}}^{\text{l.e.}}}{\tau}, \tag{2.30}$$

conserves particle number and momentum:

$$\int I_{\hat{\boldsymbol{p}}} d\rho = 0, \quad \int \boldsymbol{p} I_{\hat{\boldsymbol{p}}} d\rho = 0. \tag{2.31}$$

We find that $c = \langle\psi_{\hat{\boldsymbol{p}}'}\rangle_{\hat{\boldsymbol{p}}'}$ and $\boldsymbol{b} = 3\langle\hat{\boldsymbol{p}}'\psi_{\hat{\boldsymbol{p}}'}\rangle_{\hat{\boldsymbol{p}}'}$. By pre-emptively writing $\boldsymbol{b} \cdot \boldsymbol{p}$ in terms of a Legendre polynomial, Eq. (2.29) can be written as

$$\delta\psi_{\hat{\boldsymbol{p}}}^{\text{l.e.}} = \psi_{\hat{\boldsymbol{p}}} - \langle\psi_{\hat{\boldsymbol{p}}'}\rangle_{\hat{\boldsymbol{p}}'} - 3\langle P_1(\hat{\boldsymbol{p}} \cdot \hat{\boldsymbol{p}}')\psi_{\hat{\boldsymbol{p}}'}\rangle_{\hat{\boldsymbol{p}}'}. \tag{2.32}$$

We obtain a more general form by allowing the deviations from local equilibrium to relax at rates that depend on their angular behavior. This is achieved by expanding the collision integral in terms of spherical harmonics Y_{lm} as [19]

$$I_{\hat{\boldsymbol{p}}} = -4\pi \sum_{l=0}^{\infty} \sum_{m=-l}^{l} \frac{\langle\delta\psi_{\hat{\boldsymbol{p}}'}^{\text{l.e.}} Y_{lm}^*(\hat{\boldsymbol{p}}')\rangle_{\hat{\boldsymbol{p}}'}}{\tau_l} Y_{lm}(\hat{\boldsymbol{p}}). \tag{2.33}$$

We use a collision term in which the components of the above expansion with $l > 2$ have the same relaxation time τ. This is most easily done by adding to and subtracting from Eq. (2.33) a term similar to its right-hand side, but where τ_l is replaced by τ. With the help of a spherical harmonics closure relation, we can show that such a term is in fact equal

to the simpler relaxation time approximation Eq. (2.30). The collision integral may thus be written as

$$I_{\hat{\boldsymbol{p}}} = -\frac{\delta\psi_{\hat{\boldsymbol{p}}}^{\text{l.e.}}}{\tau} - \sum_{l=0}^{\infty}(2l+1)\left(\frac{1}{\tau_l} - \frac{1}{\tau}\right)\langle P_l(\hat{\boldsymbol{p}}\cdot\hat{\boldsymbol{p}}')\delta\psi_{\hat{\boldsymbol{p}}'}^{\text{l.e.}}\rangle_{\hat{\boldsymbol{p}}'}, \qquad (2.34)$$

where the relation

$$P_l(\hat{\boldsymbol{p}}\cdot\hat{\boldsymbol{p}}') = \frac{4\pi}{2l+1}\sum_{m=-l}^{l} Y_{lm}(\hat{\boldsymbol{p}})\,Y_{lm}^*(\hat{\boldsymbol{p}}'), \qquad (2.35)$$

has been used. All terms of the sum in Eq. (2.34) with $l > 2$ are zero by our requirement on the relaxation times $\tau_{l>2}$. Likewise, the terms $l = 0, 1$ can also be ignored by once again requiring that particle number and momentum are conserved. We are left with just the quadrupolar term $l = 2$, and consequently the collision integral can be written as

$$I_{\hat{\boldsymbol{p}}} = -\frac{1}{\tau}\left[\psi_{\hat{\boldsymbol{p}}} - \langle\psi_{\hat{\boldsymbol{p}}'}\rangle_{\hat{\boldsymbol{p}}'} - 3\langle P_1(\hat{\boldsymbol{p}}\cdot\hat{\boldsymbol{p}}')\psi_{\hat{\boldsymbol{p}}'}\rangle_{\hat{\boldsymbol{p}}'} - 5(\xi_2 - 1)\langle P_2(\hat{\boldsymbol{p}}\cdot\hat{\boldsymbol{p}}')\psi_{\hat{\boldsymbol{p}}'}\rangle_{\hat{\boldsymbol{p}}'}\right], \tag{2.36}$$

where $\xi_2 = \tau/\tau_2$.

2.2 Oscillating substrate

We will now use Eq. (2.16), the linearized Landau kinetic equation, to study the transmission of transverse sound through a film of Fermi liquid. The closely related problem of an infinite fluid layer was studied by Bekarevich and Khalatnikov [26], by Fomin [27, 28], by Flowers and Richardson [29], and by Richardson [30]. We reformulate the arguments presented in these papers in terms of the energy integrated distribution $\psi_{\hat{\boldsymbol{p}}}$ and with the modification that the fluid film have finite thickness.

Transverse sound waves are generated by an oscillating substrate in the xy plane, positioned at $z = 0$. The movement of the substrate is harmonic with velocity $\boldsymbol{u} = u\hat{\boldsymbol{x}}e^{-i\omega t}$. We assume that all points on the substrate are identical and that they oscillate in the same phase. The distribution of quasiparticles inherits this plane symmetry and depends spatially only on the z coordinate. We choose our coordinates so that the substrate oscillates along the x axis. This allows us to write the distribution function as

$$\psi_{\hat{\boldsymbol{p}}}(\boldsymbol{r}, t) = \hat{p}_x\psi(\hat{p}_z, \zeta, t), \tag{2.37}$$

where $\zeta = z/d$ is a dimensionless z coordinate, with d being the thickness of the fluid film. We have used notation $\hat{p}_x = \sin\theta\cos\phi$ and $\hat{p}_z = \cos\theta$

for the components of the momentum direction vector $\hat{\boldsymbol{p}}$, where θ is the quasiparticle propagation angle in the xz plane, measured from the positive z axis. Since $\psi_{\hat{\boldsymbol{p}}}$ is now antisymmetric with regard to $\hat{p}_x$, the zeroth-order term of the Legendre polynomial expansion can be written as

$$\langle P_0(\hat{\boldsymbol{p}} \cdot \hat{\boldsymbol{p}}')\psi_{\hat{\boldsymbol{p}}'}\rangle_{\hat{\boldsymbol{p}}'} = 0, \tag{2.38}$$

where $P_0(\hat{\boldsymbol{p}} \cdot \hat{\boldsymbol{p}}') = 1$. This is in fact a statement on the nature of transverse sound: For distribution Eq. (2.37), there is no net change in the volume of the Fermi sphere in comparison to the equilibrium state. This means that the density of particles is constant and transverse sound is thus not a density wave.

If we truncate the Legendre polynomial expansion of the quasiparticle energy in Eq. (2.17) to $l \leq 2$, the kinetic equation becomes

$$\frac{\partial}{\partial t}\left(\psi_{\hat{\boldsymbol{p}}} - \frac{F_1^s}{1 + F_1^s/3}\langle P_1(\hat{\boldsymbol{p}} \cdot \hat{\boldsymbol{p}}')\psi_{\hat{\boldsymbol{p}}'}\rangle_{\hat{\boldsymbol{p}}'} - \frac{F_2^s}{1 + F_2^s/5}\langle P_2(\hat{\boldsymbol{p}} \cdot \hat{\boldsymbol{p}}')\psi_{\hat{\boldsymbol{p}}'}\rangle_{\hat{\boldsymbol{p}}'}\right)$$

$$+ v_F \hat{\boldsymbol{p}} \cdot \nabla \psi_{\hat{\boldsymbol{p}}}$$

$$= -\frac{1}{\tau}\left[\psi_{\hat{\boldsymbol{p}}} - \langle\psi_{\hat{\boldsymbol{p}}'}\rangle_{\hat{\boldsymbol{p}}'} - 3\langle P_1(\hat{\boldsymbol{p}} \cdot \hat{\boldsymbol{p}}')\psi_{\hat{\boldsymbol{p}}'}\rangle_{\hat{\boldsymbol{p}}'} - 5(\xi_2 - 1)\langle P_2(\hat{\boldsymbol{p}} \cdot \hat{\boldsymbol{p}}')\psi_{\hat{\boldsymbol{p}}'}\rangle_{\hat{\boldsymbol{p}}'}\right]. \tag{2.39}$$

We assume that the time dependence of the quasiparticle distribution is harmonic as a result of the harmonic motion of the substrate. This is in accordance with assumptions we made in the context of linearizing the kinetic equation, that the quasiparticle distribution and energy deviate only minutely from their equilibrium values. The kinetic equation can now be rearranged as

$$\frac{\tau v_F}{a}\hat{\boldsymbol{p}} \cdot \boldsymbol{\nabla}\psi_{\hat{\boldsymbol{p}}} + \psi_{\hat{\boldsymbol{p}}} - 3b\langle P_1(\hat{\boldsymbol{p}} \cdot \hat{\boldsymbol{p}}')\psi_{\hat{\boldsymbol{p}}'}\rangle_{\hat{\boldsymbol{p}}'} - c\langle P_2(\hat{\boldsymbol{p}} \cdot \hat{\boldsymbol{p}}')\psi_{\hat{\boldsymbol{p}}'}\rangle_{\hat{\boldsymbol{p}}'} = 0, \tag{2.40}$$

where the following dimensionless constants have been used:

$$a = 1 - i\omega\tau, \tag{2.41}$$

$$b = \frac{1/a + F_1^s/3}{1 + F_1^s/3}, \tag{2.42}$$

$$c = \frac{5/2 + F_2^s}{1 + F_2^s/5} - \frac{5\xi_2}{a}. \tag{2.43}$$

We apply the definitions of the Legendre polynomials and find that the two averages in the kinetic equation may be written as

$$\langle P_1(\hat{\boldsymbol{p}} \cdot \hat{\boldsymbol{p}}')\psi_{\hat{\boldsymbol{p}}'}\rangle_{\hat{\boldsymbol{p}}'} = \frac{1}{4}\hat{p}_x g_1(\zeta), \tag{2.44}$$

$$\langle P_2(\hat{\boldsymbol{p}} \cdot \hat{\boldsymbol{p}}')\psi_{\hat{\boldsymbol{p}}'}\rangle_{\hat{\boldsymbol{p}}'} = \frac{3}{4}\hat{p}_x \hat{p}_z g_2(\zeta), \tag{2.45}$$

where

$$g_1(\zeta) = \int_{-1}^{1} d\mu(1 - \mu^2)\psi(\mu, \zeta), \tag{2.46}$$

$$g_2(\zeta) = \int_{-1}^{1} d\mu\mu(1 - \mu^2)\psi(\mu, \zeta). \tag{2.47}$$

Here $\mu = p_z = \cos\theta$. Using $\psi_{\hat{p}}$ of the form given in Eq. (2.37) and the definition $\zeta = z/d$, we obtain for the first term in the kinetic equation

$$\hat{\boldsymbol{p}} \cdot \boldsymbol{\nabla}\psi_{\hat{\boldsymbol{p}}} = \frac{\hat{p}_z\hat{p}_x}{d} \frac{\partial}{\partial\zeta}\psi(\hat{p}_z, \zeta). \tag{2.48}$$

The whole kinetic equation can be written as

$$\frac{\mu}{h} \frac{\partial}{\partial\zeta}\psi(\mu, \zeta) + \psi(\mu, \zeta) - \frac{3}{4}bg_1(\zeta) - \frac{3}{4}c\mu g_2(\zeta) = 0. \tag{2.49}$$

We have defined a dimensionless complex-valued coefficient

$$h = \frac{ad}{v_F\tau} = \frac{d}{l\xi_2} - i\Omega(1 + F_1^s/3), \tag{2.50}$$

where $l = v_F\tau_2$ is the mean free path of the quasiparticles and $\Omega = \omega d/v_F(1 + F_1^s/3)$. We integrate the kinetic equation from ζ_0 to ζ and obtain

$$\psi(\mu, \zeta) = \psi(\mu, \zeta_0)e^{\frac{h}{\mu}(\zeta_0 - \zeta)} + \frac{3}{4}\frac{h}{\mu}\int_{\zeta_0}^{\zeta} e^{\frac{h}{\mu}(\zeta' - \zeta)} \left[bg_1(\zeta') + c\mu g_2(\zeta')\right] d\zeta'. \tag{2.51}$$

This form shows that the coefficient h/μ is a complex wavenumber. The real part of h leads to an attenuation of the sound wave as it travels through the liquid. The attenuation is decreased for large values of the mean-free path l. The factor μ ensures that sound moving in a more oblique direction travels a longer distance in a given space $\delta\zeta$ than sound moving directly in the direction normal to the substrate. The imaginary part of h produces the oscillations of the sound wave.

Eq. (2.51) can be used to calculate ψ in the direction of particle propagation, so that for positive μ the particle moves in the direction of increasing ζ, and for negative μ in the direction of decreasing ζ.

2.2.1 Observable quantities

In order to make comparisons with experiments, we derive relations between distribution functions, such as $\delta n_{\hat{p}}$, and observable quantities.

This is done using the linearized kinetic equation by making comparisons to hydrodynamic conservation laws [1, 31]. We start from Eq. (2.13):

$$\frac{\partial \delta n_{\boldsymbol{p}}}{\partial t} + \boldsymbol{v_p} \cdot \boldsymbol{\nabla} \delta \bar{n}_{\boldsymbol{p}} = I_{\hat{\boldsymbol{p}}}. \tag{2.52}$$

Multiplying with the particle mass m and summing over momentum and spin states leads to the law of mass conservation

$$\frac{\partial \delta \rho}{\partial t} + m \boldsymbol{\nabla} \cdot \sum_{\boldsymbol{p}\sigma} \boldsymbol{v_p} \delta \bar{n}_{\boldsymbol{p}} = 0, \tag{2.53}$$

where $\delta \rho = m \sum_{\boldsymbol{p}\sigma} \delta n_{\boldsymbol{p}}$ is the mass density fluctuation. The right side is zero since collisions conserve particle number. Comparing to $\frac{\partial \rho}{\partial t} + \boldsymbol{\nabla} \cdot \boldsymbol{J} = 0$ one can identify the mass current

$$\boldsymbol{J} = m \sum_{\boldsymbol{p}\sigma} \boldsymbol{v_p} \delta \bar{n}_{\boldsymbol{p}} = \frac{m p_F^2}{\pi^2 \hbar^3} \langle \hat{\boldsymbol{p}} \psi_{\hat{\boldsymbol{p}}} \rangle_{\hat{\boldsymbol{p}}}, \tag{2.54}$$

where in the latter form we have once again assumed that the excitations are on the Fermi surface. The x component of mass current can be conveniently expressed in terms of the integral defined in Eq. (2.46) as

$$J_x = \frac{3}{4} m n p_F g_1(\zeta). \tag{2.55}$$

Similarly, multiplying the kinetic equation with momentum $\boldsymbol{p}$, summing over momentum and spin states and making comparison to the law of momentum conservation, $\frac{\partial \delta \boldsymbol{g}}{\partial t} + \boldsymbol{\nabla} \cdot \overset{\leftrightarrow}{\boldsymbol{\Pi}} = 0$, where $\delta \boldsymbol{g} = \sum_{\boldsymbol{p}\sigma} \boldsymbol{p} \delta n_{\boldsymbol{p}}$ is the momentum density fluctuation, allows us to identify the stress tensor $\overset{\leftrightarrow}{\boldsymbol{\Pi}}$, the components of which are given by

$$\overset{\leftrightarrow}{\Pi}_{ij} = \sum_{\boldsymbol{p}\sigma} p_i v_j \delta \bar{n}_{\boldsymbol{p}} = 3n \langle \hat{p}_i \hat{p}_j \psi_{\hat{\boldsymbol{p}}} \rangle_{\hat{\boldsymbol{p}}}, \tag{2.56}$$

where $n = p_F^3/(3\pi^2 \hbar^3)$ is the number density of particles.

The oscillating substrate is oriented with its surface normal pointing in the z direction. The shear force acting in the x direction is given by the xz-component of the stress tensor:

$$\overset{\leftrightarrow}{\Pi}_{xz} = 3n \langle \hat{p}_x \hat{p}_z \psi_{\hat{\boldsymbol{p}}} \rangle_{\hat{\boldsymbol{p}}} = \frac{3}{4} n g_2(\zeta), \tag{2.57}$$

where in the last equality Eq. (2.47) has been used.

The *transverse acoustic impedance* Z is related to the stress tensor by

$$Z = \overset{\leftrightarrow}{\Pi}_{xz}(\zeta = 0)/u, \tag{2.58}$$

where u is the oscillation amplitude of the substrate. As a consequence of having written the time-dependence of the substrate velocity in the complex form, $u \propto \exp(-i\omega t)$, the resulting acoustic impedance is also complex valued, $Z = Z' + iZ''$, where Z' is the *acoustic resistance* and Z'' the *acoustic reactance*. The force on the substrate can be written in terms of only real quantities as

$$\overset{\leftrightarrow}{\Pi}_{xz} = (Z + iZ'')u = Z'u + \frac{Z''\dot{u}}{\omega}. \tag{2.59}$$

The force proportional to acceleration is conservative and so only the resistive part of the impedance leads to energy dissipation. The reactive part can be understood to describe the portion of fluid moving in phase with the oscillating substrate.

2.2.2 Boundary conditions

In order to solve the equations of motion, Eqs. (2.51), (2.46) and (2.47), we need a way of describing the scattering of quasiparticles from the boundaries confining the Fermi liquid. These *boundary conditions* must be formulated in terms of the distribution function $\psi_{\hat{\boldsymbol{p}}}$. The boundary conditions are of central importance, since it is through them that momentum transfer between the fluid and the oscillating substrate takes place.

Arguably the most basic model for surface scattering is that of *specular*, i.e. mirror-like, reflection. The component of the reflected particle's momentum parallel to the surface is conserved while the component normal to the surface changes sign. This may be expressed as $\boldsymbol{p}_R = \boldsymbol{p} - 2\hat{\boldsymbol{n}}(\boldsymbol{p} \cdot \hat{\boldsymbol{n}})$, where $\boldsymbol{p}$ and $\boldsymbol{p}_R$ are the momenta of the particle before and after the reflection, respectively. The distributions of incoming and outgoing particles are related simply by

$$\psi_{\boldsymbol{p}_R} = \psi_{\boldsymbol{p}}. \tag{2.60}$$

In the case of the liquid film, the surface normals at the boundaries of the film point in the positive and negative z directions. For distribution $\psi_{\hat{\boldsymbol{p}}} = \hat{p}_x \psi(\hat{p}_z, \zeta)$ we obtain the specular boundary conditions

$$\psi(\mu < 0, \zeta = 1) = \psi(-\mu, \zeta = 1), \tag{2.61}$$
$$\psi(\mu > 0, \zeta = 0) = \psi(-\mu, \zeta = 0), \tag{2.62}$$

where $\mu = \hat{p}_z = \cos\theta$.

The problem with specular scattering is that there is no transfer of transverse momentum between the confining walls and the quasiparticles. This in turn means complete decoupling of the fluid from the substrate and no measured transverse impedance. Thus, specular scattering alone is not sufficient.

Another simple model for surface reflection is that of *diffuse* reflection. We may imagine that instead of being smooth and mirror-like, at microscopic scale the surface of an object consists of tiny microfacets that are oriented randomly with respect to the macroscopic surface normal. Particles hitting this rough surface are thus reflected in a random direction.

In terms of the quasiparticle distribution function, such randomization of propagation direction means that the distribution becomes isotropic. Since all quasiparticles are on the Fermi surface and have momentum magnitude p_F, the distribution of quasiparticles following a diffuse reflection is the local equilibrium distribution. For transverse oscillations, where the volume of the Fermi surface does not change, it follows that $\delta n_{\boldsymbol{p}} = \delta\bar{n}_{\boldsymbol{p}} = 0$ and as a result $\psi_{\hat{\boldsymbol{p}}} = 0$. The boundary condition for diffuse reflection at a stationary wall is given by

$$\psi_{\hat{\boldsymbol{p}}_{\text{out}}} = 0, \tag{2.63}$$

where $\hat{\boldsymbol{p}}_{\text{out}}$ signifies that the particles are traveling out from the scattering surface.

If the wall is moving, we can derive the corresponding diffuse boundary condition by considering the situation in the laboratory frame and in the rest frame of the moving wall. Since in the rest frame the reflected quasiparticles are at local equilibrium, we can write the distribution in the laboratory frame (to first order) as

$$n_{\boldsymbol{p}} = n^0(\epsilon_p^0 + \delta\epsilon_{\boldsymbol{p}} - \boldsymbol{p}\cdot\boldsymbol{u}) \approx n^0(\epsilon_p^0) + \frac{\partial n^0}{\partial\epsilon_p}(\delta\epsilon_{\boldsymbol{p}} - \boldsymbol{p}\cdot\boldsymbol{u}). \tag{2.64}$$

By writing $\delta n_{\boldsymbol{p}} = n_{\boldsymbol{p}} - n^0(\epsilon_p^0)$, this may be rearranged as

$$\delta n_{\boldsymbol{p}} - \frac{\partial n_p^0}{\partial\epsilon_p}\delta\epsilon_{\boldsymbol{p}} = -\frac{\partial n_p^0}{\partial\epsilon_p}\boldsymbol{p}\cdot\boldsymbol{u}. \tag{2.65}$$

On the left side we have $\delta\bar{n}_{\boldsymbol{p}}$, deviation from local equilibrium. Definition of $\psi_{\hat{\boldsymbol{p}}}$ in Eq. (2.15) gives

$$\psi_{\hat{\boldsymbol{p}}_{\text{out}}} = p_F\hat{\boldsymbol{p}}\cdot\boldsymbol{u}. \tag{2.66}$$

If we substitute $\psi_{\hat{\boldsymbol{p}}} = \hat{p}_x \psi(\hat{p}_z, \zeta)$ and $\boldsymbol{u} = u\hat{\boldsymbol{x}}$, the boundary condition at a diffusely reflecting moving wall becomes

$$\psi(\hat{p}_z > 0, \zeta) = p_F u. \tag{2.67}$$

The fluid is confined by two boundaries; the oscillating substrate at $\zeta = 0$ and the surface of the fluid film at $\zeta = d$. We form more general boundary conditions at each boundary by combining specular and diffuse scattering. We do this by introducing mixing parameters s_1 and s_2 that describe the specularity of the surfaces. We write

$$\psi(\mu < 0, \zeta = 1) = s_2 \psi(-\mu, \zeta = 1), \tag{2.68}$$

$$\psi(\mu > 0, \zeta = 0) = s_1 \psi(-\mu, \zeta = 0) + (1 - s_1) p_F u. \tag{2.69}$$

These boundary conditions describe a sharp specular highlight combined with a diffuse background.

It is obvious that if the surface of a real object is in fact made up of microfacets, then these are not actually oriented completely randomly. Instead, the microfacets will have a tendency to point somewhat in the direction of the macroscopic surface normal. Scattering from this surface could be simulated by broadening the specular highlight to have some finite width. A detailed discussion of this more realistic boundary condition is given in Pub. II.

2.3 Numerical implementation

In this section we outline the process of numerically solving the quasi-particle kinetic equation. The numerical method consists of forming and solving discrete versions of Eqs. (2.51), (2.46) and (2.47) using linear algebra. We begin with nondimensionalization of the relevant quantities.

We see from the boundary condition in Eq. (2.67) that the distribution ψ in Eq. (2.51) and, by extension, distributions g_1 in Eq. (2.46) and g_2 in Eq. (2.47) are proportional to $p_F u$. We can define their dimensionless counterparts,

$$\psi^e = \frac{\psi}{p_F u}, \quad g_1^e = \frac{g_1}{p_F u}, \quad g_2^e = \frac{g_2}{p_F u}. \tag{2.70}$$

In the following the superscript e will be omitted.

The steps taken in the previous chapters have reduced the problem of the oscillating substrate into the two-dimensional phase-space determined by the coordinates $\mu = \cos\theta$, the transverse component of momentum, and ζ, the distance from the oscillating substrate. Integration over μ in Eqs. (2.46) and (2.47) is done using a simple quadrature as
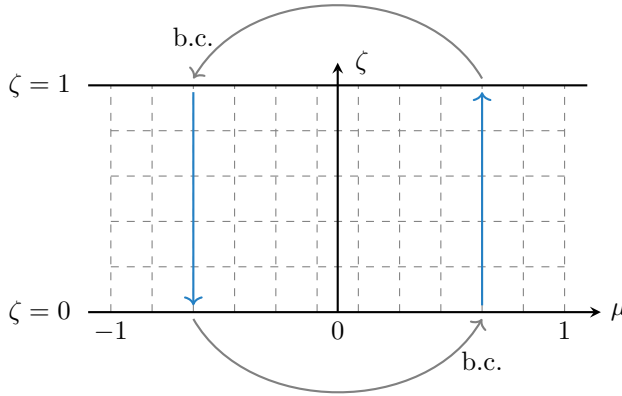
Figure 2.2: A schematic of the computational lattice. Lattice points are placed at the intersections of the dashed lines. Blue arrows show the direction of particle propagation and the gray arrows indicate how the boundary condition (b.c.) is applied.

$$\int_{-1}^{1} f(\mu)d\mu \approx \sum_{i=1}^{m} w_i f(\mu_i). \tag{2.71}$$

Weights w_i and abscissae μ_i are selected using either Gaussian quadrature or the trapezoidal method. An even number of m is used in order to avoid the propagation direction parallel to the substrate, as this direction could require special consideration.

The integral over ζ appearing in Eq. (2.51) is of the form

$$I = \int_{x_1}^{x_2} e^{\alpha x} f(x)dx, \tag{2.72}$$

where α is a complex number. The exponential part of the integrand is potentially rapidly oscillating. If the non-exponential part is linear over some short interval $[x_1, x_2]$, by applying partial integration we obtain

$$\int_{x_1}^{x_2} e^{\alpha x} f(x)dx \approx w_1 f(x_1) + w_2 f(x_2),$$
$$w_1 = \frac{e^{\alpha x_2}}{\alpha^2(x_2 - x_1)}[1 - (1 + \alpha(x_2 - x_1))e^{\alpha(x_1 - x_2)}], \tag{2.73}$$
$$w_2 = \frac{e^{\alpha x_1}}{\alpha^2(x_2 - x_1)}[1 - (1 - \alpha(x_2 - x_1))e^{\alpha(x_2 - x_1)}].$$

which is exact for $f(x) = a + bx$. We split the ζ axis into n points and use

Eq. (2.51) with the above integration formula to calculate the relation between each pair of adjacent points.

The lattice resulting from the above discretization is shown in Fig. 2.2. At each point in this lattice we have a value $\psi(\mu_i, \zeta_j)$ and at each distance ζ_j we have values $g_1(\zeta_j)$ and $g_2(\zeta_j)$. We may write all these values into a single vector in the following manner:

$$\boldsymbol{\Psi} = (\psi(\mu_1, \zeta_1), \ldots, \psi(\mu_m, \zeta_n); g_1(\zeta_1) \ldots, g_1(\zeta_n); g_2(\zeta_1), \ldots, g_2(\zeta_n)). \tag{2.74}$$

The length of this vector is $d = mn + 2m$. If the integrals in Eqs. (2.46), (2.47) and (2.51) are discretized according to the above scheme, they produce a network of linear dependencies between distributions evaluated at different grid points, which may be represented by a matrix D of dimension $d \times d$. Matrix D is a sparse matrix with $7mn - 4m$ potentially non-zero elements. If we take some values we call $\boldsymbol{\Psi}^{\text{old}}$, we may use D to calculate a new set of values $\boldsymbol{\Psi}^{\text{new}}$ as

$$\boldsymbol{\Psi}^{\text{new}} = D\boldsymbol{\Psi}^{\text{old}} + B, \tag{2.75}$$

where vector B is a result of the boundary condition at the oscillating substrate. If we search for a steady state solution, we may write $\boldsymbol{\Psi}^{\text{new}} = \boldsymbol{\Psi}^{\text{old}} = \boldsymbol{\Psi}$. We solve $\boldsymbol{\Psi}$ and obtain

$$\boldsymbol{\Psi} = (I - D)^{-1}B. \tag{2.76}$$

This equation is used to solve $\boldsymbol{\Psi}$ by calculating the inverse of $(I - D)$.

2.3.1 Limiting Cases

In this section we study three limiting cases in which the acoustic impedance of the fluid film can be calculated analytically. We expect for example that at high temperatures the Fermi liquid should behave like a classical viscous fluid, and that the results of the general theory should be in agreement with those derived from hydrodynamics. In the first two limiting cases, *damped mechanical oscillator* and *hydrodynamic limit*, the acoustic impedance is derived in a manner that is divorced from that of the general theory, and as such serves to test both the validity of the theory itself as well as the numerical process. The *ballistic gas limit* is the only limiting case derived directly from the general theory.

Damped mechanical oscillator

Under certain conditions the entire fluid film could move as a solid mass, with all parts of the film in phase with each other. A simple mechanical

analogy to this would be a moving wall attached to a mass m via a damping element. We now calculate the mechanical impedance of such a system.

We mark the positions of the wall and mass with s and x respectively, and the extension of the damping element with s_d. We thus have $x = s + s_d$. If the wall is moved, the mass experiences an accelerating force through the damping element and, therefore, the associated forces must be equal, i.e.

$$F = m\ddot{x} = -b\dot{s}_d. \tag{2.77}$$

where b describes the strength of the damping. Assuming the motion is harmonic, the velocity of the moving wall can be written as

$$u = \dot{s} = \frac{d}{dt}(x - s_d) = \left(\frac{1}{i\omega m} + \frac{1}{b}\right)F. \tag{2.78}$$

One can identify the impedance Z from $Z = F/u$. By setting $b = m/\tau$ we get

$$Z = \frac{1}{\frac{i}{m\omega} + \frac{\tau}{m}} = \frac{m\omega}{i + \omega\tau}. \tag{2.79}$$

We may write the real and imaginary parts of Z separately as

$$\mathcal{R}(Z) = Z' = \frac{m\omega^2\tau}{1 + (\omega\tau)^2}, \quad \mathcal{I}(Z) = Z'' = \frac{m\omega}{1 + (\omega\tau)^2}. \tag{2.80}$$

Clearly it is possible for the fluid to move as a solid mass only if the oscillation frequency is small enough. The oscillation wave length must be many times greater than the thickness of the fluid film for all parts of the film to be in phase.

Hydrodynamic limit

It is informative to compare the motion of a Fermi liquid to that of an ordinary liquid. In hydrodynamic theory, the equation of motion governing the dynamics of a viscous fluid is the Navier-Stokes equation. For an incompressible Newtonian fluid it may be written as [31]

$$\rho\frac{\partial \boldsymbol{v}}{\partial t} = \rho\boldsymbol{f} - \boldsymbol{\nabla}p + \mu\nabla^2\boldsymbol{v}, \tag{2.81}$$

where ρ is the density of the liquid, $\boldsymbol{f}$ describes the external forces the fluid is subject to, p is the pressure, and μ is the viscosity. In our case there are no external forces. In addition, there is no pressure gradient in the z direction. By denoting $v_x = v$, the x component of Eq. (2.81) is

$$\frac{\partial v}{\partial t} = \nu\frac{\partial^2 v}{\partial z^2}, \tag{2.82}$$

where $\nu = \mu/\rho$ is the kinematic viscocity.

The system is translationally invariant in the xy plane. The velocity of the substrate is given by $\boldsymbol{u} = \hat{\boldsymbol{x}}ue^{-i\omega t}$. We expect the fluid velocity to only depend on time and the z coordinate, and be aligned with the motion of the substrate. We write

$$\boldsymbol{v}(z,t) = \hat{\boldsymbol{x}}ue^{-i\omega t}v(z). \tag{2.83}$$

On the surface of the oscillating substrate, the fluid should move along with the oscillations and thus have the same velocity as the substrate. The top surface of the fluid is at distance d from the substrate and should be a free surface. We thus have the boundary conditions

$$v(z=0) = 1, \qquad \frac{\partial v(z)}{\partial z}\bigg|_{z=d} = 0. \tag{2.84}$$

Using the above ansatz and the boundary conditions to solve Eq. (2.81), we obtain

$$v(z) = \frac{e^{(1-i)z/\delta}}{1 + e^{2(1-i)d/\delta}} + \frac{e^{-(1-i)z/\delta}}{1 + e^{2(1-i)d/\delta}}e^{2(1-i)d/\delta}, \tag{2.85}$$

where $\delta = \sqrt{2\nu/\omega}$ is the viscous penetration depth.

In order to calculate the acoustic impedance, we first solve the viscous force caused by the fluid on the oscillating substrate. This is given by the stress tensor σ_{ij} as

$$\begin{aligned} F = -\sigma_{xz} &= -\mu\frac{\partial v_x}{\partial z} = -\mu ue^{-i\omega t}\frac{\partial v(z)}{\partial z} \\ &= -\mu ue^{-i\omega t}\frac{1-i}{\delta}\left(\frac{e^{(1-i)z/\delta}}{1 + e^{2(1-i)d/\delta}} - \frac{e^{-(1-i)z/\delta}}{1 + e^{2(1-i)d/\delta}}e^{2(1-i)d/\delta}\right). \end{aligned} \tag{2.86}$$

On the surface of the substrate we obtain

$$F(z=0) = \frac{\mu u}{\delta}(1-i)\frac{1 - e^{-2(1-i)d/\delta}}{1 + e^{-2(1-i)d/\delta}}e^{-i\omega t}. \tag{2.87}$$

Since $\frac{\mu}{\delta} = \frac{\rho\omega\delta}{2}$, the impedance can be written as

$$Z = \frac{F}{u} = \frac{\rho\omega\delta}{2}(1-i)\frac{1 - e^{-2(1-i)d/\delta}}{1 + e^{-2(1-i)d/\delta}} \tag{2.88}$$

Using the parameters of the general theory, the viscous penetration depth can be expressed as:

$$\delta = \sqrt{\frac{2\mu}{\rho\omega}} = \sqrt{\frac{2v_F^2\tau}{5\omega\xi_2}(1 + F_1^s/3)} = d\sqrt{\frac{2l}{5\Omega d}}. \tag{2.89}$$

Ballistic gas limit

At the limit of low temperature, quasiparticle collisions become increasingly rare to a point where they can be ignored. This is the domain of zero sound, where the mean free path of the quasiparticles is infinite, $l/d \to \infty$. However, this alone does not lead to any major simplification of the general theory. The equations of motion, Eqs. (2.46), (2.47) and (2.51), still have to be solved numerically. If in addition we remove the Fermi liquid interactions by setting parameters F_1^s and F_2^s to zero, the coefficients b and c become zero and Eq. (2.51) reduces to

$$\psi(\mu, \zeta) = \psi(\mu, \zeta_0) e^{\frac{h}{\mu}(\zeta_0 - \zeta)}. \tag{2.90}$$

If there are no collisions and no Fermi liquid interactions, the distribution of particles traveling out from either fluid boundary is unatteuated during the journey through the fluid film, and changes only by a phase factor. We may use the above equation to relate the distribution on the fluid surface to that on the oscillating substrate directly by setting $\zeta_0 = 0$ and $\zeta = d$, or vice versa. By also employing the boundary conditions

$$\psi(\mu < 0, \zeta = 1) = s_2 \psi(-\mu, \zeta = 1), \tag{2.91}$$

$$\psi(\mu > 0, \zeta = 0) = s_1 \psi(-\mu, \zeta = 0) + 1 - s_1, \tag{2.92}$$

we complete a rectangular loop in (μ, ζ)-space, as indicated in Fig. 2.2, and solve $\psi(\mu, \zeta)$. We obtain

$$\mu > 0 : \psi(\mu, 0) = \frac{1 - s_1}{1 - s_1 s_2 e^{-2h/\mu}}, \tag{2.93}$$

$$\mu < 0 : \psi(\mu, 0) = \frac{s_2(1 - s_1)e^{2h/\mu}}{1 - s_1 s_2 e^{-2h/\mu}}. \tag{2.94}$$

At the ballistic gas limit we have simply $h = -i\Omega$. Here, we use Eqs. (2.47), (2.57) and (2.58) to express the acoustic impedance:

$$Z = \frac{3}{4} n p_F (1 - s_1) \int_0^1 d\mu \mu (1 - \mu^2) \frac{1 - s_2 e^{2i\Omega/\mu}}{1 - s_1 s_2 e^{2i\Omega/\mu}}. \tag{2.95}$$

If using the ballistic gas limit, we set $s_1 = 0$ and $s_2 = 1$, corresponding to a fully diffuse oscillating substrate and a free fluid surface, which allows an analytical calculation of the above integral.

2.3.2   Results

Here, we present some results of the numerical calculations outlined in the previous sections. The acoustic impedance $Z = Z' + iZ''$ is calculated using the dimensionless mean free path l/d as an independent

variable, while keeping other parameters constant. We display the real and imaginary parts of the impedance separately as functions of l/d and together in a parametric representation. We express the distributions ψ, g_1 and g_2 in the units of $p_F u$. Based on Eq. (2.56), the corresponding dimensionless units for the acoustic impedance are $p_F n$. It is also useful to give acoustic impedance in other dimensionless units, $p_F n \Omega$.

The calculation depends on multiple different parameters, such as the Landau parameters F_1^s and F_2^s. The value of F_1^s is pressure dependent and well known through experiments [21]. The experimentally most important values are at zero pressure where $F_1^s = 5.4$, and at the minimum melting pressure of solid ^{3}He, i.e. at 29.3 bar, where $F_1^s = 13.3$. The value of F_2^s is not know, but is thought to have values that range between -1 and 1, based on longitudinal sound measurements [32]. The specularity of the surfaces that confine the film of Fermi liquid are controlled by parameters s_1 for the oscillating substrate and s_2 for the surface of the fluid. Both of them take values in the range $0 \leq s_i \leq 1$. Lastly, we have the dimensionless substrate oscillation frequency Ω and the relaxation time parameter ξ_2. For the latter we will use either $\xi_2 = 1$ or the estimation $\xi_2 \approx 0.35$ given in Ref. [29].

We can make some preliminary observations on the effects of some parameters. From the equation of motion in Eq. (2.39) we find that setting $F_1^s = 0$ removes the dipolar term from the quasiparticle interaction energy. Setting $F_2^s = 0$ on the other hand removes the quadrupolar component of the quasiparticle interaction energy, while conversely setting $\xi_2 = 1$ removes the corresponding term from the collision integral. Setting $s_1 = 1$ should decouple the fluid film from the oscillating substrate completely.

One requirement for the propagation of zero sound is that the sound velocity should be greater than the Fermi velocity v_F, as otherwise there will be a resonant transfer of energy between the sound wave and the quasiparticles, which leads to damping of the sound wave. This requirement can be stated as [33]

$$F_1^s + \frac{3F_2^s}{1 + F_2^s/5} > 6. \qquad (2.96)$$

In Fig. 2.3 the numerically obtained acoustic impedance is shown in a parametric representation for a small oscillation frequency, $\Omega = 0.01$, together with various analytically obtained limiting cases. We show data for different values of F_1^s, F_2^s and s_1. We first discuss the limiting cases. At the origin, the fluid film is completely decoupled from the oscillating substrate and $Z \equiv 0$. This is called the *stationary film limit*. At the end of the $Z''/p_F n \Omega$ axis, where $Z/p_F n \Omega = -i$, we have the *rigid body limit*
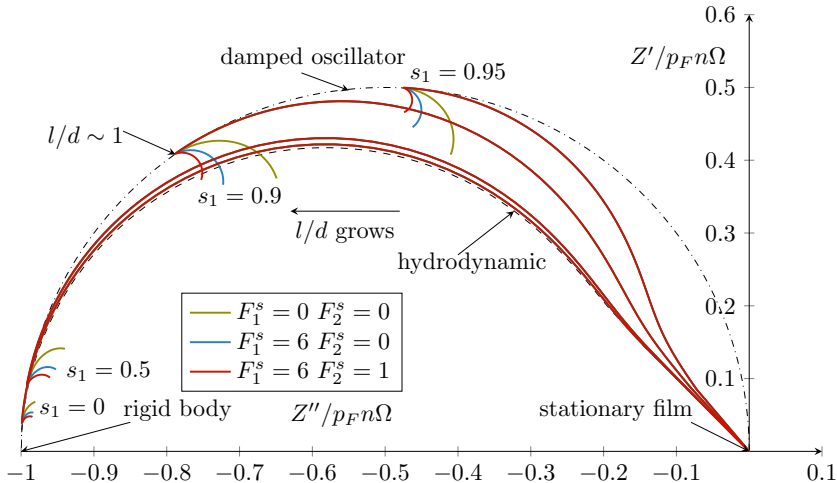
Figure 2.3: Parametric plot of $Z = Z' + iZ''$ with parameter l/d, which takes values in the range $[10^{-3}, 10^3]$. The oscillation frequency is small, $\Omega = 0.01$. Curves with different values of the Landau liquid parameters F_1^s and F_2^s, and the substrate specularity parameter s_1 are shown. $\xi_2 = 0.35$. Various limiting cases are also shown. Figure first published in Pub. I.

where the entire fluid film moves in phase with the oscillating substrate. With increasing l/d, the fluid initially follows hydrodynamic behavior, regardless of the parameters used. Plots with small values of s_1 adhere to the hydrodynamic limit for almost their entire length, while those with high values of s_1 deviate fairly quickly. At the point where $l/d \approx 1$, the propagation of any kind of transverse oscillation through the film is impossible, and the film instead behaves like a dissipative mass. At this point, the data coincides with the behavior of a damped oscillator. For large values of the mean free path, as we approach the ballistic regime where $l/d \gg 1$, we begin to see the influence of the Landau parameters.

In Fig. 2.3, the effect of substrate specularity is studied. We find that increasing s_1 can amplify the effect of the Landau parameters F_1^s and F_2^s to a degree. As specularity is increased, the film begins to decouple from the substrate. Since Z'' can be interpreted as signifying the portion of the fluid moving along with the substrate oscillations, we find that if $s_1 = 0.95$, roughly half of the fluid has decoupled from the substrate. Up to this point, decoupling increases the value of Z', leading to greater dissipation. While we have not drawn plots with $s_1 > 0.95$, we can infer that if the substrate specularity was increased further, the impedance plots would "shrink" towards the origin until finally the film
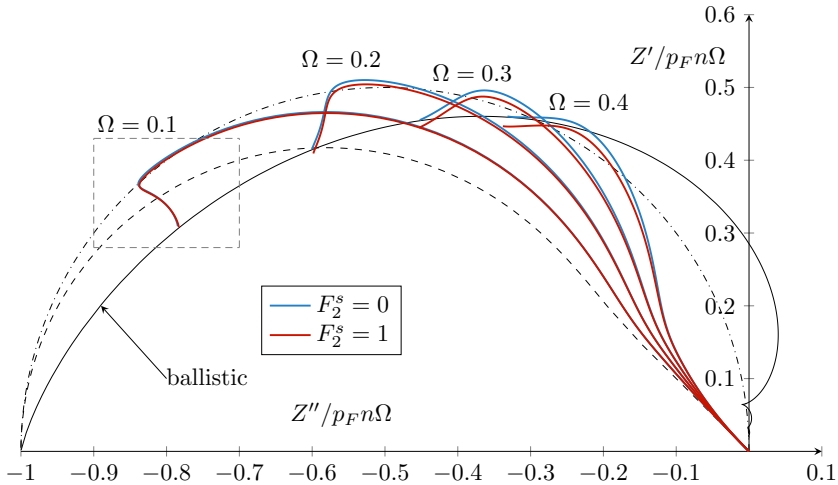
Figure 2.4: Parametric plot of $Z = Z' + iZ''$ with parameter l/d, which takes values in the range $[10^{-3}, 10^3]$. The effect of F_2^s is studied at different oscillation frequencies, if $F_1^s = 0$, $\xi_2 = 1$, $s_1 = 0$ and $s_2 = 1$. The ballistic limit is also shown. The area inside the dashed rectangle is studied in more detail in Fig. 2.5.

decouples completely. Most importantly, we find that the scale of the effects of the Landau parameters are orders of magnitude smaller than the effect of s_1, and do not lead to any significant decoupling of the fluid film, unlike s_1. Experiments reported in Refs. [16, 17], using an experimental setup corresponding to $\Omega \sim 10^{-5}$, show a thin film of normal ^{3}He decoupling from a mechanical oscillator as the temperature is lowered. In Fig. 2.3, the larger frequency of $\Omega = 10^{-3}$ is used, but there is no qualitative difference between this and smaller frequencies. In Fig. 2.3, the decoupling would correspond to a large reduction in impedance when $l/d \gg 1$. We do not see this, and thus our model cannot account for the experimentally observed decoupling in the ballistic region.

In Fig. 2.4 we show the acoustic impedance at different frequencies and with two different values of F_2^s, while keeping $F_1^s = 0$ and $\xi_2 = 1$. We have used specularity $s_1 = 0$ and $s_2 = 1$. The ballistic limit is also shown, since the plots with $F_1^s = F_2^s = 0$ use the same parameters as those used to calculate the ballistic limit in Sec. 2.3.1 and thus end on this limit. Only the $\Omega = 0.1$ curve really coincides with the damped oscillator limit if $l/d \approx 1$. This is to be expected, since at higher frequencies, the thickness of the fluid film is greater than the wavelength of the oscillations and it is thus impossible for the film to move as as solid mass. We find that in isolation, i.e. with $F_1^s = 0$ and $\xi_2 = 1$, the effect of F_2^s disappears with
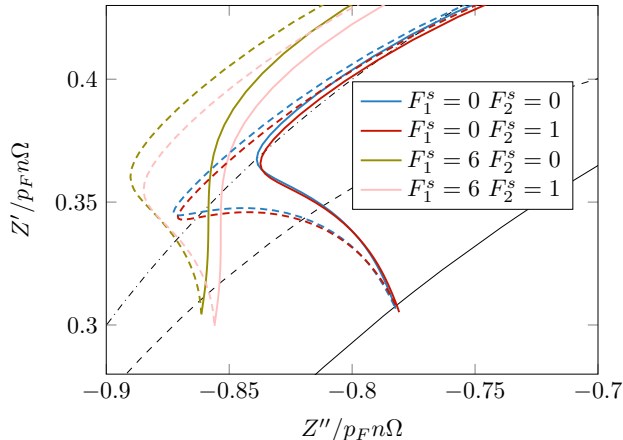
Figure 2.5: Study of the effects of parameters F_1^s, F_2^s and ξ_2 in the ballistic regime when $\Omega = 0.1$. For solid plots, $\xi_2 = 1$ and for dashed plots $\xi_2 = 0.35$. Other parameters are as in Fig. 2.4. Shown in black are the ballistic (solid), hydrodynamic (dashed) and damped oscillator (dot-dashed) limits.

decreasing Ω.

In Fig. 2.5, we make a more detailed study of how the different parameters change the behavior of the fluid film in the ballistic region. We concentrate on the case of $\Omega = 0.1$. Specularity parameters are again $s_1 = 0$ and $s_2 = 1$. First of all, we change the relaxation time parameter. We study the cases $\xi_2 = 1$ and $\xi_2 = 0.35$. We find that while ξ_2 has an effect in the region where $l/d \approx 1$, it does not affect the ballistic behavior, since the data for both values of ξ_2 end at the same point in the long mean free path limit. Moreover, we find that if we set $F_1^s = 0$, then F_2^s has hardly any effect on the behavior of the fluid film. This is likely related to the condition for the existence of zero sound, i.e. Eq. (2.96). If F_2^s has an effect on the velocity of zero sound, then its value does not matter if zero sound does not propagate.

In Fig. 2.6 we further study the effect of ξ_2. We show the real and imaginary parts of the acoustic impedance $Z = Z' + iZ''$ separately as function of l/d and in units of $p_F n$. We use two different values of F_1^s and ξ_2. The influence of ξ_2 if confined in the region around $l/d \approx 1$. This is sensible; the parameter ξ_2 is the ratio of relaxation times, i.e. $\xi_2 = \tau/\tau_2$. If all quasiparticles relax very rapidly or conversely have extremely long lifetimes, then a difference in the relaxation of the dipolar and quadrupolar components of the collision integral in Eq. (2.39) should not matter. In Fig. 2.6 we have used a large oscillation frequency $\Omega = 5$.
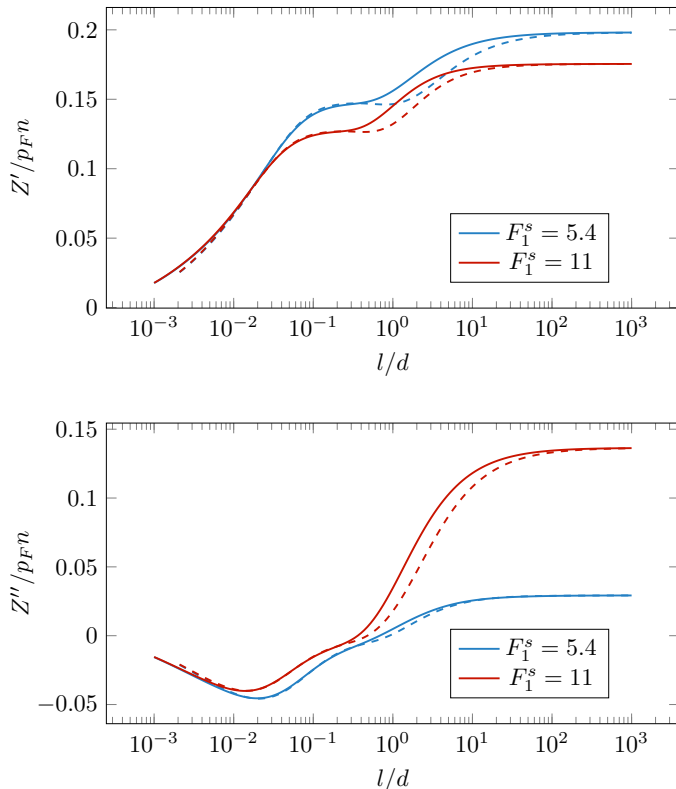
Figure 2.6: The real and imaginary parts of $Z = Z' + iZ''$ in units of $p_F n$, plotted separately as functions of l/d. The different values of F_1^s and ξ_2 have been used. For solid curves $\xi_2 = 1$ and for dashed curves $\xi_2 = 0.35$. We have used the parameter values $\Omega = 5$, $F_2^s = 0$, $s_1 = 0$ and $s_2 = 1$.

We see that the scale of the effect of F_1^s is greatly increased from that seen at small frequencies. The reason for this is that at larger frequencies, multiple wavelengths of the transverse oscillation can fit within the fluid film. This leads to resonance and antiresonance effects between the film and the substrate oscillations. As a result, the effects of the Fermi liquid interactions are amplified.

Finally, in Fig. 2.7, in an attempt to gain some insight into what constitutes a thin film of Fermi liquid, we show the impedance while using parameter values from an experiment in Ref. [34]. In the experiment, the fluid is confined between two diffusely reflecting plates. We simulate this by setting $s_1 = s_2 = 0$. The plates are separated by a distance of 25 micrometers. The pressure is 23 bar, which corresponds to $F_1^s \approx 11.8$.

Three different oscillation frequencies f have been used, 36 MHz, 60 MHz and 108 MHz. By using known values of v_F and F_1^s in

$$\Omega = \frac{2\pi f d}{v_F(1 + F_1^s/3)}, \tag{2.97}$$

we find that Ω obtains values between 31 and 93. We can display the impedance as a function of temperature by expressing the mean free path in terms of Fermi velocity v_F and relaxation time $\tau \sim 1/T^2$ as $l = v_F \tau$. We multiply the resulting acoustic impedance with $v_F(1 + F_1^s/3)$ and obtain

$$\frac{Z}{p_F n} v_F \left(1 + \frac{F_1^s}{3} \right) = \frac{Z}{p_F n} \frac{p_F}{m} = \frac{Z}{\rho}, \tag{2.98}$$

where ρ is the mass density of the liquid and we have used $m^* = m(1 + F_1^s/3)$ and $v_F = p_F/m^*$. In this form, the impedance has the dimension of velocity and is given in units of cm/s.

In Fig. 2.7, we also show results for the infinitely thick fluid layer from Refs. [29] and [30]. Difference between the infinite fluid layer and thin film results are barely perceptible for Z'/ρ, but are more apparent for Z''/ρ. Importantly, the differences arise at temperatures below the superfluid transition temperature $T_c \approx 2$ mK.

Deviation from the infinite fluid layer result is essentially chaotic. This is caused by resonance effects. For the thin film, the presence of the fluid surface is felt when a transverse sound wave traveling out from the oscillating substrate is reflected back by the fluid surface. If the reflected sound wave is in phase with the substrate oscillations when it arrives back at the substrate, it will enhance the oscillations of the substrate. This reduces the experienced impedance. Conversely, if the returning wave is in opposite phase, it will hinder the substrate oscillations, thus increasing the impedance. This means that if an experiment was devised that was sensitive to the fluid surface, for example using a thinner fluid film, then the measured impedance would be very sensitive to anything that changed the velocity or frequency of the sound waves.
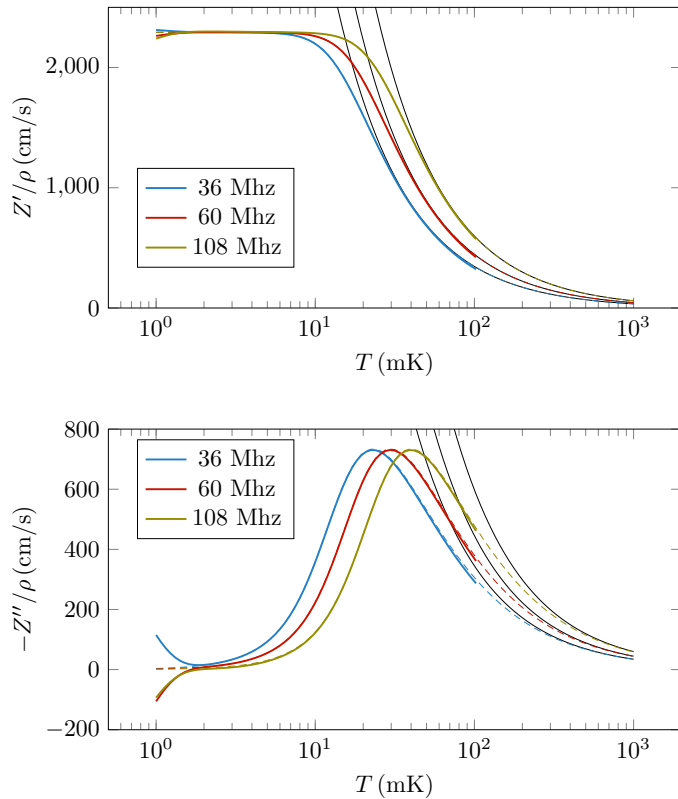
Figure 2.7: The real and imaginary parts of Z/ρ, reported in units of cm/s, shown separately as functions of T, with different oscillation frequencies f. For the imaginary part Z''/ρ, it is for some reason customary to plot $-Z''/\rho$ instead. Specularity parameters are $s_1 = s_2 = 0$. Other parameters used are $F_1^s \approx 11.8$, $F_2^s = 0$ and $\xi_2 = 0.35$. Black lines indicate hydrodynamic behavior, while dashed lines display the behavior of a fluid film of infinite thickness. Figure first published in Pub. I.

3

Moving wire in superfluid Fermi liquid

In this chapter, we investigate the flow of ^{3}He-B. We are interested in the case of a long cylindrical object, a wire, moving through a Fermi superfluid. It is expected that above the Landau velocity v_L, such motion becomes dissipative and the drag force on the object approaches the value experienced in normal liquid. The behavior of vibrating wires in ^{3}He-B has been the subject of intense study, both theoretical and experimental [35, 36, 37, 38, 39, 40, 41]. Here we concentrate on the related problem of a wire moving through ^{3}He-B with a *constant* velocity. Recent experiments seem to show that under such conditions, there is no indication of a critical velocity and the wire experiences only a marginal drag force even at velocities well above v_L [18]. The effects of Andreev reflection, and the alterations to the superflow caused by pair breaking are studied here as potential explanations for the experimentally observed low-dissipation motion.

We begin in Sec. 3.1 with an overarching view of the problem and discussion of some central concepts. In Sec. 3.2 we introduce the equations of motion that govern the dynamics of the elementary excitations of a Fermi superfluid. In Sec. 3.3 we investigate how the fluid flow is altered by pair breaking. Lastly, in Sec. 3.4 we discuss the details and the results of the numerical implementation.

3.1   Overview

By definition, a viscous fluid resists the movement of objects. Fundamentally, the resistance arises as the momentum of the object is transferred into the surrounding fluid through the creation of collective excitations

of the fluid, such as sound waves or vortices. A superfluid behaves like an ideal fluid and flows without viscosity. The underlying reason for this phenomenon is the presence of an *energy gap* in the spectrum of elementary excitations. Below a certain *critical velocity* the energy gap prevents the creation of the aforementioned carriers of momentum. The concept of a critical velocity was first discussed by Landau in the context of ^{4}He superfluid [8]. Surpassing the Landau critical velocity v_L leads to a sudden onset of viscous forces. This can be viewed as a partial breakdown of the superfluid state, where the superfluid ^{3}He is accompanied by a viscous normal liquid component. This is referred to as the two fluid model.

A weakly excited state of the superfluid can be described as the combination of a collection of elementary excitations. Microscopic theories of superfluidity are formulated in terms of these elementary excitations, called quasiparticles. Quasiparticles of supefluid theory are more complex than their normal liquid counterparts. This results from an increased number of internal degrees of freedom, such as a particle-hole characteristic.

Excitations which are able to escape the wire surface into the surrounding bulk liquid contribute directly to the drag force. The quasiparticles of a Fermi superfluid are subject to a special scattering process called *Andreev reflection*, in which a quasiparticle entering a region where the energy gap exceeds the quasiparticle's energy is reflected back along its original trajectory as a quasihole [42, 43]. Conversely, a quasihole will be reflected back as a quasiparticle. Any macroscopic object immersed in a moving fluid causes the surrounding flow field to vary spatially as the fluid is forced to flow around the object. The effective energy gap experienced by quasiparticles depends on the local superfluid flow velocity and, as a result, the flow around a macroscopic object can lead to Andreev reflections, preventing the escape of excitations.

In this chapter we investigate the drag force and critical velocity of a steadily moving wire in ^{3}He-B. This is done by studying the creation and escape of elementary excitations from the wire surface into the surrounding bulk liquid, while taking into account the changes to the superflow caused by the excitations. We concentrate on the creation of linear, or sound-like elementary excitations. In practice, it is possible that there are other dissipative mechanism at play, such as vortices in the fluid or thermally excited quasiparticles. If the flow is not steady, dissipation can also be increased by some complex dynamical effect. Experimentally it is generally found that dissipation sets in well before v_L is reached. Considering only linear excitations represents a sort of optimal case for the possibility of low-dissipative motion above v_L.
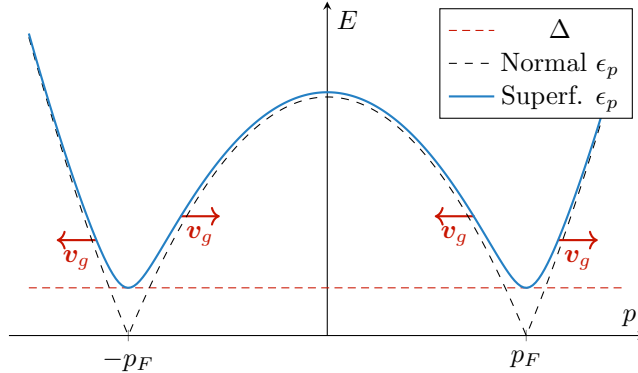
Figure 3.1: Superfluid quasiparticle excitation spectrum together with the normal state spectrum. Horizontal dashed red line depicts the energy gap Δ. Red arrows show the direction of the group velocity $\boldsymbol{v}_g$ in relation to the direction of the momentum $\boldsymbol{p}$ at vairous points. Excitations with momentum magnitude less than p_F have their group velocity pointing in the direction opposite to momentum direction, and are hole-like. The size of the energy gap has been exaggerated for visual clarity.

3.1.1 The superfluid phases of ^{3}He

At the low temperatures of a few millikelvin [2, 15], ^{3}He makes a transition into a superfluid state. The underlying cause of this phase transition is the formation of *Cooper pairs*, bound states formed by pairs of fermions. For two fermions interacting above a filled Fermi sphere, an arbitrarily weak attraction is enough to lead to the formation of a bound state. This is due to the Pauli exclusion principle, which prevents the interacting particles from occupying the states within the Fermi sphere, i.e. with $k \leq k_F$ [11].

Cooper pairing binds particles with opposite momenta, $\boldsymbol{p}$ and $-\boldsymbol{p}$. The energy of the resulting state, in which the motion of the two fermions is correlated, is negative. As a result, a filled Fermi sphere of uncorrelated fermions becomes unstable and is no longer the true ground state of the system. In the new ground state, a portion of fermions have formed into Cooper pairs. The center of mass of a Cooper pair is at rest. Thus the Cooper pairs all occupy the state with zero momentum, similar to a Bose–Einstein condensate. This is the transition to a superconducting or a superfluid state [12].

In *Bardeen–Cooper–Schrieffer* (BCS) theory of superconductivity [12] it is assumed that the ground state of the Cooper pair condensate can be described by a wave function that is the product of the wave functions

for each pair state. The Hamiltonian of the system is presented in terms
of the creation and annihilation operators of individual particles and in-
cludes a non-diagonal term describing the interaction between particles.
Diagonalization of the BCS Hamiltonian, originally performed by Bo-
goliubov [44] and Valatin [45], shows that the elementary excitations of
this system are not pure particles, but instead superpositions of a parti-
cle and a hole. These are called *Bogoliubov quasiparticles* (or sometimes
Bogoliubons). An elementary excitation is formed when a Cooper pair is
broken, meaning that a pair state is only partially occupied. The energy
of an elementary excitation with momentum $\boldsymbol{p}$ is given by the dispersion
relation [1, 46, 47]

$$\epsilon(\boldsymbol{p}) = \sqrt{\xi_p^2 + \Delta_{\boldsymbol{p}}^2}, \tag{3.1}$$

where $\xi_p = p^2/2m^* - \epsilon_F$ is the kinetic energy measured from the Fermi
surface. This is the energy of normal Fermi liquid quasiparticles in Eq.
(2.3). For low energy excitations this can be linearized as $\xi_p \approx v_F(p -
p_F)$. Here $\Delta_{\boldsymbol{p}}$ is the minimum excitation energy, the energy gap. The
dispersion relation Eq. (3.1) is shown in Fig. 3.1, assuming a constant
gap, $\Delta_{\boldsymbol{p}} = \Delta$. Unlike in the normal state, excitations on the Fermi
surface have non-zero energy. The energy gap $\Delta_{\boldsymbol{p}}$ can be thought of as
the binding energy of a Cooper pair at $T = 0$. In order to produce an
excitation, a Cooper pair must first be broken.

The group velocity $\boldsymbol{v}_g$ of an excitation is given by the slope of the
dispersion relation, $\boldsymbol{v}_g = \partial \epsilon_{\boldsymbol{p}}/\partial \boldsymbol{p}$. In Fig. 3.1 the direction of the group
velocity is depicted at certain places on the dispersion curve. Excitations
can be created both above and below the Fermi surface. For excitations
with $|p| < p_F$, the group velocity and the momentum are antiparallel.
Such excitations have a negative effective mass and have hole-like char-
acteristics.

The wave function of a system of fermions must be antisymmetric
with respect to the exchange of particles. BCS theory of superconduc-
tivity originally describes the Cooper pairing of electrons in a conductor.
The possible solutions to the Cooper pair spatial wave function consist of
a radial component and a spherical harmonic. For a BCS Cooper pair,
the lowest energy solution is the symmetric s-wave with zero angular
momentum, $l = 0$. As a consequence, the spin component of the wave
function is antisymmetric. This is called *singlet pairing*, where the total
spin of the pair is zero, $S = 0$, and the pair wave function is given by

$$|\Psi\rangle = \psi_0 \left(|\uparrow\downarrow\rangle - |\downarrow\uparrow\rangle \right), \tag{3.2}$$

where ψ_0 is the spatial component of the wave function and the arrows
represent the spins of the particles composing the pair.

In contrast to Cooper pairs of BCS theory, ^{3}He Cooper pairs have a complicated internal structure. The fact that superfluid ^{3}He remains sensitive to external magnetic fields means that the Cooper pairs have non-zero total spin, namely $S = 1$, with three possible values for the spin projection, $S_z = -1, 0, 1$. This is called *triplet pairing*. The spin component of the wave function is symmetric and the wave function itself may be written

$$|\Psi\rangle = \psi_{1,+1}|\uparrow\uparrow\rangle + \psi_{1,0}\left(|\uparrow\downarrow\rangle + |\downarrow\uparrow\rangle\right) + \psi_{1,-1}|\downarrow\downarrow\rangle, \qquad (3.3)$$

where ψ_{S,S_z} are the spatial wave functions of the three spin substates and the subscripts indicate the values total spin and the spin projection. The spatial component of the wave function must now be antisymmetric. The hard core repulsion between ^{3}He atoms also suggests that the spatial component should be one that disappears if the interatomic distance goes to zero, thus preventing the atoms from overlapping. Such conditions are satisfied by states with odd angular momentum, $l = 1, 3, 5, ...$ [46]. The state with the lowest energy is the one realized in nature. This is found to be the antisymmetric p-wave with $l = 1$ [1]. Since the angular momentum also has three possible projections $l_z = -1, 0, 1$, the result is nine-fold complexity in comparison to a Cooper pair in a superconductor [46]. One consequence of this complexity is that ^{3}He has multiple superfluid phases.

in the absence of an external magnetic field, ^{3}He has two superfluid phases, the anisotropic A phase and the isotropic B phase. Isotropy here means that ^{3}He-B is an equal superposition of all of the substates with different spin projection S_z, whereas in ^{3}He-A one of these substates, namely that with $S_z = 0$, is unoccupied. There is also a third phase, called A_1, which is only stable in an external magnetic field, and in which only the $S_z = 1$ substate is occupied. We will be dealing solely with ^{3}He-B in which, at equilibrium, the energy gap Δ is also isotropic [14, 46].

3.1.2 Critical velocity and pair breaking

If an object moves in a superfluid with a velocity which is higher than the so-called critical velocity, it begins to experience dissipative forces, as excitations are generated in the superfluid. We consider the excitations produced by pair breaking on the surface of an object moving with velocity $\boldsymbol{v}$ with respect to the rest frame of the fluid. Here, we assume the object is small, so that the flow of superfluid is not disturbed by the object and the flow velocity is the same everywhere. We can consider the dispersion relation in Eq. (3.1) in a reference frame moving along with
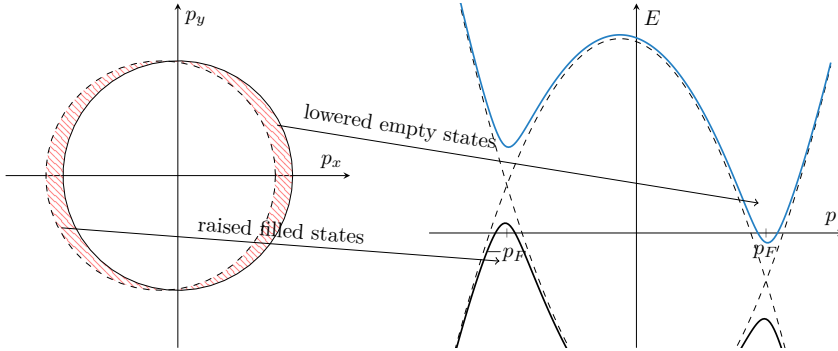
Figure 3.2: Left: Fermi surface displaced by movement in the negative x direction. Right: Quasiparticle energy Eq. (3.4) in a frame of reference moving with velocity $v > v_L$ to the left. The figure shows both the positive and negative branches of the square root in Eq. (3.4), in blue and black respectively. Energy states with positive momentum are lowered, while states with negative momentum are raised. Positive momentum states close to the Fermi surface have negative energy.

the object at velocity $\boldsymbol{v}$. By Galilean transformation, in this frame an excitation has the energy

$$\epsilon(\boldsymbol{p}) = \sqrt{\xi_p^2 + \Delta^2} - \boldsymbol{p} \cdot \boldsymbol{v}. \tag{3.4}$$

If we concentrate on just the Fermi surface where $\xi_p = 0$, the above equation simplifies to $\epsilon = \Delta - p_F \hat{\boldsymbol{p}} \cdot \boldsymbol{v}$. This is the minimum excitation energy, or energy gap in a moving frame of reference. If the frame of reference is moving at such a velocity that $p_F \hat{\boldsymbol{p}} \cdot \boldsymbol{v} > \Delta$, the excitation has negative energy. This condition is first satisfied at the *Landau critical velocity*, $v_L = \Delta/p_F$ by excitations traveling along motion of the object, i.e. with $\hat{\boldsymbol{p}} \cdot \boldsymbol{v} = v_L$.

The dispersion relation in Eq. (3.4) is depicted on the right in Fig. 3.2. This is called the *semiconductor picture*. In the semiconductor picture, in the ground state of the superfluid, all negative branch states are considered to be filled with quasiparticles. An excitation with momentum $\boldsymbol{p}$ can thus be formed in two alternative ways; either a quasiparticle with momentum $\boldsymbol{p}$ can be added into the positive branch, or a negative branch quasiparticle with momentum $-\boldsymbol{p}$ can be removed. Both of these options result in an excitation with momentum $\boldsymbol{p}$.

If an object moves through superfluid ^{3}He, then in the rest frame of the object the distribution of quasiparticles is tilted as shown in Fig. 3.2. If the velocity of the object surpasses the Landau critical velocity,
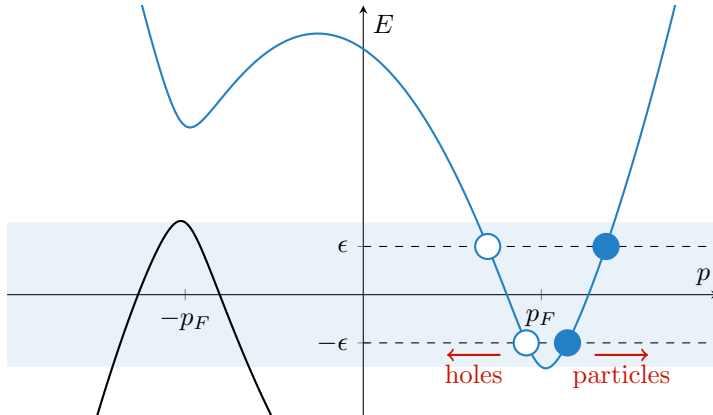
Figure 3.3: Production of Bogoliubov quasiparticle pairs. The energy range in which quasiparticles can be created is marked in blue. Energy conservation $\epsilon_1 + \epsilon_2 = 0$ can be satisfied by the creation of a pair that consists of two quasiparticles, two quasiholes, or a quasiparticle and a quasihole.

then there are some empty states with negative energy. Thus it is energetically favorable to produce excitations in these states. Moreover, in the semiconductor picture there exists a range of energies where there are both filled and empty states. The moving object can now scatter quasiparticles from the filled states to the empty ones.

An elementary excitation of the superfluid ground state, i.e. a Bogoliubov quasiparticle, is formed by having a pair state be occupied by only a single ^{3}He quasiparticle. Scattering from a moving object, a process which destroys Cooper pairs but conserves the number of ^{3}He quasiparticles, must then produce two elementary excitations, as a ^{3}He quasiparticle is removed from one state and placed into another [48]. Even though the produced excitations transfer momentum away from the moving object, we can assume that for a single instance of scattering this transfer is small and to first order the energy of the moving object is unchanged. It follows that for the produced pair of excitations, $\epsilon_1 + \epsilon_2 = 0$, where ϵ_1 and ϵ_2 are the energies of the two excitations. This is clearly first possible at the critical velocity which allows $\epsilon_1 = \epsilon_2 = 0$. Above the critical velocity v_L there is a range on energies,

$$- |\Delta - p_F \hat{\boldsymbol{p}} \cdot \boldsymbol{v}| \leq \epsilon_1 \leq |\Delta - p_F \hat{\boldsymbol{p}} \cdot \boldsymbol{v}|, \tag{3.5}$$

in which an excitation can be created. The other produced excitation has the energy $\epsilon_2 = -\epsilon_1$. The creation of quasiparticle pairs is depicted

in Fig. 3.3. Scattering from the moving object produces beams of quasi-particles and quasiholes traveling in opposite directions.

3.2   Equations of motion

Our study of the motion of superfluid ^{3}He is based on the quasiclassical theory of Fermi superfluids. Details of this theory are found in Ref. [47]. The idea behind quasiclassical theory is to represent the complex interaction between Fermi liquid quasiparticles using phenomenological parameters. The similarity between this and Landau's Fermi liquid theory is not a coincidence, as quasiclassical theory is in essence a more general version of Landau's theory. The state of the liquid is represented by quasiclassical propagators, from which certain internal degrees of freedom, such as the quasiparticle energy, have been integrated out. These "unnecessary" degrees of freedom are removed and replaced by the phenomenological parameters before undertaking computationally expensive calculations.

The following is an outline of the dynamic equations of the low-frequency, $\hbar\omega \ll \Delta$, and long-wavelength, $\hbar k v_F \ll \Delta$, limit of the general quasiclassical theory. This limit is derived from the general theory by expanding the dynamic equations in terms of $\hbar\omega/\Delta$ and $\hbar k v_F/\Delta$ and considering only the leading order terms. The resulting equations are presented in Sec. 7 of Ref. [47]. All energies are small in comparison to the Fermi energy, $\xi_p, \Delta, u, a, \epsilon \ll v_F p_F$.

The energy of a quasiparticle excitation with momentum $\boldsymbol{p}$ in the quasiclassical theory is

$$\epsilon(\boldsymbol{p}, \boldsymbol{r}, t) = \sqrt{|\xi_p + u(\hat{\boldsymbol{p}}, \boldsymbol{r}, t)|^2 + |\Delta(\hat{\boldsymbol{p}}, \boldsymbol{r}, t)|^2} + a(\hat{\boldsymbol{p}}, \boldsymbol{r}, t). \qquad (3.6)$$

Here, $u(\hat{\boldsymbol{p}}, \boldsymbol{r}, t)$ and $a(\hat{\boldsymbol{p}}, \boldsymbol{r}, t)$ are effective potentials or *molecular fields* that describe the quasiparticle-quasiparticle interaction. They are even and odd with respect to momentum, i.e. $u(-\hat{\boldsymbol{p}}) = u(\hat{\boldsymbol{p}})$ and $a(-\hat{\boldsymbol{p}}) = -a(\hat{\boldsymbol{p}})$. Clearly $u(\hat{\boldsymbol{p}}, \boldsymbol{r}, t)$ acts to shift the chemical potential in a manner similar to the definition of local equilibrium in the context of normal liquid. The potential $a(\hat{\boldsymbol{p}}, \boldsymbol{r}, t)$ is analogous to the interaction term added in the normal liquid case to ensure Galilean invariance.

If we fix the direction of momentum, energy depends only on the magnitude of momentum through ξ_p. For each value of the energy, there are two possible choices of ξ_p. It is convenient to split the distribution of elementary excitations into two *branches*, so that

$$f(\boldsymbol{r}, \xi, t) = \begin{cases} \phi_{B1}(\boldsymbol{r}, \epsilon(\boldsymbol{r}, \xi_p, t), t), & \text{if } \xi_p + u > 0, \\ \phi_{B2}(\boldsymbol{r}, \epsilon(\boldsymbol{r}, \xi_p, t), t), & \text{if } \xi_p + u < 0. \end{cases} \qquad (3.7)$$

The group velocity $\boldsymbol{v}_g$ of an excitation is given by the slope of its dispersion relation, $\boldsymbol{v}_g = \partial\epsilon/\partial\boldsymbol{p}$. It follows that excitations in branch ϕ_{B1} have a group velocity in the same direction as their momentum and are thus particle-like, while excitations in ϕ_{B2} have a group velocity that points against their momentum and are hole-like. The two branches ϕ_{B1} and ϕ_{B2} represent the distributions of the particle- and hole-like Bogoliubov quasiparticles, respectively. In the quasiclassical theory, the two distributions are symmetrized and obtain values in the range $[-1/2, 1/2]$. The value $1/2$ corresponds to a filled state and the value $-1/2$ to an empty state. The equilibrium distributions at temperature T is given by

$$\phi_{B1} = \phi_{B2} = -\frac{1}{2}\tanh\left(\epsilon/2T\right), \tag{3.8}$$

which at $T = 0$ simplifies to $\phi_{B1} = \phi_{B2} = 1/2 - \theta(\epsilon)$. In a reference frame moving with velocity $\boldsymbol{v}$, the distributions are Galilei transformed as $\phi_{Bi}(\hat{\boldsymbol{p}}, \epsilon) \to \phi_{Bi}(\hat{\boldsymbol{p}}, \epsilon + p_F\hat{\boldsymbol{p}}\cdot\boldsymbol{v})$. In the case of the zero-temperature equilibrium distribution this becomes $\phi_{Bi} = 1/2 - \theta(\epsilon + p_F\hat{\boldsymbol{p}}\cdot\boldsymbol{v})$.

In Ref. [47], the equations that describe the dynamics of distributions ϕ_{B1} and ϕ_{B2} are derived using techniques based on Green's functions. At the low-frequency long-wavelength limit it is possible to arrive at the same equations in a much simpler manner. By studying the total time evolution of the two distributions, using the dispersion relation in Eq. (3.6), we find Boltzmann-like kinetic equations

$$\frac{\partial\phi_{B1}}{\partial t} + \nu^{-1}v_F\hat{\boldsymbol{p}}\cdot\boldsymbol{\nabla}\phi_{B1} + \left[\nu^{-1}\frac{\partial u}{\partial t} + \frac{\partial a}{\partial t} + \frac{|\Delta|}{\tilde{\epsilon}}\frac{\partial|\Delta|}{\partial t}\right]\frac{\partial\phi_{B1}}{\partial\epsilon} = I_{B1}, \tag{3.9}$$

$$\frac{\partial\phi_{B2}}{\partial t} - \nu^{-1}v_F\hat{\boldsymbol{p}}\cdot\boldsymbol{\nabla}\phi_{B2} + \left[-\nu^{-1}\frac{\partial u}{\partial t} + \frac{\partial a}{\partial t} + \frac{|\Delta|}{\tilde{\epsilon}}\frac{\partial|\Delta|}{\partial t}\right]\frac{\partial\phi_{B2}}{\partial\epsilon} = I_{B2}, \tag{3.10}$$

where $\nu = |\tilde{\epsilon}|/\sqrt{\tilde{\epsilon}^2 - |\Delta|^2}$, and we have defined $\tilde{\epsilon} = \epsilon - a$. I_{Bi} is a collision term as in the context of normal liquid. We consider only a time-independent and collisionless case, in which the kinetic equations reduce to

$$\hat{\boldsymbol{p}}\cdot\boldsymbol{\nabla}\phi_{B1} = 0, \quad \hat{\boldsymbol{p}}\cdot\boldsymbol{\nabla}\phi_{B2} = 0, \tag{3.11}$$

which simply state that the distributions ϕ_{B1} and ϕ_{B2} are constant along the trajectory of a quasiparticle.

The Boltzmann-like equations for the distributions ϕ_{B1} and ϕ_{B2} are accompanied by self-consistency equations for the molecular fields $u(\hat{\boldsymbol{p}}, \boldsymbol{r}, t)$

and $a(\hat{\boldsymbol{p}}, \boldsymbol{r}, t)$, and for the gap $\Delta(\hat{\boldsymbol{p}}, \boldsymbol{r}, t)$, which can be written as

$$
u(\hat{\boldsymbol{p}}) = \frac{U}{1 + F_0^s}
$$
$$
+ \frac{1}{2} \int \frac{d\Omega'_p}{4\pi} A^s(\hat{\boldsymbol{p}} \cdot \hat{\boldsymbol{p}}') \int_{-E_c}^{E_c} d\epsilon \, \Theta(\epsilon, \hat{\boldsymbol{p}}') \left[\phi_{B1}(\epsilon, \hat{\boldsymbol{p}}') - \phi_{B2}(\epsilon, \hat{\boldsymbol{p}}') \right],
$$
(3.12)

$$
a(\hat{\boldsymbol{p}}) = -v_F \boldsymbol{A} \cdot \hat{\boldsymbol{p}}
$$
$$
+ \frac{1}{2} \int \frac{d\Omega'_p}{4\pi} A^s(\hat{\boldsymbol{p}} \cdot \hat{\boldsymbol{p}}') \int_{-E_c}^{E_c} d\epsilon \, N(\epsilon, \hat{\boldsymbol{p}}') \left[\phi_{B1}(\epsilon, \hat{\boldsymbol{p}}') + \phi_{B2}(\epsilon, \hat{\boldsymbol{p}}') \right],
$$
(3.13)

$$
\Delta(\hat{\boldsymbol{p}}) = -\frac{1}{2} \int \frac{d\Omega'_p}{4\pi} V(\hat{\boldsymbol{p}} \cdot \hat{\boldsymbol{p}}')
$$
$$
\times \int_{-E_c}^{E_c} d\epsilon \, N(\epsilon, \hat{\boldsymbol{p}}') \left[\phi_{B1}(\epsilon, \hat{\boldsymbol{p}}') + \phi_{B2}(\epsilon, \hat{\boldsymbol{p}}') \right] \frac{\Delta(\hat{\boldsymbol{p}}')}{\epsilon - a(\hat{\boldsymbol{p}}')},
$$
(3.14)

where

$$
\Theta(\epsilon, \hat{\boldsymbol{p}}) = \theta \left([\epsilon - a(\hat{\boldsymbol{p}})]^2 - |\Delta(\hat{\boldsymbol{p}})|^2 \right),
$$
(3.15)

$$
N(\epsilon, \hat{\boldsymbol{p}}) = \frac{|\epsilon - a(\hat{\boldsymbol{p}})|}{\sqrt{[\epsilon - a(\hat{\boldsymbol{p}})]^2 - |\Delta(\hat{\boldsymbol{p}})|^2}} \Theta(\epsilon, \hat{\boldsymbol{p}}),
$$
(3.16)

$$
U = U_{\text{ext}} + \frac{\hbar}{2}\dot{\psi}, \quad \boldsymbol{A} = \boldsymbol{A}_{\text{ext}} - \frac{\hbar}{2}\boldsymbol{\nabla}\psi, \quad \boldsymbol{v}_s = \frac{\hbar}{2m}\boldsymbol{\nabla}\psi, \quad (3.17)
$$

$$
A^s(\hat{\boldsymbol{p}} \cdot \hat{\boldsymbol{p}}') = \sum_{l=0}^{\infty} A_l^s P_l(\hat{\boldsymbol{p}} \cdot \hat{\boldsymbol{p}}'), \quad A_l^s = \frac{F_l^s}{1 + F_l^s/(2l+1)}, \quad (3.18)
$$

where $\theta(x)$ is the Heaviside step function. Here $\int d\Omega_p$ denotes integration over a unit sphere of $\hat{\boldsymbol{p}}$. $N(\epsilon, \hat{\boldsymbol{p}})$ is the density of states given in units $N(0) = mp_F/2\pi^2\hbar^3$. $U_{\text{ext}}(\boldsymbol{r}, t)$ and $\boldsymbol{A}_{\text{ext}}(\boldsymbol{r}, t)$ are external fields, which we assume to be zero. $V(\hat{\boldsymbol{p}} \cdot \hat{\boldsymbol{p}}')$ describes the effective potential between the components of a Cooper pair. Eq. (3.18) is a Legendre-polynomial expansion of the quasiparticle interaction energy $A^s(\hat{\boldsymbol{p}} \cdot \hat{\boldsymbol{p}}')$ in terms of symmetric Landau parameters F_l^s, familiar from Landau's Fermi liquid theory. The limit of integration E_c is a computational cut-off energy.

In order to simplify our calculations, we assume a constant Δ. This assumption entails that the fluid velocity on the surface of the object does not greatly exceed $v_L/2$, as pair breaking begins to distort the gap once the critical velocity is exceeded [1, 49].

In the time independent and collisionless case, neither $u(\hat{\boldsymbol{p}}, \boldsymbol{r}, t)$ nor $a(\hat{\boldsymbol{p}}, \boldsymbol{r}, t)$ appear in the kinetic equation, while $a(\hat{\boldsymbol{p}}, \boldsymbol{r}, t)$ still appears in

the definition $\tilde{\epsilon} = \epsilon - a$. This means that $u(\hat{\boldsymbol{p}}, \boldsymbol{r}, t)$ does not affect the kinetics, but we must ensure that $a(\hat{\boldsymbol{p}}, \boldsymbol{r}, t)$ is self-consistent since it depends explicitly on itself. We concentrate solely on the field $a(\hat{\boldsymbol{p}}, \boldsymbol{r}, t)$ and Eq. (3.13).

Since $a(\hat{\boldsymbol{p}}, \boldsymbol{r}, t)$ is antisymmetric with respect to momentum, only the odd terms in the polynomial expansion of $A^s(\hat{\boldsymbol{p}} \cdot \hat{\boldsymbol{p}}')$ can be nonzero. We truncate the polynomial expansion at $l = 1$, and assume that the effects of higher terms are negligible. The self-consistency equation of $a(\hat{\boldsymbol{p}}, \boldsymbol{r}, t)$ in Eq. 3.13 can now be written

$$
a(\hat{\boldsymbol{p}}) = m v_F \boldsymbol{v}_s \cdot \hat{\boldsymbol{p}}
$$
$$
+ \frac{1}{2} \frac{F_1^s}{1 + F_1^s/3} \int \frac{d\Omega'_p}{4\pi} \hat{\boldsymbol{p}} \cdot \hat{\boldsymbol{p}}' \int_{-E_c}^{E_c} d\epsilon N(\epsilon, \hat{\boldsymbol{p}}') \left[\phi_{B1}(\epsilon, \hat{\boldsymbol{p}}') + \phi_{B2}(\epsilon, \hat{\boldsymbol{p}}') \right].
$$
$$(3.19)$$

We find that we can separate the momentum dependency from a and write $a(\hat{\boldsymbol{p}}, \boldsymbol{r}, t) = \boldsymbol{\alpha}(\boldsymbol{r}, t) \cdot \hat{\boldsymbol{p}}$. From Eq. (3.19), one can also calculate that in the absence of excitations ($\phi_{B1} = \phi_{B2} = -1/2$), $\boldsymbol{\alpha} = p_F \boldsymbol{v}_s$. The field $\boldsymbol{\alpha}$ describes the local tilting of the distribution function as depicted in Fig. 3.2.

Force on the wire is calculated from the stress tensor

$$
\overset{\leftrightarrow}{\boldsymbol{\Pi}}(\boldsymbol{r}, t) = v_F p_F N(0) \int \frac{d\Omega}{4\pi} \hat{\boldsymbol{p}} \, \hat{\boldsymbol{p}} \int_{-E_c}^{E_c} d\epsilon \, \Theta(\epsilon, \hat{\boldsymbol{p}}) \left[\phi_{B1}(\epsilon, \hat{\boldsymbol{p}}) - \phi_{B2}(\epsilon, \hat{\boldsymbol{p}}) \right].
$$
$$(3.20)$$

Force on a surface with area dA and normal $\hat{\boldsymbol{n}}$ is $dF = (\hat{\boldsymbol{n}} \cdot \overset{\leftrightarrow}{\boldsymbol{\Pi}}) dA$. The total drag force on the wire can be calculated in cylindrical coordinates as

$$
\boldsymbol{F}(t) = l \int_{-\pi}^{\pi} R d\varphi \hat{\boldsymbol{n}} \cdot \overset{\leftrightarrow}{\boldsymbol{\Pi}}(R, \varphi, t), \tag{3.21}
$$

where l is the length of the wire and R its radius.

The *mass current density* is given by

$$
\boldsymbol{j}(\boldsymbol{r}, t) = m v_F N(0) \int \frac{d\Omega_p}{4\pi} \hat{\boldsymbol{p}} \int_{-E_c}^{E_c} d\epsilon \, N(\epsilon, \hat{\boldsymbol{p}}') \left[\phi_{B1}(\epsilon, \hat{\boldsymbol{p}}') + \phi_{B2}(\epsilon, \hat{\boldsymbol{p}}') \right].
$$
$$(3.22)$$

We also define, at a given energy, the *number current density of excitations* [50]:

$$
\boldsymbol{j}_e(\boldsymbol{r}, t, \epsilon) = v_F N(0) \int \frac{d\Omega_p}{4\pi} \hat{\boldsymbol{p}} \, \Theta(\epsilon, \hat{\boldsymbol{p}}) \left[\phi_{B1}(\epsilon, \hat{\boldsymbol{p}}) - \phi_{B2}(\epsilon, \hat{\boldsymbol{p}}) \right]. \tag{3.23}
$$

Comparing this to the stress tensor Eq. (3.20), we can make the interpretation that the net force on the wire is caused by the excitation current, each escaping excitation carrying away momentum $p_F \hat{\boldsymbol{p}}$.

3.2.1   Andreev reflection

Andreev reflection is a scattering process in which a particle-type excitation is converted into a hole-type excitation and reflected back along its original trajectory, or vice versa [42]. It can take place in materials where the superconducting energy gap $\boldsymbol{\Delta}(\boldsymbol{r})$ changes significantly on the scale of the superconducting coherence length ξ_0. The most often considered example of this is an electron moving through the interface between a superconductor and a normal metal. In the context of wires moving in ^{3}He-B, Andreev reflection has been studied as it pertains to the movements of thermally excited quasiparticles [39, 40]. It is also an essential component in any realistic microscopic modeling of quasiparticle reflections from a surface, since the energy gap is suppressed at the interface of a superfluid and an object [43, 51]. Here, we focus on the effects Andreev reflection has on the propagation of quasiparticles produced by pair breaking.

Andreev reflection results from the interplay of conservation of energy, momentum and particle number. Due to energy conservation, a particle may not enter into a region where the local energy gap is greater than the energy of the particle. At the same time, there is no hard scattering potential on such a boundary that could impart a momentum impulse of the order of the Fermi momentum p_F to the particle, which is what is required for ordinary reflection to take place. Instead, a hole is reflected back and a Cooper pair is produced on the other side of the boundary. The hole has nearly identical momentum as the initial particle, changed only slightly by the transition through the Fermi surface, and travels backwards along the same trajectory. This is called *retroreflection*. Cooper pairing takes place between particles with opposite momenta, so the total momentum of the produced Cooper pair is zero. Momentum and particle number are thus conserved.

The energy of an excitation is given by the dispersion relation in Eq. (3.6). Assuming a constant Δ, the minimum allowed excitation energy is

$$E_{\min} = \Delta + a(\hat{\boldsymbol{p}}, \boldsymbol{r}) = \Delta + \hat{\boldsymbol{p}} \cdot \boldsymbol{\alpha}(\boldsymbol{r}). \qquad (3.24)$$

The effective energy gap experienced by a quasiparticle thus depends on the direction of its momentum $\hat{\boldsymbol{p}}$ and the local value of the field $\boldsymbol{\alpha}(\boldsymbol{r})$. If a macroscopic object is immersed in a flowing liquid, there are unavoidable gradients in the flow velocity as the fluid is forced to divert around the object. This produces a situation similar to that on the boundary of a normal metal and a superconductor; an energy gap that depends on position and momentum direction, and can change as the quasiparticles travel through the liquid. In this way quasiparticles can be Andreev
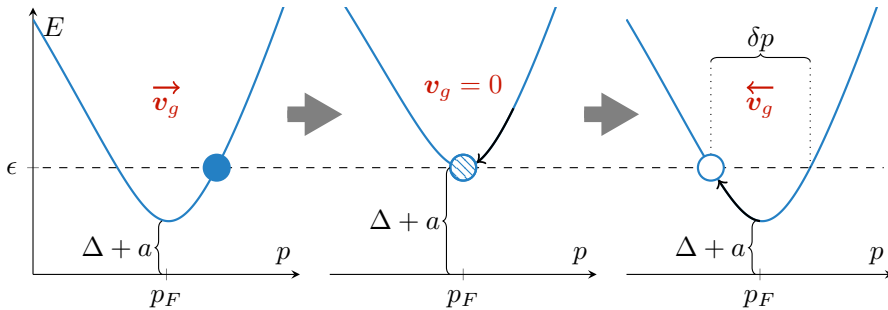
Figure 3.4: A particle-like excitation is Andreev reflected by the changing effective energy gap. Initially the quasiparticle has group velocity to the right and energy $\epsilon > \Delta + a(\hat{\boldsymbol{p}}, \boldsymbol{r})$. Reaching a region where $\epsilon < \Delta + a(\hat{\boldsymbol{p}}, \boldsymbol{r})$, it is prevented from traveling further, instead changing its particle-hole nature and traveling back along its original trajectory. There is only a minor change in momentum, $\delta p \ll p_F$ when the quasiparticle is transported through the Fermi surface.

reflected by the superflow. This process is depicted in Fig. 3.4.

In the quasiclassical theory of Fermi superfluids, Andreev reflection is present as a boundary condition for the two branches of the quasiparticle distribution function. If the quasiparticle is entering a region where the local energy gap is greater than the quasiparticle's energy, then on the boundary of this region $[\epsilon - a(\hat{\boldsymbol{p}}, \boldsymbol{r})] - |\Delta(\hat{\boldsymbol{p}}, \boldsymbol{r})|^2 = 0$ and [47]

$$\phi_{B1}(\hat{\boldsymbol{p}}, \epsilon, \boldsymbol{r}) = \phi_{B2}(\hat{\boldsymbol{p}}, \epsilon, \boldsymbol{r}). \tag{3.25}$$

This is called *branch conversion*. Branch conversion can also occur as a result of a collision process, either with the object moving through the liquid or with other quasiparticles described by the collision integrals I_{Bi} in Eqs. (3.9) and (3.10). The latter possibility is ignored in our model.

3.3 Superfluid flow past a cylinder

In this section we will discuss the flow of Fermi superfluid past a cylindrical object and our methods for finding a self-consistent flow in the presence of pair breaking. First however, we discuss the flow when pair breaking is not present.

3.3.1 Potential flow

A flow that is irrotational,, i.e. $\boldsymbol{\nabla} \times \boldsymbol{v} = 0$, is called *potential flow*, since the fluid velocity can be expressed as the gradient of a *velocity potential*

ψ, i.e. $\boldsymbol{v} = \boldsymbol{\nabla}\psi$. Mass transport is related to the probability current of the mass carriers

$$\boldsymbol{J} = -\frac{i\hbar}{2m}\left(\Psi^*\boldsymbol{\nabla}\Psi - \Psi\boldsymbol{\nabla}\Psi^*\right). \tag{3.26}$$

Because the order parameter for ³He-B, which can be understood to be the wave function of the mass carriers, may be written in terms of a real quantity multiplied by a complex phase factor, $\Psi = R(\boldsymbol{r})e^{i\psi(\boldsymbol{r})}$, superfluid velocity $\boldsymbol{v}_s$ must be proportional to the gradient of the phase [1, 52]:

$$\boldsymbol{v}_s = \frac{\hbar}{2m}\boldsymbol{\nabla}\psi(\boldsymbol{r}), \tag{3.27}$$

where the factor $1/2$ follows from each Cooper pair consisting of two particles and m is the mass of the bare fermion.

Flow past an object must satisfy the continuity equation

$$\frac{\partial\rho}{\partial t} + \boldsymbol{\nabla}\cdot\boldsymbol{j} = 0, \tag{3.28}$$

where ρ is the mass density and $\boldsymbol{j} = \rho\boldsymbol{v}$ is the mass current density. In the time-independent case, this recudes to $\boldsymbol{\nabla}\cdot\boldsymbol{j} = 0$, which means that the fluid is incompressible. The condition of incompressibility implies that the phase ψ satisfies the Laplace equation

$$\nabla^2\psi = \frac{1}{r}\frac{\partial}{\partial r}\left(r\frac{\partial\psi}{\partial r}\right) + \frac{1}{r^2}\frac{\partial^2\psi}{\partial\varphi^2} + \frac{\partial^2\psi}{\partial z^2} = 0, \tag{3.29}$$

where the Laplace operator ∇^2 has been expressed in cylindrical coordinates. For a cylindrical object aligned with the z axis, the flow is invariant in the z direction and the last term of the Laplace operator is zero.

In addition to the Laplace equation, a velocity potential has to satisfy appropriate boundary conditions. In the case of flow past an object, there should be no flow through the surface of the object. Therefore

$$\hat{\boldsymbol{n}}(\varphi)\cdot\boldsymbol{v}(R,\varphi) = 0, \tag{3.30}$$

where it has been assumed that the object is cylindrcal. Here $\hat{\boldsymbol{n}}$ is the surface normal of the object and R is its radius. Far from the object, the flow velocity should approach a constant value. For a superfluid flow past a cylindrical object with radius R aligned along the z axis moving at velocity $v\hat{\boldsymbol{x}}$, a phase that satisfies these conditions is given in the rest frame of the cylinder as

$$\frac{\hbar}{2m}\psi(r,\varphi) = -vr\left(1 + \frac{R^2}{r^2}\right)\cos\varphi. \tag{3.31}$$
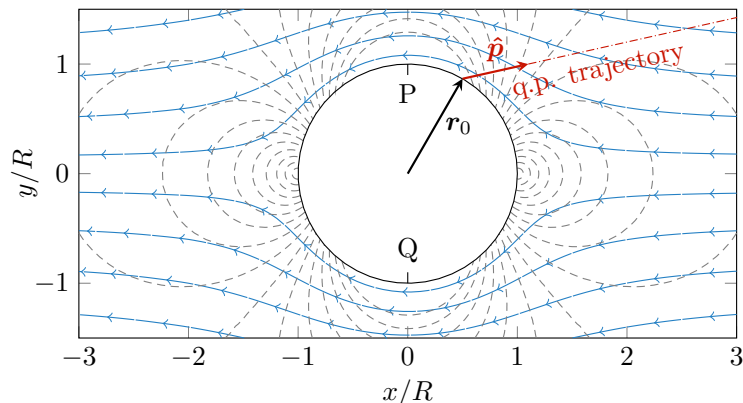
Figure 3.5: Ideal flow past a cylinder in a reference frame where the cylinder is stationary. Far away from the cylinder the fluid is moving with velocity $-v\boldsymbol{x}$. Streamlines show the direction of flow, while the dashed lines are contours of constant speed, placed at intervals of $0.1v$. On the points directly on the front and back of the cylinder the flow velocity is zero. At points P and Q the flow velocity is $-2v\boldsymbol{x}$. The trajectory of a quasiparticle starting from position $\boldsymbol{r}_0$ in direction $\hat{\boldsymbol{p}}$ is shown in red.

The flow generated by this velocity potential is depicted in Fig. 3.5. An important feature of the flow is that at points P and Q the fluid flows at twice the velocity it has far from the cylinder. If the flow is also inviscid, it does not generate a drag force on moving objects. A fluid that is both incompressible and inviscid is called *ideal*.

3.3.2 Effects of pair breaking

Below the Landau critical velocity v_L, superfluid ^{3}He behaves like an irrotational ideal fluid. If v_L is exceeded anywhere in the fluid where there is also a mechanism for scattering quasiparticles, pair breaking will begin to take place. A cylindrical object begins to scatter quasiparticles first at points P and Q if the asymptotic fluid velocity, the velocity far from the object, reaches $v_L/2$. If the velocity is further increased, the regions of pair breaking will expand out from points P and Q to cover more of the cylinder surface.

Pair breaking produces excitations in the form of quasiparticles. These quasiparticles are created at the wire and travel out into the surrounding liquid, carrying away momentum. This produced flow of quasiparticles will then alter the flow of liquid near the wire, thus also changing the

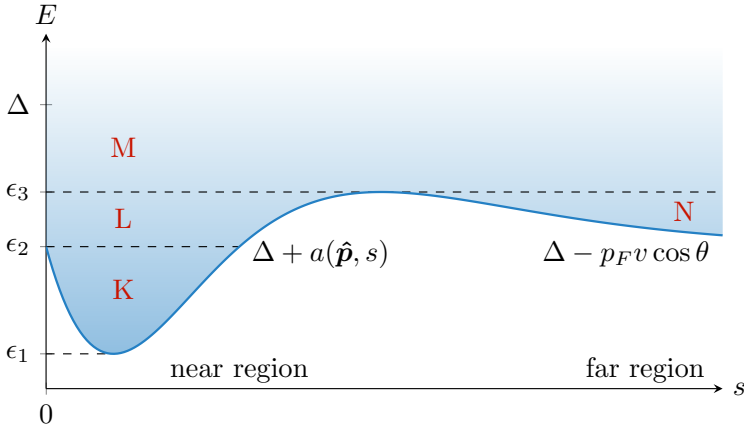Figure 3.6: Allowed quasiparticle energies along a trajectory $\boldsymbol{r} = \boldsymbol{r}_0 + s\hat{\boldsymbol{p}}$. The trajectory starts from the surface of the wire at $s = 0$. The region below curve $\Delta + a(\hat{\boldsymbol{p}}, s)$ is the energy gap where quasiparticles cannot exist. K, L, M and N denote the energy ranges categorized by access to the wire surface and the far region of the fluid, as discussed in the text.

fluid velocity on the surface of the wire.

We have to study the propagation of quasiparticles. Starting from some location $\boldsymbol{r}_0$, the trajectory of a quasiparticle with momentum $\hat{\boldsymbol{p}}$ can be parametrized as $\boldsymbol{r} = \boldsymbol{r}_0 + s\hat{\boldsymbol{p}}$, where $\boldsymbol{r}_0$ is fixed and $s \in \mathbb{R}$. We define the following energies along such a trajectory:

$$\epsilon_1(\hat{\boldsymbol{p}}, \boldsymbol{r}_0) = \min_{\boldsymbol{r}} \left[a(\hat{\boldsymbol{p}}, \boldsymbol{r}) \right] + \Delta, \quad \text{minimum gap along trajectory,}$$

$$\epsilon_2(\hat{\boldsymbol{p}}, \boldsymbol{r}_0) = a(\hat{\boldsymbol{p}}, \boldsymbol{r}_0) + \Delta, \quad\quad\quad\quad\quad \text{gap at point } \boldsymbol{r}_0, \quad (3.32)$$

$$\epsilon_3(\hat{\boldsymbol{p}}, \boldsymbol{r}_0) = \max_{\boldsymbol{r}} \left[a(\hat{\boldsymbol{p}}, \boldsymbol{r}) \right] + \Delta, \quad \text{maximum gap along trajectory.}$$

The minimum allowed energy, or effective energy gap $\Delta + a(\hat{\boldsymbol{p}}, \boldsymbol{r})$ along a trajectory that starts from the wire surface is pictured in Fig. 3.6.

Quasiparticles arriving from the far region in Fig. 3.6 are only able to reach the wire surface if they are in energy range M where the energy of the particle $E > \epsilon_3$. Quasiparticles in the energy range N are Andreev reflected, since at some point along their trajectory the local energy gap exceeds their energy. If quasiparticles approaching from the far region are present, for example if $T > 0$ and there are thermally excited quasi-particles, only those in region M can contribute to the drag force on the wire.

If the critical velocity is surpassed on the wire surface, $\epsilon_2 < 0$ and the wire begins to scatter quasiparticles into region L. However, if $\epsilon_2 < \epsilon_3$,

the resulting quasiparticles will be Andreev reflected by the flow field and thus do not contribute to the drag force. It is only if $\epsilon_3 < 0$ that quasiparticles in states M, with unrestricted access to the far region of the liquid, are produced by pair breaking.

It is also possible for there to exist quasiparticle states K with energy $\epsilon_1 < \epsilon < \epsilon_2$. There is no scattering into these states, since they have no access to the wire surface.

The condition that $\epsilon_3 < 0$ for quasiparticles to escape is predicated on the assumption that quasiparticles are only created at $\epsilon \leq 0$. However we know that once ϵ_2 is below zero, there is a range of energies in which quasiparticles can be created,

$$-|\epsilon_2| \leq \epsilon \leq |\epsilon_2|, \tag{3.33}$$

since in the semiconductor picture there will be filled states with positive energy which can scatter into the empty states with positive energy, thus producing quasiparticles with positive energy. The quasiparticles are fermions and follow Pauli exclusion principle, and are created in pairs. If a quasiparticle pair, where the positive energy particle has energy $\epsilon > \epsilon_3$ is created, then the positive energy particle is able to escape, while the negative energy particle may not. This leaves the negative energy state filled, which prevents the creation of another pair with the same energy and momentum. We assume that the system has reached a state of equilibrium where all the confined negative energy states of type L are filled. If a pair is created at the Fermi surface and $\epsilon_3 < 0$, then both members of the pair are able to escape, leaving behind an empty state to be filled again.

3.3.3 Self-consistent flow

In this section we will investigate how ideal flow is modified by the excitations produced by pair breaking. The excitations carry mass current, as indicated by Eq. (3.22). In order to find a self-consistent solution to the flow, we have to find fields $a(\hat{\boldsymbol{p}}, \boldsymbol{r})$ and $\boldsymbol{v}_s(\hat{\boldsymbol{p}}, \boldsymbol{r})$ that satisfy both self-consistency Eq. (3.19) for $a(\hat{\boldsymbol{p}}, \boldsymbol{r})$ and continuity equation $\boldsymbol{\nabla} \cdot \boldsymbol{j} = 0$. In practice, this must be done through an iterative process.

We begin work on the self-consistency Eq. (3.19). We assume that the cylinder is large in comparison to the superfluid coherence length, $R \gg \xi_0 = \hbar v_F / 2\pi k_B T_c$. We also assume the that $T = 0$ so that there are no thermally excited quasiparticles. We will also neglect quasiparticle-quasiparticle collisions. An example of the other extreme where quasiparticle-quasiparticle collisions dominate the dynamics in the near region of the wire is discussed in Sec. VII of Pub. III.

We separate momentum dependency from a by writing $a(\hat{\boldsymbol{p}}, \boldsymbol{r}) = \boldsymbol{\alpha}(\boldsymbol{r}) \cdot \hat{\boldsymbol{p}}$ and form a corresponding self-consistency equation for the field $\boldsymbol{\alpha}(\boldsymbol{r})$ as

$$\left(1 + \frac{F_1^s}{3}\right) \boldsymbol{\alpha}(\boldsymbol{r}) = p_F \boldsymbol{v}_s(\boldsymbol{r}) + \frac{F_1^s}{2} \tilde{\boldsymbol{I}}_{\boldsymbol{\alpha}}(\boldsymbol{r}), \qquad (3.34)$$

where

$$\tilde{\boldsymbol{I}}_{\boldsymbol{\alpha}}(\boldsymbol{r}) = \int \frac{d\Omega}{4\pi} \hat{\boldsymbol{p}} \int_{-E_c}^{E_c} d\epsilon\, N(\hat{\boldsymbol{p}}, \epsilon, \boldsymbol{r}) [\phi_{B1}(\hat{\boldsymbol{p}}, \epsilon, \boldsymbol{r}) + \phi_{B2}(\hat{\boldsymbol{p}}, \epsilon, \boldsymbol{r})], \quad (3.35)$$

with

$$N(\hat{\boldsymbol{p}}, \epsilon, \boldsymbol{r}) = \frac{|\epsilon - \boldsymbol{\alpha}(\boldsymbol{r}) \cdot \hat{\boldsymbol{p}}|}{\sqrt{(\epsilon - \boldsymbol{\alpha}(\boldsymbol{r}) \cdot \hat{\boldsymbol{p}})^2 - |\Delta|^2}} \theta([\epsilon - \boldsymbol{\alpha}(\boldsymbol{r}) \cdot \hat{\boldsymbol{p}}]^2 - |\Delta|^2). \quad (3.36)$$

Mass current density $\boldsymbol{j}$ can be stated in terms of Eq. (3.35) as

$$\boldsymbol{j} = m v_F N(0) \tilde{\boldsymbol{I}}_{\boldsymbol{\alpha}}(\boldsymbol{r}). \qquad (3.37)$$

The integrand in Eq. (3.35) is non-zero only if $(\epsilon - a)^2 - |\Delta|^2 > 0$, or in other words if

$$\epsilon > a(\hat{\boldsymbol{p}}, \boldsymbol{r}) + |\Delta(\hat{\boldsymbol{p}}, \boldsymbol{r})| = E_+(\hat{\boldsymbol{p}}, \boldsymbol{r}) \quad \text{or} \qquad (3.38)$$
$$\epsilon < a(\hat{\boldsymbol{p}}, \boldsymbol{r}) - |\Delta(\hat{\boldsymbol{p}}, \boldsymbol{r})| = E_-(\hat{\boldsymbol{p}}, \boldsymbol{r}), \qquad (3.39)$$

where we have defined energies E_+ and E_-. Since $a(-\hat{\boldsymbol{p}}, \boldsymbol{r}) = -a(\hat{\boldsymbol{p}}, \boldsymbol{r})$ we find that $E_+(-\hat{\boldsymbol{p}}, \boldsymbol{r}) = -E_-(\hat{\boldsymbol{p}}, \boldsymbol{r})$. A similar relation exists for the distributions, $\phi_{B1}(-\hat{\boldsymbol{p}}, -\epsilon, \boldsymbol{r}) = -\phi_{B2}(\hat{\boldsymbol{p}}, \epsilon, \boldsymbol{r})$. Assuming that the energies E_+ and E_- are within the interval $[-E_c, E_c]$, we can split the integration into two parts, one on the interval $[E_+, E_c]$ and the other on $[-E_c, E_-]$. With a change of variables $\hat{\boldsymbol{p}} \to -\hat{\boldsymbol{p}}$ and $\epsilon \to -\epsilon$, we can show that the resulting two terms are equal. The integral may thus be written as

$$\tilde{\boldsymbol{I}}_{\boldsymbol{\alpha}}(\boldsymbol{r}) = 2 \int \frac{d\Omega}{4\pi} \hat{\boldsymbol{p}} \int_{E_+(\hat{\boldsymbol{p}}, \boldsymbol{r})}^{E_c} d\epsilon\, \nu(\hat{\boldsymbol{p}}, \epsilon, \boldsymbol{r}) [\phi_{B1}(\hat{\boldsymbol{p}}, \epsilon, \boldsymbol{r}) + \phi_{B2}(\hat{\boldsymbol{p}}, \epsilon, \boldsymbol{r})]. \quad (3.40)$$

where

$$\nu(\hat{\boldsymbol{p}}, \epsilon, \boldsymbol{r}) = \frac{|\epsilon - \boldsymbol{\alpha}(\boldsymbol{r}) \cdot \hat{\boldsymbol{p}}|}{\sqrt{(\epsilon - \boldsymbol{\alpha}(\boldsymbol{r}) \cdot \hat{\boldsymbol{p}})^2 - |\Delta|^2}}. \qquad (3.41)$$

One of our underlying assumptions is that the wire surface is the only source of quasiparticles. At zero temperature there are no thermally excited quasiparticles. In addition we are neglecting quasiparticle-quasiparticle collisions. This means that only momentum states that

encounter the wire at some point along their trajectory, have a change of being occupied. If we shift the distributions ϕ_{B1} and ϕ_{B2} by $1/2$, we can only concern ourselves with trajectories that hit the wire, since for any other trajectory the integrand will be zero. We write

$$
\begin{aligned}
\tilde{\boldsymbol{I}}_{\boldsymbol{\alpha}}(\boldsymbol{r}) = {} & 2 \int \frac{d\Omega}{4\pi} \hat{\boldsymbol{p}} \int_{E_+(\hat{\boldsymbol{p}},\boldsymbol{r})}^{E_c} d\epsilon\, \nu(\hat{\boldsymbol{p}}, \epsilon, \boldsymbol{r}) \left[-\frac{1}{2} - \frac{1}{2} \right] \\
& + 2 \int_{\text{hit}} \frac{d\Omega}{4\pi} \hat{\boldsymbol{p}} \int_{E_+(\hat{\boldsymbol{p}},\boldsymbol{r})}^{E_c} d\epsilon\, \nu(\hat{\boldsymbol{p}}, \epsilon, \boldsymbol{r}) \\
& \times \left[\left(\phi_{B1}(\hat{\boldsymbol{p}}, \epsilon, \boldsymbol{r}) + \frac{1}{2} \right) + \left(\phi_{B2}(\hat{\boldsymbol{p}}, \epsilon, \boldsymbol{r}) + \frac{1}{2} \right) \right],
\end{aligned}
\tag{3.42}
$$

where $\int_{\text{hit}}$ signifies the integration over momentum directions that encounter the wire. The first integral can be calculated analytically. We obtain

$$
\tilde{\boldsymbol{I}}_{\boldsymbol{\alpha}}(\boldsymbol{r}) = \frac{2}{3} \boldsymbol{\alpha}(\boldsymbol{r}) + 2\boldsymbol{I}_{\boldsymbol{\alpha}}(\boldsymbol{r}),
\tag{3.43}
$$

where

$$
\begin{aligned}
\boldsymbol{I}_{\boldsymbol{\alpha}}(\boldsymbol{r}) = {} & \int_{\text{hit}} \frac{d\Omega}{4\pi} \hat{\boldsymbol{p}} \int_{E_+(\hat{\boldsymbol{p}},\boldsymbol{r})}^{E_c} d\epsilon\, \nu(\hat{\boldsymbol{p}}, \epsilon, \boldsymbol{r}) \\
& \times \left[\left(\phi_{B1}(\hat{\boldsymbol{p}}, \epsilon, \boldsymbol{r}) + \frac{1}{2} \right) + \left(\phi_{B2}(\hat{\boldsymbol{p}}, \epsilon, \boldsymbol{r}) + \frac{1}{2} \right) \right].
\end{aligned}
\tag{3.44}
$$

In terms of $\boldsymbol{I}_{\boldsymbol{\alpha}}(\boldsymbol{r})$ the self-consistency equation for $\boldsymbol{\alpha}(\boldsymbol{r})$ becomes

$$
\boldsymbol{\alpha}(\boldsymbol{r}) = p_F \boldsymbol{v}_s(\boldsymbol{r}) + F_1^s \boldsymbol{I}_{\boldsymbol{\alpha}}(\boldsymbol{r}).
\tag{3.45}
$$

Similarly, the mass current density can be written as

$$
\boldsymbol{j}(\boldsymbol{r}) = 2m v_F N(0) \left(\frac{p_F}{3} \boldsymbol{v}_s(\boldsymbol{r}) + \left(1 + \frac{F_1^s}{3} \right) \boldsymbol{I}_{\boldsymbol{\alpha}}(\boldsymbol{r}) \right).
\tag{3.46}
$$

This explicitly shows that the mass current, in addition to the component caused by the superflow $\boldsymbol{v}_s$, also has a component that depends on the presence of excitations. Each excitation carries the mass of a Fermi liquid quasiparticle, $m^* = (1 + F_1^s/3)m$. However, the separation is not as clear as the above equation makes it seem since, for a self-consistent flow, changes caused by the excitations will also be included in $\boldsymbol{v}_s$.

Based on the kinetic equation (3.11), we know that in the time-independent and collisionless case the distributions of quasiparticles ϕ_{Bi} are constant along the trajectory of a quasiparticle. This means that

along their entire trajectory, quasiparticles will have the same distribution that they have at the point where they originate. If the quasiparticles originate from the wire, their distribution will be that given by a boundary condition $\phi_{Bi}^{\text{bc}}(\hat{\boldsymbol{p}}, R\hat{\boldsymbol{r}}, \epsilon)$ at the wire surface. At a point of Andreev reflection with $[\epsilon - a(\hat{\boldsymbol{p}}, \boldsymbol{r})]^2 - |\Delta(\hat{\boldsymbol{p}}, \boldsymbol{r})|^2 = 0$, the distributions are equal, $\phi_{B1}(\hat{\boldsymbol{p}}, \boldsymbol{r}, \epsilon) = \phi_{B2}(\hat{\boldsymbol{p}}, \boldsymbol{r}, \epsilon)$. For example, for given momentum and energy, the distribution of outgoing hole-type quasiparticles from the site of Andreev reflection is the same as the distribution of incoming particle-type excitations. Within the gap, $[\epsilon - a(\hat{\boldsymbol{p}}, \boldsymbol{r})]^2 - |\Delta(\hat{\boldsymbol{p}}, \boldsymbol{r})|^2 < 0$ and the distributions are not defined.

The energy integration in Eq. (3.44) can be split into intervals where the distributions $\phi_{B1}(\hat{\boldsymbol{p}}, \boldsymbol{r}, \epsilon)$ and $\phi_{B2}(\hat{\boldsymbol{p}}, \boldsymbol{r}, \epsilon)$ have known values. First, we define the following limiting energy values at some point $\boldsymbol{r} = \boldsymbol{r}_0 + s\hat{\boldsymbol{p}}$ on the trajectory of a quasiparticle:

$$
\begin{aligned}
\epsilon_0(\hat{\boldsymbol{p}}, \boldsymbol{r}) &= E_+(\hat{\boldsymbol{p}}, \boldsymbol{r}) = a(\hat{\boldsymbol{p}}, \boldsymbol{r}) + \Delta, \\
\epsilon_2(\hat{\boldsymbol{p}}, \boldsymbol{r}) &= a_{\text{max}<}(\hat{\boldsymbol{p}}, \boldsymbol{r}) + \Delta, \\
\epsilon_3(\hat{\boldsymbol{p}}, \boldsymbol{r}) &= a_{\text{max}>}(\hat{\boldsymbol{p}}, \boldsymbol{r}) + \Delta, \\
\epsilon_{\text{max}}(\hat{\boldsymbol{p}}, \boldsymbol{r}) &= \max\{\epsilon_2, \epsilon_3\} = a_{\text{max}}(\hat{\boldsymbol{p}}, \boldsymbol{r}) + \Delta, \\
\epsilon_{\text{min}}(\hat{\boldsymbol{p}}, \boldsymbol{r}) &= \min\{\epsilon_2, \epsilon_3\}.
\end{aligned}
\tag{3.47}
$$

Here $a_{\text{max}<}$ is the maximum value of a along the trajectory of a quasiparticle towards the wire, and $a_{\text{max}>}$ the same, but away from the wire. Finally, a_{max} is the maximum value along the whole particle trajectory. The energy integration for a given momentum direction can be divided along these energies as

$$
\int_{E_+}^{E_c} d\epsilon = \int_{\epsilon_0}^{\epsilon_{\text{min}}} d\epsilon + \int_{\epsilon_2}^{\epsilon_{\text{max}}} d\epsilon + \int_{\epsilon_{\text{max}}}^{E_c} d\epsilon,
\tag{3.48}
$$

where the different parts of the integral correspond to regions K, L and M of Fig. 3.6, respectively. States K are the only type of states with no access to the wire surface. We refer to these states as *trapped* states, and mark their distribution with ϕ_{Bi}^{trap}.

Eq. (3.44) thus becomes

$$\boldsymbol{I_\alpha}(\boldsymbol{r}) = \int_{\text{hit}+} \frac{d\Omega_p}{4\pi} \hat{\boldsymbol{p}} \int_{\epsilon_{\max}}^{E_c} d\epsilon\, \nu(\hat{\boldsymbol{p}}, \epsilon, \boldsymbol{r}) \left[\phi_{B1}^{\text{bc}}(\hat{\boldsymbol{p}}, \epsilon, \boldsymbol{r}) + \frac{1}{2} \right]$$

Particle states M, which have free access from the wire surface to the bulk liquid.

$$+2 \int_{\text{hit}+} \frac{d\Omega_p}{4\pi} \hat{\boldsymbol{p}} \int_{\epsilon_2}^{\epsilon_{\max}} d\epsilon\, \nu(\hat{\boldsymbol{p}}, \epsilon, \boldsymbol{r}) \left[\phi_{B1}^{\text{bc}}(\hat{\boldsymbol{p}}, \epsilon, \boldsymbol{r}) + \frac{1}{2} \right]$$

Particle states L propagating out from the wire, and hole states that have been Andreev reflected and are propagating back towards the wire.

$$+ \int_{\text{hit}-} \frac{d\Omega_p}{4\pi} \hat{\boldsymbol{p}} \int_{\epsilon_{\max}}^{E_c} d\epsilon\, \nu(\hat{\boldsymbol{p}}, \epsilon, \boldsymbol{r}) \left[\phi_{B2}^{\text{bc}}(\hat{\boldsymbol{p}}, \epsilon, \boldsymbol{r}) + \frac{1}{2} \right]$$

Hole states M, which have free access from the wire surface to the bulk liquid.

$$+2 \int_{\text{hit}-} \frac{d\Omega_p}{4\pi} \hat{\boldsymbol{p}} \int_{\epsilon_2}^{\epsilon_{\max}} d\epsilon\, \nu(\hat{\boldsymbol{p}}, \epsilon, \boldsymbol{r}) \left[\phi_{B2}^{\text{bc}}(\hat{\boldsymbol{p}}, \epsilon, \boldsymbol{r}) + \frac{1}{2} \right]$$

Hole states L propagating out from the wire, and particle states that have been Andreev reflected and are propagating back towards the wire.

$$+2 \int_{\text{hit}} \frac{d\Omega_p}{4\pi} \hat{\boldsymbol{p}} \int_{\epsilon_0}^{\epsilon_{\min}} d\epsilon\, \nu(\hat{\boldsymbol{p}}, \epsilon, \boldsymbol{r}) \left[\phi_{Bi}^{\text{trap}}(\hat{\boldsymbol{p}}, \epsilon, \boldsymbol{r}) + \frac{1}{2} \right].$$

Trapped states K. Includes hole and particle states propagating (3.49) in both directions, towards and away from the wire in a sequence of Andreev reflections. Since all states are Andreev reflected, hole and particle states have the same distribution ϕ_{Bi}^{trap}.

All other possible integration intervals will be over states propagating from the far regions of the liquid to the wire surface, which by our assumptions are unoccupied.

When calculating the force on the wire, the stress tensor is evaluated on the surface of the wire. A similar process as above applied to the stress tensor in Eq. (3.20) leads to

$$\overset{\leftrightarrow}{\boldsymbol{\Pi}}(\boldsymbol{r}) = 2 v_F p_F N(0) \int_{\hat{\boldsymbol{n}}\cdot\hat{\boldsymbol{p}}>0} \frac{d\Omega_p}{4\pi} \hat{\boldsymbol{p}}\,\hat{\boldsymbol{p}} \int_{\epsilon_{\max}}^{E_c} d\epsilon \left[\phi_{B1}^{\text{bc}}(\hat{\boldsymbol{p}}, \epsilon, \boldsymbol{r}) + \frac{1}{2} \right]$$
$$- 2 v_F p_F N(0) \int_{\hat{\boldsymbol{n}}\cdot\hat{\boldsymbol{p}}<0} \frac{d\Omega_p}{4\pi} \hat{\boldsymbol{p}}\,\hat{\boldsymbol{p}} \int_{\epsilon_{\max}}^{E_c} d\epsilon \left[\phi_{B2}^{\text{bc}}(\hat{\boldsymbol{p}}, \epsilon, \boldsymbol{r}) + \frac{1}{2} \right],$$

(3.50)

where $\boldsymbol{r}$ is now some point on the wire surface. In the integrals over momentum direction we have taken into account that all quasiparticle trajectories intersect the wire surface.

In Sec. III of Pub. III, a boundary condition describing the diffuse scattering of quasiparticles from a planar surface is introduced. This

boundary condition gives the distributions of scattered quasiparticles and is formulated with the explicit goal of satisfying the continuity of mass current $\hat{\boldsymbol{n}}\cdot\boldsymbol{j} = 0$ and excitation number current $\hat{\boldsymbol{n}}\cdot\boldsymbol{j}_e = 0$ at the boundary. These continuity conditions are discussed in App. B. In Sec. V of Pub. III it is shown that when no quasiparticles are able to escape from the near region of the wire, i.e. below the critical velocity, the distributions of quasiparticles scattered from the wire surface are given by the equilibrium distribution $\phi_{Bi}^{\mathrm{b.c}} = 1/2 - \theta(\epsilon)$. We thus expect that using the equilibrium distribution gives the correct value for the critical velocity. In Sec. V of Pub. III the drag force on the wire is also calculated assuming that the flow field around the wire is not modified by pair breaking. It is discovered that using the distribution $\phi_{Bi}^{\mathrm{b.c}} = 1/2 - \theta(\epsilon)$ for the reflected quasiparticles even above the critical velocity does not differ qualitatively from using the diffuse boundary condition introduced in Sec. III of Pub. III.

When calculating the self-consistent field, we will use the equilibrium distributions $\phi_{Bi}^{\mathrm{b.c}} = 1/2 - \theta(\epsilon)$. Our reasons for this are two-fold. First, the integrals in Eqs. (3.44) and (3.50) are simplified, since the distributions are step functions and so only change the limits of energy integration. Second, in the mass current and excitation number current conserving boundary condition, the distributions $\phi_{Bi}^{\mathrm{b.c}}$ can depend on the value that $a(\hat{\boldsymbol{p}}, \boldsymbol{r})$ takes anywhere in the fluid, which means that the distributions have to be constantly re-evaluated on every iteration step. This is computationally impractical.

For the distribution $\phi_{Bi}^{\mathrm{trap}}$ of trapped states in region K, we make two different simple suppositions, which we will call *model 1* and *model 2*. In model 1, we assume that the trapped K states are all empty, since they cannot reach the wire. This is in line with a steady-state view of the system. In model 2, we assume that when the wire first began accelerating, the states in region K had access to the wire surface, but were later blocked off as the wire gained speed and the extant $\boldsymbol{\alpha}$-field was formed. In such a case, those K states that have wire-intersecting trajectories are in equilibrium with the wire surface. Since we already only consider states that intersect the wire, the two models can be summarized as

$$
\begin{aligned}
\text{model 1}: &\begin{cases} \phi_{Bi}^{\mathrm{bc}} &= 1/2 - \theta(\epsilon), \\ \phi_{Bi}^{\mathrm{trap}} &= 1/2 - \theta(\epsilon - a), \end{cases} \\
\text{model 2}: &\begin{cases} \phi_{Bi}^{\mathrm{bc}} &= 1/2 - \theta(\epsilon), \\ \phi_{Bi}^{\mathrm{trap}} &= 1/2 - \theta(\epsilon). \end{cases}
\end{aligned}
\tag{3.51}
$$

Making the above substitutions in Eq. (3.49) yields

$$
\begin{aligned}
\boldsymbol{I}_1(\boldsymbol{r}) = {} & \int_{\text{hit}} \frac{d\Omega_p}{2\pi} \hat{\boldsymbol{p}}\, \theta[-a_{\max<}(\hat{\boldsymbol{p}}, \boldsymbol{r}) - \Delta] \\
& \times \left(\sqrt{a(\hat{\boldsymbol{p}}, \boldsymbol{r})^2 - \Delta^2} - \sqrt{[a_{\max<}(\hat{\boldsymbol{p}}, \boldsymbol{r}) - a(\hat{\boldsymbol{p}}, \boldsymbol{r}) + \Delta]^2 - \Delta^2} \right) \\
& - \int_{\text{hit}} \frac{d\Omega_p}{4\pi} \hat{\boldsymbol{p}}\, \theta[-a_{\max}(\hat{\boldsymbol{p}}, \boldsymbol{r}) - \Delta] \\
& \times \left(\sqrt{a(\hat{\boldsymbol{p}}, \boldsymbol{r})^2 - \Delta^2} - \sqrt{[a_{\max}(\hat{\boldsymbol{p}}, \boldsymbol{r}) - a(\hat{\boldsymbol{p}}, \boldsymbol{r}) + \Delta]^2 - \Delta^2} \right),
\end{aligned}
\tag{3.52}
$$

and

$$
\begin{aligned}
\boldsymbol{I}_2(\boldsymbol{r}) = {} & \int_{\text{hit}} \frac{d\Omega_p}{2\pi} \hat{\boldsymbol{p}}\, \theta[-a(\hat{\boldsymbol{p}}, \boldsymbol{r}) - \Delta] \sqrt{a(\hat{\boldsymbol{p}}, \boldsymbol{r})^2 - \Delta^2} \\
& - \int_{\text{hit}} \frac{d\Omega_p}{2\pi} \hat{\boldsymbol{p}}\, \theta[-a_{\max>}(\hat{\boldsymbol{p}}, \boldsymbol{r}) - \Delta] \\
& \times \left(\sqrt{a(\hat{\boldsymbol{p}}, \boldsymbol{r})^2 - \Delta^2} - \sqrt{[a_{\max>}(\hat{\boldsymbol{p}}, \boldsymbol{r}) - a(\hat{\boldsymbol{p}}, \boldsymbol{r}) + \Delta]^2 - \Delta^2} \right) \\
& + \int_{\text{hit}} \frac{d\Omega_p}{4\pi} \hat{\boldsymbol{p}}\, \theta[-a_{\max}(\hat{\boldsymbol{p}}, \boldsymbol{r}) - \Delta] \\
& \times \left(\sqrt{a(\hat{\boldsymbol{p}}, \boldsymbol{r})^2 - \Delta^2} - \sqrt{[a_{\max}(\hat{\boldsymbol{p}}, \boldsymbol{r}) - a(\hat{\boldsymbol{p}}, \boldsymbol{r}) + \Delta]^2 - \Delta^2} \right).
\end{aligned}
\tag{3.53}
$$

These integrals have to be evaluated numerically.

The force on the wire given in Eq. (3.21) requires calculation of $\hat{\boldsymbol{n}} \cdot \overset{\leftrightarrow}{\boldsymbol{\Pi}}$. Using the equilibrium distribution $\phi_{Bi}^{\text{bc}} = 1/2 - \theta(\epsilon)$ in Eq. (3.50) yields

$$
\hat{\boldsymbol{n}} \cdot \overset{\leftrightarrow}{\boldsymbol{\Pi}} = -2v_F p_F N(0) \int \frac{d\Omega_p}{4\pi} \hat{\boldsymbol{p}} |\hat{\boldsymbol{n}} \cdot \hat{\boldsymbol{p}}|\, \theta[-a_{\max}(\hat{\boldsymbol{p}}, \boldsymbol{r}) - \Delta]\, (a_{\max}(\hat{\boldsymbol{p}}, \boldsymbol{r}) + \Delta).
\tag{3.54}
$$

3.4 Numerical implementation

This section offers a brief discussion on the numerical methods employed in calculating self-consistent flow around a cylinder moving at supercritical velocities. At the end of this section results of the numerical calculation are presented.

There are three equations that govern self-consistent flow. First, the self-consistency equation for $\boldsymbol{\alpha}$ was given in Eq. (3.45) as

$$
\boldsymbol{\alpha}(\boldsymbol{r}) = p_F \boldsymbol{v}_s(\boldsymbol{r}) + F_1^s \boldsymbol{I}_i(\boldsymbol{r}).
\tag{3.55}
$$

Secondly, the continuity equation $\boldsymbol{\nabla} \cdot \boldsymbol{j}(\boldsymbol{r}) = 0$. In the steady state using Eq. (3.46), we obtain Poisson's equation

$$\nabla^2 \psi(\boldsymbol{r}) = -\frac{2m}{\hbar p_F}(3 + F_1^s)\boldsymbol{\nabla} \cdot \boldsymbol{I}_i(\boldsymbol{r}). \tag{3.56}$$

It is similar to the Laplace equation that was used to determine the flow of ideal fluid, with the addition of a source term of the right side that depends on the excitations. If there are no excitations, then $\boldsymbol{I}_i(\boldsymbol{r}) \equiv 0$ and the flow is ideal. Finally, the flow velocity is given by

$$\boldsymbol{v}_s(\boldsymbol{r}) = \frac{\hbar}{2m}\boldsymbol{\nabla}\psi(\boldsymbol{r}). \tag{3.57}$$

Solution for the self-consistent flow is obtained by finding $\boldsymbol{v}_s$ (or $\boldsymbol{\alpha}$) for which both Eq. (3.55) and Eq. (3.56) are satisfied. In practice, this is done through an iterative numerical process.

We make a transformation to unitless variables using

$$\begin{aligned}
\boldsymbol{\alpha} &= p_F v\tilde{\boldsymbol{\alpha}}, \\
\boldsymbol{I} &= p_F v\tilde{\boldsymbol{I}}, \\
\Delta &= p_F v\tilde{\Delta}, \\
\epsilon &= p_F v\tilde{\epsilon}, \\
\boldsymbol{v}_s &= v\tilde{\boldsymbol{v}}_s, \\
r &= R\tilde{r}, \\
\psi &= \frac{2mvR}{\hbar}\tilde{\psi}.
\end{aligned} \tag{3.58}$$

In the following, we do not write the tildes over the unitless quantities. In addition, we study the problem in terms of deviation from ideal flow, $\delta\boldsymbol{v}_s = \boldsymbol{v}_s - \boldsymbol{v}_0$. The equations governing self-consistent flow can thus be written as

$$\boldsymbol{\alpha}(\boldsymbol{r}) = \delta\boldsymbol{v}_s(\boldsymbol{r}) + \boldsymbol{v}_0 + F_1^s\boldsymbol{I}_i(\boldsymbol{r}), \tag{3.59}$$

$$\nabla^2\delta\psi(\boldsymbol{r}) = -(3 + F_1^s)\boldsymbol{\nabla} \cdot \boldsymbol{I}_i(\boldsymbol{r}), \tag{3.60}$$

$$\boldsymbol{\nabla}\delta\psi(\boldsymbol{r}) = \delta\boldsymbol{v}_s(\boldsymbol{r}). \tag{3.61}$$

In our numerical solution, we define a lattice of points around the wire, with point (j, k) having polar coordinates (r_j, φ_k) where $r_j = R + j\,\delta r$ and $\varphi_k = \delta\varphi/2 + k\,\delta\varphi$. Lattice spacings are typically of order $\delta r \sim 10^{-2}$ and of $\delta\varphi \sim 10^{-2}$. A schematic of the lattice is shown in Fig. 3.7. In practice, we can limit ourselves to only a single quadrant of the space surrounding the wire, so that $1 \leq r_j \leq R_\infty$ and $\delta\varphi/2 \leq \varphi_k \leq (\pi - \delta\varphi)/2$.
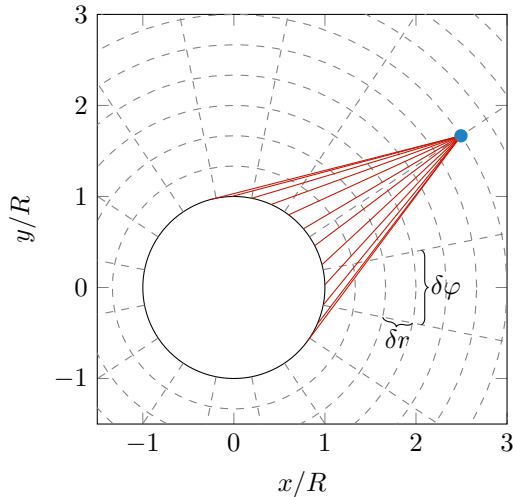
Figure 3.7: Schematic of the lattice used in the numerical computation. Lattice points are placed at the intersection of the dashed lines. A lattice point has been highlighted in blue. Quasiparticle trajectories in the $r\varphi$ plane that originate from the cylinder surface and end at the highlighted lattice point are show in red. In the numerical solution, the trajectories are selected so that they are equally spaced on the surface of the cylinder.

This is a result of symmetry conditions. Because the wire is cylindrical and far from the wire the liquid flows in the $-\hat{\boldsymbol{x}}$ direction, the flow has mirror symmetry over the x axis. In a reflection over the y axis, the flow is antisymmetric. This is due to a time reversal symmetry; reversing the direction of the wire's motion should produce the same result as reversing the direction of time.

The above group of equations is solved at each point of the lattice. Derivatives are calculated using the *finite difference* method. If evaluating the integrals over momentum directions appearing in Eqs. (3.52) and (3.53) at some given lattice point at position $\boldsymbol{r}_0$, we have to find the value of $a(\hat{\boldsymbol{p}}, s)$ on trajectories $\boldsymbol{r} = \boldsymbol{r}_0 + s\hat{\boldsymbol{p}}$ that meet the wire surface. Such trajectories are selected so that on the surface of the wire they are spaced equidistantly. This ensures that at the edges of the cylinder, as seen from point $\boldsymbol{r}_0$, the trajectories are spaced more tightly. We expect that on these trajectories, which are nearly tangential to the wire, $a(\hat{\boldsymbol{p}}, s)$ will change rapidly between adjacent trajectories and greater accuracy is thus needed. The trajectories obviously will not pass directly through the lattice points (r_j, φ_k) and thus we interpolate fields $\boldsymbol{\alpha}$ and $\boldsymbol{v}_s$ to find their values in the spaces between. The integrals over momentum
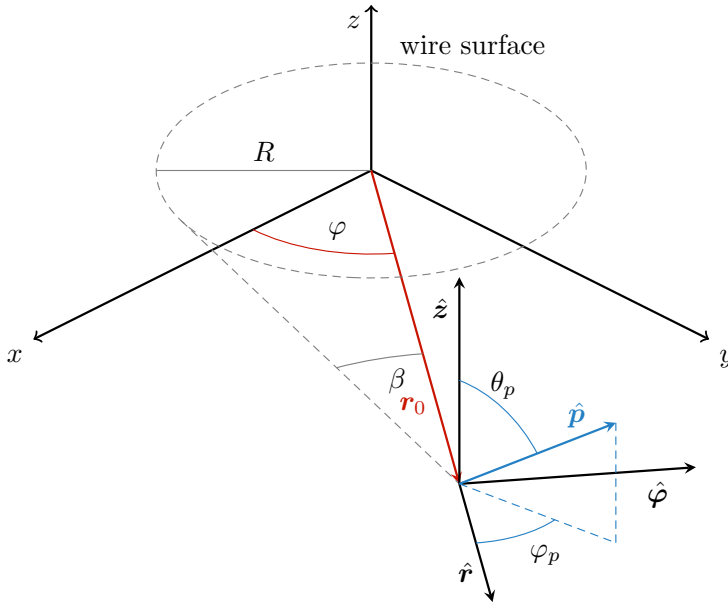
Figure 3.8: A schematic showing vectors $\boldsymbol{r}_0$ and $\hat{\boldsymbol{p}}$ and the relevant coordinate axes and angles. Coordinate φ is the polar angle of position $\boldsymbol{r}_0$ measured from the positive x axis. The direction of $\hat{\boldsymbol{p}}$ is given in spherical coordinates with angles θ_p and φ_p. The dashed gray circle depicts the cross section of a wire with radius R. At point $\boldsymbol{r}_0$ the angular size of the wire is 2β.

direction are evaluated using the trapezoidal method.

The algorithm for solving Eqs. (3.59), (3.60) and (3.61) goes as follows. First, we choose some initial value for field $\boldsymbol{v}_s$. The usual choice is to use the ideal flow field $\boldsymbol{v}_0$ at the given wire velocity v, in which case we have $\delta\boldsymbol{v}_s(\boldsymbol{r}) \equiv 0$. Then, a fixed-point iteration (*Newton-Raphson method*) is used to solve the corresponding $\boldsymbol{\alpha}$ from Eq. (3.59). Once $\boldsymbol{\alpha}$ has converged, we use Eq. (3.60) to solve the corresponding $\delta\psi$. From this, a new $\delta\boldsymbol{v}_s$ can be calculated using Eq. (3.61). The new $\delta\boldsymbol{v}_s$ is then plugged back into Eq. (3.59) and the process is repeated untill $\delta\boldsymbol{v}_s$ converges. When calculating $\delta\boldsymbol{v}_s$ from Eq. (3.61), we use the method of *succesive under-relaxation* in an attempt to introduce stability to the iterative process.

3.4.1 Choice of coordinates

In order to complete the integration over momentum directions, we use two different sets of coordinates. We fix the origin of a cylindrical coordinate system at the center of the moving wire. The z axis is aligned with the wire, and we denote with φ and r the polar angle and the distance from the wire center. We denote the location of the point at which we evaluate Eqs. (3.52) and (3.53) with $\boldsymbol{r}_0$. Centered on the point $\boldsymbol{r}_0$ we have a set of spherical coordinates which we use to parametrize the direction of momentum vector $\hat{\boldsymbol{p}}$. These coordinates are oriented so that angle $\varphi_p = 0$ points along vector $\boldsymbol{r}_0$ and θ_p is measured from $\hat{\boldsymbol{z}}$. These choices are depicted in Fig. 3.8. In the cylindrical coordinates we can parametrize the momentum direction as

$$\hat{\boldsymbol{p}} = \sin\theta_p \cos\varphi_p \hat{\boldsymbol{r}} + \sin\theta_p \sin\varphi_p \hat{\boldsymbol{\varphi}} + \cos\theta_p \hat{\boldsymbol{z}}. \tag{3.62}$$

The system is translationally invariant in the z direction and $\boldsymbol{\alpha} \cdot \hat{\boldsymbol{z}} = 0$. We write $a_{\max}(\hat{\boldsymbol{p}}) = \sin\theta_p a_{\max}(\varphi_p)$. If $\hat{\boldsymbol{p}}$ points too far out of the $r\varphi$ plane, then the Heaviside step function appearing in the integrals of Eqs. (3.52) and (3.53) is zero. Making use of this fact and the symmetry of the integrand around the angle $\theta_p = \pi/2$, we can write for example that

$$\int_{\text{hit}} \frac{d\Omega_p}{4\pi} \hat{\boldsymbol{p}} \, \theta[-a_{\max}(\hat{\boldsymbol{p}}, \boldsymbol{r}) - \Delta]$$
$$\times \left(\sqrt{a(\hat{\boldsymbol{p}}, \boldsymbol{r})^2 - \Delta^2} - \sqrt{[a_{\max}(\hat{\boldsymbol{p}}, \boldsymbol{r}) - a(\hat{\boldsymbol{p}}, \boldsymbol{r}) + \Delta]^2 - \Delta^2} \right)$$
$$= \frac{1}{4\pi} \int_{-\beta}^{\beta} d\varphi_p \theta[-a_{\max}(\varphi_p) - \Delta] \begin{pmatrix} \cos\varphi_p \\ \sin\varphi_p \\ 0 \end{pmatrix} \int_{\theta_l(\varphi_p)}^{\pi/2} d\theta_p \sin^2\theta_p$$
$$\times \left(\sqrt{a(\varphi_p)^2 \sin^2\theta_p - \Delta^2} - \sqrt{([a_{\max}(\varphi_p) - a(\varphi_p)] \sin\theta_p + \Delta)^2 + \Delta^2} \right),$$
$$\tag{3.63}$$

where $\beta = \arcsin(R/r)$, so that $[\pi - \beta, \pi + \beta]$ is the range of angle φ_p occluded by the wire and $\theta_l(\varphi_p) = \arcsin\left(-\frac{\Delta}{a_{\max}(\varphi_p)}\right)$.

3.4.2 Iterative methods

Newton-Raphson method is an iterative process for finding the roots (or zeroes) of a function $f(x)$ [53]:

$$x_{n+1} = x_n - \frac{f(x_n)}{f'(x_n)}. \tag{3.64}$$

With a sufficiently good initial guess for x_0, the starting value of the iteration, the above recursion will converge on a value that satisfies $f(x) = 0$. For a system of non-linear equations, the Newton-Raphson method takes the form

$$\boldsymbol{x}_{n+1} = \boldsymbol{x}_n - \boldsymbol{J}_{\boldsymbol{f}}^{-1}(\boldsymbol{x}_n)\boldsymbol{f}(\boldsymbol{x}_n), \qquad (3.65)$$

where $\boldsymbol{J}_{\boldsymbol{f}}(\boldsymbol{x})$ is the *Jacobian matrix* of $\boldsymbol{f}(\boldsymbol{x})$ and $\boldsymbol{x}$ is a vector holding all the variables on which $\boldsymbol{f}$ depends. The elements of $\boldsymbol{J}_{\boldsymbol{f}}(\boldsymbol{x})$ hold partial derivatives of $\boldsymbol{f}(\boldsymbol{x})$ with respect to each component of $\boldsymbol{x}$. Herein lies a difficulty. Since quasiparticles traveling out from the wire surface can in principle be reflected back at any point along their trajectory, there is no way for us to know what form the Jacobian will take beforehand. We must use a method that does not employ the Jacobian.

We are looking for a solution to $\boldsymbol{\alpha} = \boldsymbol{f}(\boldsymbol{\alpha})$, where f is the right side of Eq. (3.59). If we define a new function that satisfies $g(\boldsymbol{\alpha}) = \boldsymbol{\alpha} - \boldsymbol{f}(\boldsymbol{\alpha})$, we can use the Newton-Raphson method in finding the zeroes of $g(\boldsymbol{\alpha})$. By inserting $g(\boldsymbol{\alpha})$ into the Newton-Raphson formula, we can write the recursion

$$\boldsymbol{\alpha}^{(k+1)} = \boldsymbol{\alpha}^{(k)} - \frac{g(\boldsymbol{\alpha}^{(k)})}{g'(\boldsymbol{\alpha}^{(k)})} = \boldsymbol{\alpha}^{(k)} - \frac{\boldsymbol{\alpha}^{(k)} - \boldsymbol{f}(\boldsymbol{\alpha}^{(k)})}{1 - M}. \qquad (3.66)$$

The derivative of $\boldsymbol{f}(\boldsymbol{\alpha})$ has been replaced by the parameter M.

We can understand what value M should take by the following reasoning. Assume that the equation

$$x = f(x) \qquad (3.67)$$

has a fixed point at $x = a$. A fixed point iteration $x_{n+1} = f(x_n)$ will converge only if the derivative of the function at the fixed point satisfies $|f'(a)| < 1$. By adding Mx to either side of Eq. (3.67), we can form a new equation that has the same roots as Eq. (3.67), given by

$$x = \frac{f(x) + Mx}{1 + M} = g(x). \qquad (3.68)$$

The derivative $g'(x)$ can now be adjusted with the parameter M to satisfy $|g'(a)| < 1$. In practice, $M = 2$ seems a good choice.

If solving $\delta\boldsymbol{v}_s$ from Eq. (3.60), we first "mix" $\delta\psi$ with the value it had on the previous iteration step, with a mixing parameter τ. This is called successive under-relaxation [53], and can be written as

$$\delta\psi^{(k)} = \tau\delta\psi_C^{(k)} + (1 - \tau)\delta\psi^{(k-1)}, \qquad (3.69)$$

where $\delta\psi_C^{(k)}$ has been solved from the continuity equation Eq. (3.60) at iteration step k and $0 < \tau < 1$. This effectively slows down the
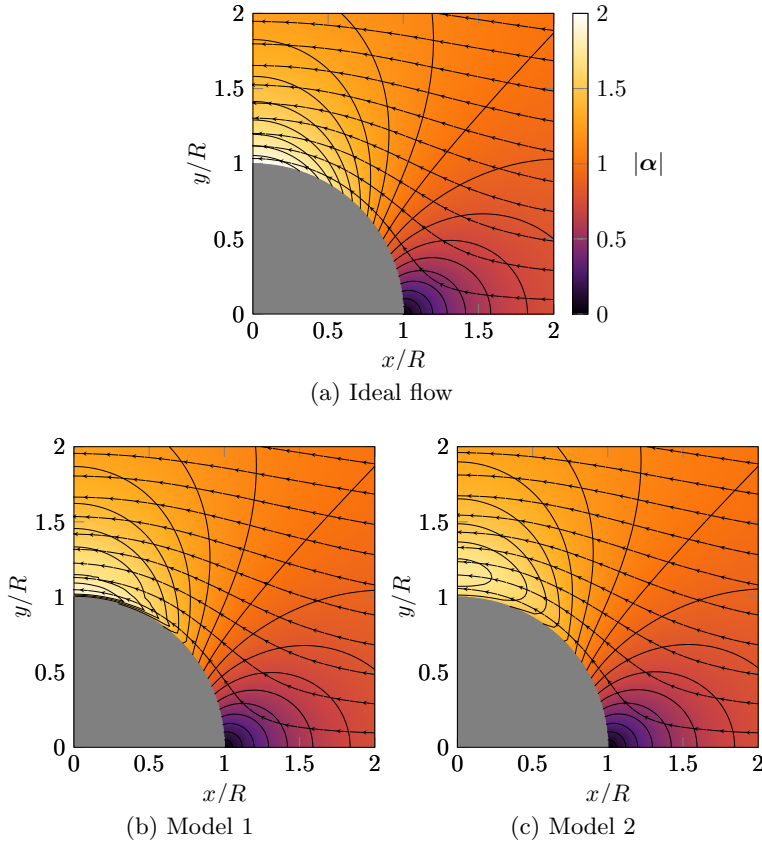
(a) Ideal flow

(b) Model 1

(c) Model 2

Figure 3.9: The field $\boldsymbol{\alpha}$ in units $p_F v$ at $v = 0.8 v_L$. The gray segment of a disk represents the cylinder. The color gradient signifies magnitude, $|\boldsymbol{\alpha}|$, and the stream lines the direction of $\boldsymbol{\alpha}$. Contours of constant $|\boldsymbol{\alpha}|$ are displayed at intervals of $0.1 p_F v$. The color scaling is the same in all figures. Figure first published in Pub. III.

convergence, introducing a modicum of stability as oscillation around the steady state solution is avoided. The method is more commonly applied as successive over-relaxation, in which the convergence of an iteration can be accelerated by using $1 < \tau < 2$.

3.4.3   Results

Here, we present some results of the numerical calculations outlined in the previous section. These are mostly the results found in Sec. VI of Pub. III with some additional analysis and comments. In all calculations we have assumed zero temperature, constant gap, and $F_1^s = 5.4$, corresponding to zero pressure in liquid ^{3}He.
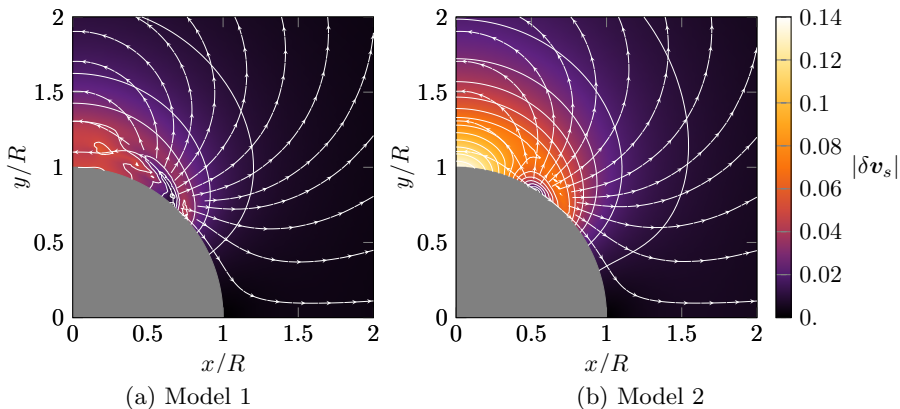
(a) Model 1   (b) Model 2

Figure 3.10: Deviation from the ideal flow, $\delta\boldsymbol{v}_s$, in units of v at $v = 0.8v_L$, corresponding to the quasiparticle potentials in Fig. 3.9(b) and Fig. 3.9(c). The gray segment of a disk represents the cylinder. The color gradient signifies $|\delta\boldsymbol{v}_s|$, and the stream lines the direction of flow. Contour lines of constant $|\delta\boldsymbol{v}_s|$ are displayed at intervals $0.01v$. The ideal flow is modified in a manner that diverts the liquid from the regions where critical velocity is exceeded locally. Figure first published in Pub. III.

Fig. 3.9 displays numerical results for the self-consistent $\boldsymbol{\alpha}$-field. Wire velocity is $v = 0.8v_L$. As a point of comparison, Fig. 3.9a displays the ideal flow field, given by the potential in Eq. (3.31). Results for model 1, corresponding to Eq. (3.52) are shown in Fig. 3.9b and results for model 2, corresponding to Eq. (3.53) are shown in Fig. 3.9c. Far from the wire the fields are the same, but close to the wire surface magnitude of $\boldsymbol{\alpha}$ is suppressed in both model 1 and model 2, to the point that the field maximum detaches from the wire surface. This feature is much more pronounced in Model 2. Suppression of $\boldsymbol{\alpha}$ at the wire surface means that fewer quasiparticles will scatter and subsequently there will be fewer excitations.

Fig. 3.10 shows results for $\delta\boldsymbol{v}_s = \boldsymbol{v}_s - \boldsymbol{v}_0$, deviation from ideal flow, corresponding to the $\boldsymbol{\alpha}$-fields show in Figs. 3.9b and 3.9c. As is expected, the flow is modified only in the region close to the wire. For both models, the flow is driven to circumvent the region close to the wire surface, effectively 'shielding' the wire from the incoming flow. This effect is much larger for model 2.

From Fig. 3.10 it seems that current is not conserved, since everywhere along the y axis there is a deviation $\delta\boldsymbol{v}_s$ from ideal flow that points in the direction of the negative x axis, which means that overall more superflow is going past the wire than in the ideal case. However, from
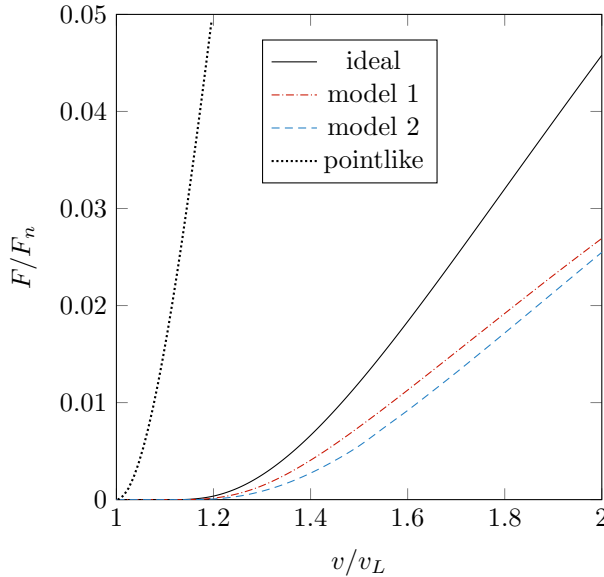
Figure 3.11: Drag force exerted on a macroscopic cylinder $(R \gg \xi_0)$ as a function of velocity in the collisionless approximation. The force is calculated for three different flow fields, the ideal flow, model 1, and model 2. The force on a microscopic pointlike object is also shown for comparison. The force in each case is reported in units of force in normal liquid on an object with the same dimension.

Eq. (3.46) we know that the total mass current $\boldsymbol{j}$ includes also a component that depends on excitations. This opposing mass current carried by excitations ensures that $\boldsymbol{j}$ is conserved.

The calculated drag force on the wire is shown in Fig. 3.11. The force is measured in units of force on a cylinder moving in a normal state Fermi liquid using a diffuse boundary condition, which is given by [54]

$$\boldsymbol{F}_n = \frac{43\pi}{48} p_F n_f v l R, \tag{3.70}$$

where $n_f = p_F^3 / 3\pi^2 \hbar^3$ is the number density of fermions, v is the velocity of the wire, and l and R are the length and radius of the wire, respectively. For comparison, the force on a microscopic pointlike object

$$\boldsymbol{F} = \theta(v - v_L) \frac{(v - v_L)^2 (v + v_L)}{v^3} \boldsymbol{F}_n, \tag{3.71}$$

is also shown in Fig. 3.11. For details see Sec. IV of Pub. III.

A cylindrical object begins to scatter quasiparticles at $v = v_L/2$, but the escape of quasiparticles into the far regions of the liquid becomes

possible only if $v = v_L$. We expect the drag force to set in beyond this
velocity. From Fig. 3.11 we find that for the pointlike microscopic object,
the ciritical velocity is v_L as expected. For the cylindrical object how-
ever, the critical velocity is increased, roughly to $1.12 v_L$. The spatially
varying flow field near the macroscopic wire is preventing the escape of
quasiparticles. Comparing ideal flow to model 1 and model 2, we find
that the critical velocity is the same for all models. However, the force
for both model 1 and model 2 is reduced in comparison to ideal flow;
self-consistent flow either reduces scattering since $\boldsymbol{\alpha}$ is reduced on the
wire surface, or is more effective at preventing the escape of quasiparti-
cles. In all cases, the calculated force is greatly reduced from the force
in a normal liquid, being roughly of the order of 10^{-2} in the units of F_n.

Fig. 3.12 displays the value of the effective energy gap $\Delta + a(\hat{\boldsymbol{p}}, s)$
along a specific trajectory starting from point $(r = R, \varphi = \pi/2)$ on the
surface of the wire and heading out in the positive x direction at two
different wire velocities, $v = 0.8 v_L$, which is below the calculated critical
velocity, and $v = 2 v_L$. At $v = 0.8 v_L$, even though there is a siginifi-
cant difference in the effective energy gap in the near region of the wire
between the two models and the ideal flow case, the maximum value of
$a(\hat{\boldsymbol{p}}, s) + \Delta$ along the trajectory is roughly the same. Moreover, the value
is positive, which means that along this trajectory the quasiparticles are
all Andreev reflected. At $v = 2 v_L$ we find that the maximum value along
trajectory is below zero and differs slightly between the models. For such
a trajectory the effect of the reduced magnitude of $\boldsymbol{\alpha}$ on the wire surface
is also very evident. Gap on the wire surface is much lower for ideal flow,
which means that there is vastly more scattering.
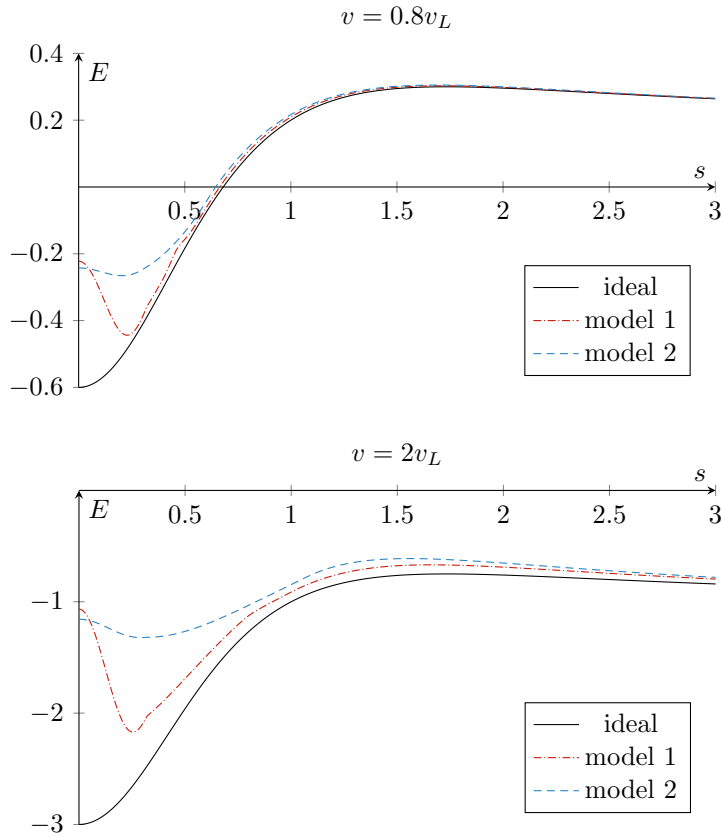
Figure 3.12: Effective energy gap $\Delta + a(\hat{\boldsymbol{p}}, s)$ in units of Δ at different wire velocities along a trajectory starting from point $(r = R, \varphi = \pi/2)$ at the top of the wire cross section and heading in direction $\hat{\boldsymbol{x}}$, calculated for three different flow fields, the ideal flow, model 1, and model 2. Position on the trajectory, s, is given in units of wire radius R.

4

Conclusion

In this thesis we have studied the motion of objects immersed in both normal and superfluid Fermi liquid. In the first half we concentrated on the phenomenon of transverse zero sound, and its propagation through a thin film of Fermi liquid. We applied the kinetic equations of Fermi liquid theory to the determination of the linear response of a Fermi liquid film to the transverse oscillations of a substrate. We calculated the acoustic impedance of the fluid film over a broad range of values for the mean free path of the Fermi liquid quasiparticles. This allowed us to investigate the linear response under various conditions, ranging from the collision dominated hydrodynamic region to the ballistic region. We investigated the combined effects of Fermi liquid interactions and surface specularity. We found that we cannot explain the experimentally observed decoupling of the fluid [16, 17], without requiring unreasonably high surface specularity, and even then the decoupling is not related to the Fermi liquid interactions. A possible continuation of this work would be to consider the motion of a Fermi superfluid.

In the latter portion of the thesis, the supercritical motion of a wire moving in superfluid ^{3}He was investigated. Using the quasiclassical theory of Fermi superfluids, we developed a model describing the dynamics of elementary excitations in the vicinity of a macroscopic cylinder moving in a Fermi superfluid. Based on this model, we studied how the motion of the cylinder alters the flow of the surrounding superfluid and calculated the drag force on the wire. We found that the critical velocity of the wire is increased from the expected value of v_L to roughly $1.12v_L$. We also found that the force on the wire is reduced by a factor of $\sim 10^{-2}$ in comparison to the normal state value, although this is still quite far of from the experimentally reported value of $\sim 10^{-5}$ [18].

In the latter project there are many possibilities for improvement. We

have ignored the effects of quasiparticle collisions. The way the model treats the scattering of quasiparticles from the wire surface could also be improved. Most obviously, we could apply the boundary condition detailed in Sec. III of Pub. III when calculating the self-consistent flow above the critical velocity. In addition, we could consider the effects of gap suppression near the wire. We could also include time dependence in the model. This could allow an accurate determinations of the distribution of quasiparticles in those states that are trapped by the superfluid flow, of which we made only general assumptions that we called model 1 and model 2. This work could also serve as a starting point to the study of the related, time dependent problem of a vibrating wire.

Appendix A

Effective mass of Fermi liquid quasiparticles

In this appendix the relation between the effective mass of Fermi liquid quasiparticles m^* and the first symmetric Landau parameter F_1^s is calculated. We study a system of fermions using a reference frame moving with some velocity $\boldsymbol{u}$. Since, according to Landau's theory, the number of quasiparticles in the system is the same as the number of particles, the addition of a single quasiparticle with momentum $\boldsymbol{p}$ increases the mass of the system by m, the bare particle mass. This means that in the moving frame, the momentum of the whole system is increased by $\boldsymbol{p} - m\boldsymbol{u}$. The increase in energy of the whole system can be identified with the energy of this added particle. Calculating this energy in the moving frame we get

$$\epsilon'_{\boldsymbol{p}-m\boldsymbol{u}} = \frac{|\boldsymbol{p} - m\boldsymbol{u}|^2}{2m} = \epsilon_{\boldsymbol{p}} - m\boldsymbol{p} \cdot \boldsymbol{u} + \frac{1}{2}mu^2, \tag{A.1}$$

where $\epsilon_{\boldsymbol{p}} = p^2/(2m)$. Since the momentum $\boldsymbol{p}$ is arbitrary, we may write

$$\epsilon'_{\boldsymbol{p}} = \epsilon_{\boldsymbol{p}+m\boldsymbol{u}} - \boldsymbol{p} \cdot \boldsymbol{u} - \frac{1}{2}mu^2. \tag{A.2}$$

Here, assuming that $m\boldsymbol{u} \ll \boldsymbol{p}$, we can expand $\epsilon_{\boldsymbol{p}+m\boldsymbol{u}}$ as a Taylor series as

$$\begin{aligned}
\epsilon_{\boldsymbol{p}+m\boldsymbol{u}} &= \epsilon_{\boldsymbol{p}} + m\boldsymbol{u} \cdot \nabla_{\boldsymbol{p}}\epsilon_{\boldsymbol{p}} + \dots \\
&= \epsilon_{\boldsymbol{p}} + \frac{m}{m^*}p_F \boldsymbol{u} \cdot \hat{\boldsymbol{p}} + \dots,
\end{aligned} \tag{A.3}$$

where in the last equality it has been assumed that the quasiparticle is on the Fermi surface, and the definition of Fermi velocity $v_F = p_F/m^*$

has been used. By dropping the quadratic term from the energy equation we obtain

$$\epsilon'_{\boldsymbol{p}} = \epsilon_{\boldsymbol{p}} + (\frac{m}{m^*} - 1)p_F \boldsymbol{u} \cdot \hat{\boldsymbol{p}}. \tag{A.4}$$

On the other hand, the ground state distribution has been shifted in the moving frame and is centered around $-m\boldsymbol{u}$. This corresponds with the middle figure in Fig. 2.1b. A shifted Fermi surface leads to a non-zero quasiparticle interaction energy. If $\boldsymbol{u}$ is fairly small, we can express the distribution in the moving frame using the series expansion

$$n'_{\boldsymbol{p}} = n^0_{\boldsymbol{p}+m\boldsymbol{u}} = n^0_{\boldsymbol{p}} + m\boldsymbol{u} \cdot \nabla_{\boldsymbol{p}} n^0_{\boldsymbol{p}} + \dots \tag{A.5}$$

At low temperatures, $n^0_{\boldsymbol{p}}$ resembles a step function and is thus isotropic. We have that $\delta n'_{\boldsymbol{p}} = m\boldsymbol{u} \cdot \hat{\boldsymbol{p}} \, \partial n^0_{\boldsymbol{p}} / \partial p = -m\boldsymbol{u} \cdot \hat{\boldsymbol{p}} \, \delta(p - p_F)$. Accordingly, we find that the energy integrated distribution can be written as

$$\phi_{\hat{\boldsymbol{p}}} = -mv_F \boldsymbol{u} \cdot \hat{\boldsymbol{p}} = -\frac{m}{m^*} p_F P_1(\boldsymbol{u} \cdot \hat{\boldsymbol{p}}). \tag{A.6}$$

In the last equality, we have used $P_1(x) = x$. The orthogonality of Legendre polynomials means that with this distribution, only the $l = 1$ term is non-zero after the averaging over momentum directions in Eq. (2.17). We obtain the energy

$$\epsilon'_{\boldsymbol{p}} = \epsilon_{\boldsymbol{p}} - \frac{m}{m^*} p_F \frac{F^s_1}{3} \boldsymbol{u} \cdot \hat{\boldsymbol{p}}. \tag{A.7}$$

By comparing our two results for the quasiparticle energy we find that

$$\frac{m^*}{m} = 1 + \frac{F^s_1}{3}. \tag{A.8}$$

This is the same relation as in Eq. (2.21).

Appendix B

Superfluid diffuse boundary condition

In Pub. III, a boundary condition for the diffuse reflection of Fermi superfluid quasiparticles from a planar surface is introduced and applied to the problem of a moving wire. This boundary condition is specifically formulated to satisfy the conditions for mass and excitations conservation. The components of mass current $\boldsymbol{j}$ and excitation number current $\boldsymbol{j}_e$ perpendicular to a planar surface should vanish, i.e. $\hat{\boldsymbol{n}} \cdot \boldsymbol{j} = \hat{\boldsymbol{n}} \cdot \boldsymbol{j}_e = 0$, where $\hat{\boldsymbol{n}}$ is the surface normal. The objective of this appendix is to verify that these conditions hold.

We begin by restating the diffuse boundary condition. We define

$$
\begin{aligned}
A(\epsilon) = &\int_{\hat{\boldsymbol{n}} \cdot \hat{\boldsymbol{p}} < 0} d\Omega_p |\hat{\boldsymbol{n}} \cdot \hat{\boldsymbol{p}}| N(\hat{\boldsymbol{p}}, \epsilon) \phi_{B1}(\hat{\boldsymbol{p}}, \epsilon) \\
& - \int_{\hat{\boldsymbol{n}} \cdot \hat{\boldsymbol{p}} > 0} d\Omega_p |\hat{\boldsymbol{n}} \cdot \hat{\boldsymbol{p}}| N(\hat{\boldsymbol{p}}, \epsilon) \phi_{B2}(\hat{\boldsymbol{p}}, \epsilon),
\end{aligned}
\tag{B.1}
$$

$$
\begin{aligned}
B(\epsilon) = &\int_{\hat{\boldsymbol{n}} \cdot \hat{\boldsymbol{p}} < 0} d\Omega_p |\hat{\boldsymbol{n}} \cdot \hat{\boldsymbol{p}}| \Theta(\hat{\boldsymbol{p}}, \epsilon) \phi_{B1}(\hat{\boldsymbol{p}}, \epsilon) \\
& + \int_{\hat{\boldsymbol{n}} \cdot \hat{\boldsymbol{p}} > 0} d\Omega_p |\hat{\boldsymbol{n}} \cdot \hat{\boldsymbol{p}}| \Theta(\hat{\boldsymbol{p}}, \epsilon) \phi_{B2}(\hat{\boldsymbol{p}}, \epsilon),
\end{aligned}
\tag{B.2}
$$

where

$$
\Theta(\hat{\boldsymbol{p}}, \epsilon) = \theta([\epsilon - a(\hat{\boldsymbol{p}})]^2 - |\Delta(\hat{\boldsymbol{p}})|^2),
\tag{B.3}
$$

$$
\nu(\hat{\boldsymbol{p}}, \epsilon) = \frac{|\epsilon - a(\hat{\boldsymbol{p}})|}{\sqrt{[\epsilon - a(\hat{\boldsymbol{p}})]^2 - |\Delta(\hat{\boldsymbol{p}})|^2}},
\tag{B.4}
$$

$$
N(\hat{\boldsymbol{p}}, \epsilon) = \nu(\hat{\boldsymbol{p}}, \epsilon) \Theta(\hat{\boldsymbol{p}}, \epsilon).
\tag{B.5}
$$

The distributions of reflected quasiparticles can be written in terms of incoming particle distributions as

$$\phi_{B1}(\hat{\boldsymbol{p}}, \hat{\boldsymbol{n}} \cdot \hat{\boldsymbol{p}} > 0, \epsilon) = \frac{g(\epsilon)}{2} \left[\nu^{-1}(\hat{\boldsymbol{p}}, \epsilon) A(\epsilon) + B(\epsilon) \right], \qquad \text{(B.6)}$$

$$\phi_{B2}(\hat{\boldsymbol{p}}, \hat{\boldsymbol{n}} \cdot \hat{\boldsymbol{p}} < 0, \epsilon) = \frac{g(\epsilon)}{2} \left[-\nu^{-1}(\hat{\boldsymbol{p}}, \epsilon) A(\epsilon) + B(\epsilon) \right], \qquad \text{(B.7)}$$

where we have used the normalization factor

$$g^{-1}(\epsilon) = \int_{\hat{\boldsymbol{n}} \cdot \hat{\boldsymbol{p}} > 0} d\Omega_p \, \hat{\boldsymbol{n}} \cdot \hat{\boldsymbol{p}} \, \Theta(\hat{\boldsymbol{p}}, \epsilon). \qquad \text{(B.8)}$$

Here we verify that on the surface of the wire the boundary condition satisfies $\hat{\boldsymbol{n}} \cdot \boldsymbol{j} = 0$ and $\hat{\boldsymbol{n}} \cdot \boldsymbol{j}_e = 0$ at arbitrary energy. These conditions may be written as

$$\hat{\boldsymbol{n}} \cdot \boldsymbol{j} = 0 : \int \frac{d\Omega_p}{4\pi} \hat{\boldsymbol{n}} \cdot \hat{\boldsymbol{p}} \, N(\hat{\boldsymbol{p}}, \epsilon)[\phi_{B1}(\hat{\boldsymbol{p}}, \epsilon) + \phi_{B2}(\hat{\boldsymbol{p}}, \epsilon)] = 0,$$
$$\hat{\boldsymbol{n}} \cdot \boldsymbol{j}_e = 0 : \int \frac{d\Omega_p}{4\pi} \hat{\boldsymbol{n}} \cdot \hat{\boldsymbol{p}} \, \Theta(\hat{\boldsymbol{p}}, \epsilon)[\phi_{B1}(\hat{\boldsymbol{p}}, \epsilon) - \phi_{B2}(\hat{\boldsymbol{p}}, \epsilon)] = 0. \qquad \text{(B.9)}$$

Concentrating on the first equation, conservation of mass, we split the integration over momentum direction to those pointing towards ($\hat{\boldsymbol{n}} \cdot \hat{\boldsymbol{p}} < 0$) and away from ($\hat{\boldsymbol{n}} \cdot \hat{\boldsymbol{p}} > 0$) the wire. We can categorize the distributions as

$$\hat{\boldsymbol{n}} \cdot \hat{\boldsymbol{p}} > 0 : \begin{cases} \phi_{B1} = \text{reflected particles,} \\ \phi_{B2} = \text{incoming holes,} \end{cases}$$
$$\hat{\boldsymbol{n}} \cdot \hat{\boldsymbol{p}} < 0 : \begin{cases} \phi_{B1} = \text{incoming particles,} \\ \phi_{B2} = \text{reflected holes.} \end{cases} \qquad \text{(B.10)}$$

For the reflected distributions, we insert boundary conditions in Eq. (B.6) and Eq. (B.7) into Eqs. (B.9) and obtain

$$\int_{\hat{\boldsymbol{n}} \cdot \hat{\boldsymbol{p}} > 0} \frac{d\Omega_p}{4\pi} \hat{\boldsymbol{n}} \cdot \hat{\boldsymbol{p}} \, N(\hat{\boldsymbol{p}}, \epsilon) \left(\frac{g(\epsilon)}{2} \left[\nu^{-1}(\hat{\boldsymbol{p}}, \epsilon) A(\epsilon) + B(\epsilon) \right] + \phi_{B2}(\hat{\boldsymbol{p}}, \epsilon) \right) +$$
$$\int_{\hat{\boldsymbol{n}} \cdot \hat{\boldsymbol{p}} < 0} \frac{d\Omega_p}{4\pi} \hat{\boldsymbol{n}} \cdot \hat{\boldsymbol{p}} \, N(\hat{\boldsymbol{p}}, \epsilon) \left(\phi_{B1}(\hat{\boldsymbol{p}}, \epsilon) + \frac{g(\epsilon)}{2} \left[-\nu^{-1}(\hat{\boldsymbol{p}}, \epsilon) A(\epsilon) + B(\epsilon) \right] \right) = 0. \qquad \text{(B.11)}$$

Moving those parts of the integrands which do not depend on $\hat{\boldsymbol{p}}$ outside

of the integrals and using the definition of $\nu(\hat{\boldsymbol{p}}, \epsilon)$, Eq. (B.4), we obtain

$$
\begin{aligned}
&\frac{g}{2} A \int_{\hat{\boldsymbol{n}} \cdot \hat{\boldsymbol{p}}>0} \frac{d\Omega_p}{4\pi} \hat{\boldsymbol{n}} \cdot \hat{\boldsymbol{p}} \, \Theta + \frac{g}{2} B \int_{\hat{\boldsymbol{n}} \cdot \hat{\boldsymbol{p}}>0} \frac{d\Omega_p}{4\pi} \hat{\boldsymbol{n}} \cdot \hat{\boldsymbol{p}} \, N \\
&+ \int_{\hat{\boldsymbol{n}} \cdot \hat{\boldsymbol{p}}>0} \frac{d\Omega_p}{4\pi} \hat{\boldsymbol{n}} \cdot \hat{\boldsymbol{p}} \, N \phi_{B2} + \int_{\hat{\boldsymbol{n}} \cdot \hat{\boldsymbol{p}}<0} \frac{d\Omega_p}{4\pi} \hat{\boldsymbol{n}} \cdot \hat{\boldsymbol{p}} \, N \phi_{B1} \\
&- \frac{g}{2} A \int_{\hat{\boldsymbol{n}} \cdot \hat{\boldsymbol{p}}<0} \frac{d\Omega_p}{4\pi} \hat{\boldsymbol{n}} \cdot \hat{\boldsymbol{p}} \, \Theta + \frac{g}{2} B \int_{\hat{\boldsymbol{n}} \cdot \hat{\boldsymbol{p}}<0} \frac{d\Omega_p}{4\pi} \hat{\boldsymbol{n}} \cdot \hat{\boldsymbol{p}} \, N = 0.
\end{aligned} \tag{B.12}
$$

We employ a change of variables from momentum direction $\hat{\boldsymbol{p}}$ in the specularly reflected momentum direction $\underline{\hat{\boldsymbol{p}}} = \hat{\boldsymbol{p}} - 2\hat{\boldsymbol{n}}(\hat{\boldsymbol{n}} \cdot \hat{\boldsymbol{p}})$. We also apply the identity

$$
\hat{\boldsymbol{n}} \cdot \underline{\hat{\boldsymbol{p}}} = \hat{\boldsymbol{n}} \cdot \hat{\boldsymbol{p}} - 2\hat{\boldsymbol{n}} \cdot \hat{\boldsymbol{n}}(\hat{\boldsymbol{n}} \cdot \hat{\boldsymbol{p}}) = -\hat{\boldsymbol{n}} \cdot \hat{\boldsymbol{p}}. \tag{B.13}
$$

If there is no flow through the wire, $\boldsymbol{\alpha} \cdot \hat{\boldsymbol{n}} = 0$, then

$$
\boldsymbol{\alpha} \cdot \underline{\hat{\boldsymbol{p}}} = \boldsymbol{\alpha} \cdot \hat{\boldsymbol{p}} - 2\boldsymbol{\alpha} \cdot \hat{\boldsymbol{n}}(\hat{\boldsymbol{n}} \cdot \hat{\boldsymbol{p}}) = \boldsymbol{\alpha} \cdot \hat{\boldsymbol{p}}. \tag{B.14}
$$

If in addition $|\Delta(\underline{\hat{\boldsymbol{p}}})| = |\Delta(\hat{\boldsymbol{p}})|$, we obtain the symmetry relations

$$
\Theta(\underline{\hat{\boldsymbol{p}}}, \epsilon) = \Theta(\hat{\boldsymbol{p}}, \epsilon), \tag{B.15}
$$

$$
N(\underline{\hat{\boldsymbol{p}}}, \epsilon) = N(\hat{\boldsymbol{p}}, \epsilon). \tag{B.16}
$$

Using the change of variables $\hat{\boldsymbol{p}} \to \underline{\hat{\boldsymbol{p}}}$ on some of the integrals where $\hat{\boldsymbol{n}} \cdot \hat{\boldsymbol{p}} < 0$, we obtain

$$
\begin{aligned}
&\frac{g}{2} A \overbrace{\int_{\hat{\boldsymbol{n}} \cdot \hat{\boldsymbol{p}}>0} \frac{d\Omega_p}{4\pi} \hat{\boldsymbol{n}} \cdot \hat{\boldsymbol{p}} \, \Theta}^{g^{-1}} + \frac{g}{2} B \int_{\hat{\boldsymbol{n}} \cdot \hat{\boldsymbol{p}}>0} \frac{d\Omega_p}{4\pi} \hat{\boldsymbol{n}} \cdot \hat{\boldsymbol{p}} \, N \\
&+ \int_{\hat{\boldsymbol{n}} \cdot \hat{\boldsymbol{p}}>0} \frac{d\Omega_p}{4\pi} |\hat{\boldsymbol{n}} \cdot \hat{\boldsymbol{p}}| \, N \phi_{B2} - \int_{\hat{\boldsymbol{n}} \cdot \hat{\boldsymbol{p}}<0} \frac{d\Omega_p}{4\pi} |\hat{\boldsymbol{n}} \cdot \hat{\boldsymbol{p}}| \, N \phi_{B1} \\
&+ \frac{g}{2} A \underbrace{\int_{\hat{\boldsymbol{n}} \cdot \hat{\boldsymbol{p}}>0} \frac{d\Omega_p}{4\pi} \hat{\boldsymbol{n}} \cdot \hat{\boldsymbol{p}} \, \Theta}_{g^{-1}} - \frac{g}{2} B \int_{\hat{\boldsymbol{n}} \cdot \hat{\boldsymbol{p}}>0} \frac{d\Omega_p}{4\pi} \hat{\boldsymbol{n}} \cdot \hat{\boldsymbol{p}} \, N = 0,
\end{aligned} \tag{B.17}
$$

where the appearance of g^{-1} has been pointed out. The second and sixth terms on the left side cancel. Using the definition of A in Eq. (B.1) in the above equation, we find that the condition $\hat{\boldsymbol{n}} \cdot \boldsymbol{j} = 0$ is satisfied for all values of A.

For the excitation current $\boldsymbol{j}_e$ a similar process leads to

$$
\frac{g}{2}A\int_{\hat{\boldsymbol{n}}\cdot\hat{\boldsymbol{p}}>0}\frac{d\Omega_p}{4\pi}\hat{\boldsymbol{n}}\cdot\hat{\boldsymbol{p}}\,\Theta\nu^{-1}+\overbrace{\frac{g}{2}B\int_{\hat{\boldsymbol{n}}\cdot\hat{\boldsymbol{p}}>0}\frac{d\Omega_p}{4\pi}\hat{\boldsymbol{n}}\cdot\hat{\boldsymbol{p}}\,\Theta}^{g^{-1}}
$$

$$
-\int_{\hat{\boldsymbol{n}}\cdot\hat{\boldsymbol{p}}>0}\frac{d\Omega_p}{4\pi}|\hat{\boldsymbol{n}}\cdot\hat{\boldsymbol{p}}|\,\Theta\phi_{B2}-\int_{\hat{\boldsymbol{n}}\cdot\hat{\boldsymbol{p}}<0}\frac{d\Omega_p}{4\pi}|\hat{\boldsymbol{n}}\cdot\hat{\boldsymbol{p}}|\,\Theta\phi_{B1} \tag{B.18}
$$

$$
-\frac{g}{2}A\int_{\hat{\boldsymbol{n}}\cdot\hat{\boldsymbol{p}}>0}\frac{d\Omega_p}{4\pi}\hat{\boldsymbol{n}}\cdot\hat{\boldsymbol{p}}\,\Theta\nu^{-1}+\frac{g}{2}B\underbrace{\int_{\hat{\boldsymbol{n}}\cdot\hat{\boldsymbol{p}}>0}\frac{d\Omega_p}{4\pi}\hat{\boldsymbol{n}}\cdot\hat{\boldsymbol{p}}\,\Theta}_{g^{-1}}=0.
$$

The first and fifth terms on the left side cancel. Using the definition of B in Eq. (B.2) in the above equation, we find that the condition $\hat{\boldsymbol{n}}\cdot\boldsymbol{j}_e=0$ is satisfied for all values of B.

Bibliography

[1] D. Vollhardt, P. Wölfe, *The superfluid Phases of Helium 3* (Dover Publications, New York, 2013).

[2] D. D. Osheroff, R. C. Richardson, and D. M. Lee, Phys. Rev. Lett. **28** 885 (1972).

[3] H. Kamerlingh Onnes, Proc. R. Acad. Amsterdam **11** 168 (1911).

[4] S. N. Bose, Zeitschrift für Physik **26**, 178–181 (1924).

[5] P. L. Kapitza, Nature **141**, 74 (1938).

[6] J. F. Allen and A. D. Misener, Nature **141**, 75 (1938).

[7] F. London, Nature **141**, 643 (1938).

[8] L. Landau, J. Phys. USSR **5**, 71 (1941).

[9] L. D. Landau, Zh. Eksp. Teor. Fiz. **30**, 1058 (1956) [Sov. Phys. JETP **3**, 920 (1957)].

[10] L. D. Landau, Zh. Eksp. Teor. Fiz. **32**, 59 (1957) [Sov. Phys. JETP **5**, 101 (1957)].

[11] L. N. Cooper, Phys. Rev. **104**, 1189 (1956).

[12] J. Bardeen, L. N. Cooper and J. R. Schrieffer, Phys. Rev. **108**, 1175 (1957).

[13] P. W. Anderson and P. Morel, Phys. Rev. **123**, 1911 (1961).

[14] R. Balian and N. R. Werthamer, Phys. Rev. **131**, 1553 (1963).

[15] D. D. Osheroff, W. J. Gully, R. C. Richardson, and D. M. Lee, Phys. Rev. Lett. **29** 920 (1972).

[16] A. Casey, J. Parpia, R. Schanen, B. Cowan, and J. Saunders, Phys. Rev. Lett. **92**, 255301 (2004).

[17] S. G. Dimov, R. G. Bennett, B. Ilic, S. S. Verbridge, L. V. Levitin, A. D. Fefferman, A. Casey, J. Saunders, and J. M. Parpia, J. Low Temp. Phys.**158**, 155 (2010).

[18] D. I. Bradley, S. N. Fisher, A. M. Guénault, R. P. Haley, C. R. Lawson, G. R. Pickett, R. Schanen, M. Skyba, V. Tsepelin, and D. E. Zmeev, Nat. Phys. **12**, 1017 (2016).

[19] G. Baym and C. Pethick, *Landau Fermi-liquid Theory: Concepts and Applications* (Wiley, New York, 1991).

[20] D. Pines and P. Nozieres, *The theory of quantum liquids, Vol. 1 Normal Fermi liquids* (W. A. Benjamin, New York, 1966).

[21] D. S. Greywall, Phys. Rev. B. **33**, 7520 (1986).

[22] J. C. Wheatley, Rev. Mod. Phys. **47**, 415 (1975).

[23] H. H. Hensley, Y. Lee, P. Hamot, T. Mizusaki, and W. P. Halperin, J. Low Temp. Phys. **89**, 501 (1992).

[24] L. R. Corruccini, D. D. Osheroff, D. M. Lee, and R. C. Richardson, Phys. Rev. Lett. **27**, 650 (1971).

[25] H. Smith and H. Højgaard Jensen, *Transport Phenomena* (Clarendon Press, Oxford, 1989).

[26] I. L. Bekarevich and I.M. Khalatnikov, Zh, Eksp. Teor. Fiz. **39**, 1699 (1960) [Sov. Phys. JETP **12**, 1187 (1961)].

[27] A. Fomin, Zh, Eksp. Teor. Fiz. **54**, 1881 (1968) [Sov. Phys. JETP **27**, 1010 (1968)].

[28] A. Fomin, Pis'ma Zh. Eksp. Teor. Fiz. **24**, 90 (1976) [JETP Lett. **24**, 77 (1976)].

[29] E. Flowers and R. Richardson, Phys. Rev. B, vol. **17**, 1238 (1978).

[30] R. Richardson, Phys. Rev. B, vol. **18**, 6122 (1978).

[31] L. D. Landau and E. M. Lifshitz, *Fluid Mechanics* (Pergamon Press, Oxford, 1987).

[32] B. N. Engel and G. G. Ihas, Phys. Rev. Lett. **55**, 955 (1985).

[33] W. P. Halperin and E. Varoquaux, in *Helium Three*, edited by W.P. Halperin and L.P. Pitaevskii (Elsevier, Amsterdam, 1990), pp. 353.

[34] P. R. Roach and J. B. Ketterson, Phys. Lett. **36**, 736 (1976).

[35] C. Lambert, Physica B **165**&**166**, 653 (1990).

[36] C. Lambert, Physica B **178**, 294 (1992).

[37] S. N. Fisher, A. M. Guénault, C. J. Kennedy, and G. R. Pickett, Phys. Rev. Lett. **63**, 2566 (1989).

[38] S. N. Fisher, G. R. Pickett, and R. J. Watts-Tobin, J. Low Temp. Phys. **83**, 225 (1991).

[39] M. P. Enrico, S. N. Fisher, and R. J. Watts-Tobin, J. Low Temp. Phys. **98**, 81 (1995).

[40] M. P. Enrico and R. J. Watts-Tobin, J. Low Temp. Phys. **102**, 103 (1996).

[41] C. A. M. Castelijns, K. F. Coates, A. M. Guénault, S. G. Mussett, and G. R. Pickett, Phys. Rev. Lett. **56**, 69 (1986).

[42] A. F. Andreev, Zh. Eksp. Teor. Fiz. **46**, 1823 (1964) [Sov. Phys. JETP **19**, 1228 (1964)].

[43] J. Kurkijärvi and D. Rainer, in *Helium Three*, edited by W.P. Halperin and L.P. Pitaevskii (Elsevier, Amsterdam, 1990), pp. 313-352.

[44] N. N. Bogoliubov, Nuovo Cimento **7**, 794 (1958); Zh. Eksp. Teor. Fiz. **34**, 58 (1958) [Sov. Phys. JTEP **7**, 41 (1958)].

[45] J. G. Valatin, Nuovo Cimento **7**, 843 (1958).

[46] A.J. Leggett, Rev. Mod. Phys. **47**, 331 (1975).

[47] J. W. Serene and D. Raine, Phys. Rep. **101**, 221 (1983).

[48] M. Tinkham, *Introduction to Superconductivity* (McGraw-Hill, New York, 1996).

[49] D. Vollhardt, K. Maki, and N. Schopohl, J. Low Temp. Phys. **39**, 79 (1980).

[50] B. Ashauer, *Emission von Quasiteilchen durch bewegte Objekte in suprafluidem* ^{3}*Helium-B*, Ph.D. thesis, University of Bayreuth, 1989.

[51] G. Kieselmann and D. Rainer, Z. Phys. B **52**, 267 (1983).

[52] E. V. Thuneberg, J. Low Temp. Phys. **122** 657 (2000).

[53] W. H. Press, S. A. Teukolsky, W. T. Vetterling, and B. P. Flannery, *Numerical Recipes: The Art of Scientific Computing* (Cambridge, 2007), Third Edition.

[54] T. H. Virtanen and E. V. Thuneberg, AIP Conf. Proc. **850**, 113 (2006).

Original publications